

## Finite Element Analysis of Precast Prestressed Beam-Column Concrete Connection in Seismic Construction

Master's Thesis in the International Master's Programme in Structural Engineering

DANIEL CAMARENA

Department of Civil and Environmental Engineering  
*Division of Structural Engineering*  
*Concrete Structures*  
CHALMERS UNIVERSITY OF TECHNOLOGY  
Göteborg, Sweden 2006  
Master's Thesis 2006:28



MASTER'S THESIS 2006:28

# Finite Element Analysis of Precast Prestressed Beam-Column Concrete Connection in Seismic Construction

Master's Thesis in the International Master's Programme in Structural Engineering

DANIEL CAMARENA

Department of Civil and Environmental Engineering  
*Division of Structural Engineering*  
*Concrete Structures*  
CHALMERS UNIVERSITY OF TECHNOLOGY  
Göteborg, Sweden 2006



Finite Element Analysis of Precast Prestressed Beam-Column Concrete Seismic Connection

Master's Thesis in the International Master's Programme in Structural Engineering  
DANIEL CAMARENA

© DANIEL CAMARENA, 2006

Master's Thesis 2006:28  
Department of Civil and Environmental Engineering  
Division of Structural Engineering  
Concrete Structures  
Chalmers University of Technology  
SE-412 96 Göteborg  
Sweden  
Telephone: + 46 (0)31-772 1000

Cover: Description and geometry of the selected and analysed beam-column concrete connection

Chalmers Reproservice / Department of Civil and Environmental Engineering  
Göteborg, Sweden 2006



# Finite Element Analysis of Precast Prestressed Beam-Column Concrete Seismic Connection

Master's Thesis in the International Master's Programme in Structural Engineering

DANIEL CAMARENA

Department of Civil and Environmental Engineering

Division of Structural Engineering

Concrete Structures

Chalmers University of Technology

## ABSTRACT

In the past decade, a large number of precast concrete structures have been built all over many earthquake prone countries. This has been one answer to past statements of uneconomical construction and that construction activity should be automated.

The connections between precast members normally constitute the weakest link in the structure, and the satisfactory performance and economy of precast concrete structures depend to a great extent on the proper selection and design of the connections.

In the design of earthquake resistant structures that incorporate precast concrete elements the main difficulty has been to find efficient and economical methods for connecting the precast concrete members together, and create connections that give adequate strength, stiffness and ductility.

The aim of the master's project was to select by means of conceptual design and to examine by finite element analysis and analytical models the effectiveness of a precast prestressed beam-column concrete connection of a jointed system and to discuss alternative solutions.

Various choices of structural solutions were to be studied within the project with regard to serviceability, production methods, maintenance and costs. The works should include literature studies and FE-analyses with the DIANA V9 program.

This thesis presents the results of the finite element analysis to examine the effectiveness of a precast prestressed beam-column concrete connection of a jointed system and compares it with an analytical model.

Results show that the seismic efficiency and the structural response of the analysed beam-column concrete connection under monolithic horizontal imposed displacement are satisfactory. The comparison of the finite element analysis and the analytical calculations converge quite well in the non-linear response. The design of the column of the selected beam-column concrete connection could be improved.

Key words: Connections; jointed system; ductile connection; hybrid; precast concrete; prestress; post-tensioning; finite element analysis; seismic design.



# Contents

ABSTRACT	I
CONTENTS	III
PREFACE	VII
NOTATIONS	VIII
1 BASIC CONCEPT	1
1.1 Types of concrete connections in moment resisting frames	1
1.1.1 Equivalent monolithic systems	1
1.1.2 Jointed systems	2
1.2 Manufacture and erection issues	4
1.3 Acceptance of Precast Concrete in Seismic Regions	6
2 PROJECT DESCRIPTION	7
2.1 Purpose	7
2.2 Goal and objectives	7
2.3 Scope and limitations	7
2.4 Research approach and methodology	8
2.5 Outline of the thesis	8
3 CONCEPTUAL ANALYSIS	10
3.1 Possible solutions of ductile connections	10
3.1.1 Alternative 1	10
3.1.2 Alternative 2	11
3.1.3 Alternative 3	11
3.1.4 Alternative 4	12
3.1.5 Alternative 5	13
3.1.6 Alternative 6	14
3.1.7 Alternative 7	15
3.1.8 Alternative 8	16
3.1.9 Alternative 9	17
3.1.10 Alternative 10	18
3.2 Evaluation of the connections	19
3.2.1 Decisive parameters	19
3.3 Comparison	23
3.4 Conclusion	23
4 PRELIMINARY STRUCTURAL ANALYSIS	25
4.1 Frame model	25
4.2 Results	29

5	DETAILED DESIGN AND FINAL GEOMETRY	31
5.1	Design concept	31
5.2	Sectional response	32
5.3	Maximum prestress	32
5.3.1	Steel stresses in secondary tendons	32
5.3.2	Concrete stresses	32
5.4	Energy dissipation	32
5.5	Detailing requirements	33
5.5.1	Beam and column design	33
5.5.2	Slab interaction	33
5.5.3	Protection of post-tensioned steel	33
5.5.4	Concrete confinement	33
5.5.5	Ties through weak planes	33
5.5.6	Position of secondary tendons	34
5.6	Final geometry and design	34
6	FINITE ELEMENT ANALYSIS	39
6.1	Material constitutive models	39
6.1.1	Concrete	39
6.1.2	Steel bars and tendons	42
6.1.3	Mortar and rubber pad	42
6.2	Finite element model	43
6.2.1	Geometry	44
6.2.2	Mesh	45
6.2.3	Boundary conditions	46
6.2.4	Loads and imposed displacement	47
6.2.5	Post-tensioned tendons	48
6.2.6	Thickness and material properties	49
6.3	Preliminary linear analysis	52
6.4	Non-linear analysis	59
6.4.1	Displacements	60
6.4.2	Cracking and stresses	62
6.4.3	Loss of prestress in the tendons and yielding of reinforcing steel	70
6.4.4	Force-drift curve	73
7	RESULTS VALIDATION WITH ANALYTICAL MODELLING	76
7.1	Moment rotation analysis procedure	76
7.2	Comparison of moment-drift curve	82
8	RECOMMENDATIONS AND CONCLUSIONS	84
8.1	Column capacity	84
8.2	Recommendations for further research	84
8.3	Final conclusions	85





## Preface

This master project is a part of an experimental program on precast structures that is been carried out at the European Centre for Training and Research in Earthquake Engineering and at the European School for Advance Studies in Reduction of Seismic Risk (ROSE School), Italy. The main goal of the program is to obtain mechanical information and to study the performance of innovative precast prestressed concrete connections, the research program involves the testing of one-third scale beam-column precast connection sub-assembly.

The master's project was carried out between September 2005 and March 2006 at the European School for Advance Studies in Reduction of Seismic Risk (ROSE School), Italy and at the Department of Structural Engineering, Concrete Structures, Chalmers University of Technology, Sweden.

I would like to express my gratitude to my supervisors at ROSE School, researchers Davide Bolognini and Ph.D. Roberto Nascimbene, who guided and enlightened me, and Ph.D. Rui Pinho for giving me the opportunity to take part in the project. I would also like to extend my thanks to my examiner and supervisor at Chalmers University of Technology professor M.Sc.C.E. Ph.D. Björn Engström for his help and advice, to my opponent Farzad Faridafshin for his comments and to my family and friends for their support during my stay in Sweden and Italy.

Göteborg March 2006

Daniel Camarena

## Notations

### Roman upper case letters

$A$	Area of cross-section
$E$	Modulus of elasticity
$G$	Fracture energy
$M$	Bending moment
$S_d$	Spectral acceleration
$T$	Fundamental period of vibration
$V$	Shear force

### Roman lower case letters

$a_g$	Peak ground acceleration (PGA)
$b$	Section width
$f_c$	Concrete compressive strength
$f_y$	Yield strength
$f_2$	Concrete compressive strength in cracked concrete
$h$	Section height
$u$	Displacement

### Greek letters

$\sigma$	Stress
$\varepsilon$	Strain
$\varepsilon_1$	Principal tensile strain
$\varepsilon_2$	Principal compressive strain
$\phi$	Diameter
$\nu$	Poisson's ratio
$\rho$	Density

## **Abbreviations**

EC1	Eurocode 1: Actions on Structures
EC2	Eurocode 2: Design of Concrete Structures
EC8	Eurocode 8: Design of Structures for Earthquake Resistance
FE	Finite Element
FEM	Finite Element Method
PRESS	PREcast Seismic Structural Systems
TCY	System that denotes Tension/Compression Yielding
fib	federation internationale du beton



# 1 Basic Concept

Connections are one of the most essential parts in prefabricated structures. The behaviour of a precast structure will to a large extent depend on the behaviour of the connections. This is valid for seismic and non-seismic construction.

Precast concrete connections must fulfil requirements with respect to resistance, performance, manufacture, transportation, erection, safety and other criteria. Their principal function is to transfer forces across joints so that interaction between precast units is obtained. This interaction can be achieved in multiple ways; therefore, there are many types of connections.

This chapter will give an overview of the subject, mostly with regard to seismic beam to column precast concrete connections and more in detail with non-emulative ductile connections.

## 1.1 Types of concrete connections in moment resisting frames

The fib bulletin 27, fib (2003) defines two broad categories of precast concrete connections of moment resisting frames: either “equivalent monolithic” systems, or “jointed” systems. The main difference between the two systems relates to the modality of accommodating the inelastic demand.

### 1.1.1 Equivalent monolithic systems

The equivalent monolithic system or cast-in-place emulation (wet connections) is subdivided in two categories: strong connections of limited ductility and ductile connections.

Strong connections of limited ductility are designed to be sufficiently strong so that the yielding occurs elsewhere in the structure.

An in the other hand ductile connections of equivalent monolithic systems are designed for the required strength and a plastic hinge is expected to occur in the beam at the column face in a severe earthquake and yield penetration will occur in the connection region. An example of a ductile connection can be seen in Figure 1.1.

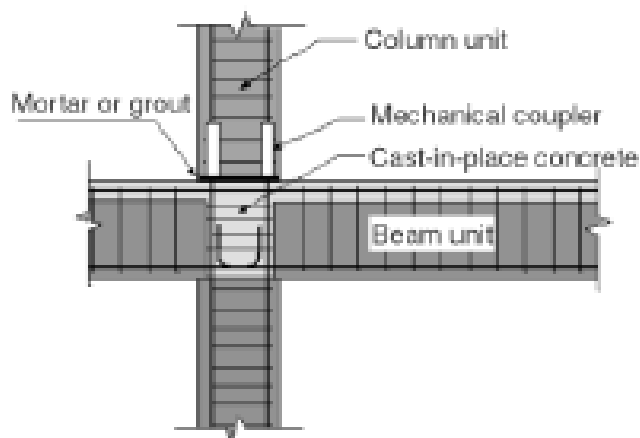


*Figure 1.1 Typical arrangement of a beam-column concrete connection according to the equivalent monolithic system (emulative approach).*

The emulation cast-in-place (equivalent monolithic) reinforced concrete approach is commonly accepted in the main international building codes and also among precasters in many earthquake prone countries. This type of connections will not be considered any more in this thesis.

## **1.1.2 Jointed systems**

In the jointed system the connections are weaker than the adjacent precast concrete elements. Jointed systems do not emulate the performance of cast-in-place concrete construction. It can be subdivided into two subcategories: connections of limited ductility and ductile connections.

### **1.1.2.1 Connections of limited ductility**

Connections of limited ductility for jointed systems are usually dry connections formed by welding or bolting reinforced bars or plates or steel embedments, and dry packing and grouting. These connections do not behave as typical connections in monolithic construction and generally have limited ductility.

### **1.1.2.2 Ductile connections**

Ductile connections of jointed systems are generally dry connections in which unbonded post-tensioned tendons are used to connect the precast concrete elements together. Such connections can be designed to perform in a ductile manner. The post-

elastic deformations of the member are concentrated at the interface of the precast concrete elements where a crack opens and closes. The unbonded post-tensioned tendons remain in the elastic range.

Development of precast concrete structures for seismic areas under the PRESS (PREcast Seismic Structural Systems) program [Priestley (1996)] resulted in the experimental validation of the seismic efficiency of different innovative typologies of ductile beam-column connections of jointed systems. The basic scheme of such connections is the adoption of “unbonded” concepts, in the form of unbonded post-tensioned bars or tendons, partially ungrouted reinforcing bars of mild steel or a combination of the above.

One of the innovative connections used in the PRESS program is the “Hybrid System”, which uses unbonded tendons together with additional mild steel as longitudinal reinforcement in order to supply energy dissipation capacity. This system, if well designed and constructed, will perform at least as satisfactorily as ductile connections of equivalent monolithic systems, and has the added advantage of reducing damage and of being self-centring after an earthquake. This system has been used in the Paramount building located in San Francisco, which is actually the tallest precast building in a high seismic zone in the United States, see Figure 1.2.

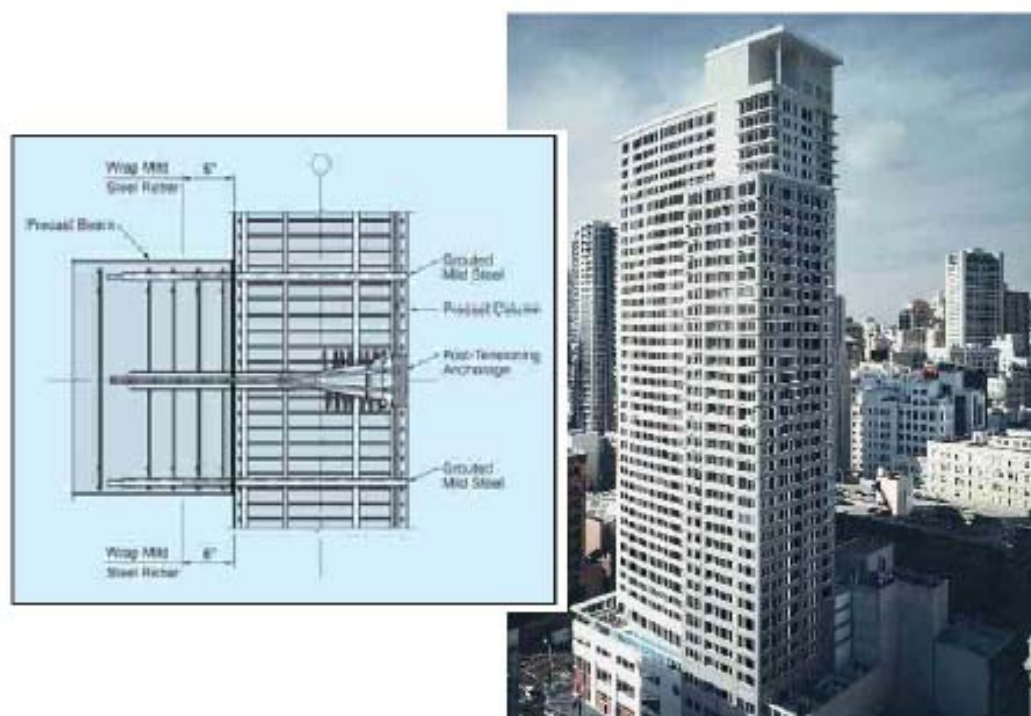


Figure 1.2 View of the Paramount building and reinforcing details of exterior column [Englekirk (2002)].

Another research program within the same current as of the PRESS program was developed in Japan. The project proposes a new structural system that estimates in beforehand degrees of losses due to severe earthquakes. Concrete ductile connections or Mild-PRESS joints designed with the so-called “damage controlled seismic design” are presented in Nakano et al (2001).

The target of the project was to be able to estimate the amount of economic and functional losses, which might be caused by severe earthquakes, as well as to reduce the waste of natural resources and energy. The basic idea is that precast elements should be maintained in the elastic range and the inelastic demand is accommodated within the connection itself. Reduced level of damage in the precast beams, when compared with analogous cast-in-place solutions, is therefore expected.

An example of the Mild-PRESS joint system is the International Stadium of Yokohama, see Figure 1.3.

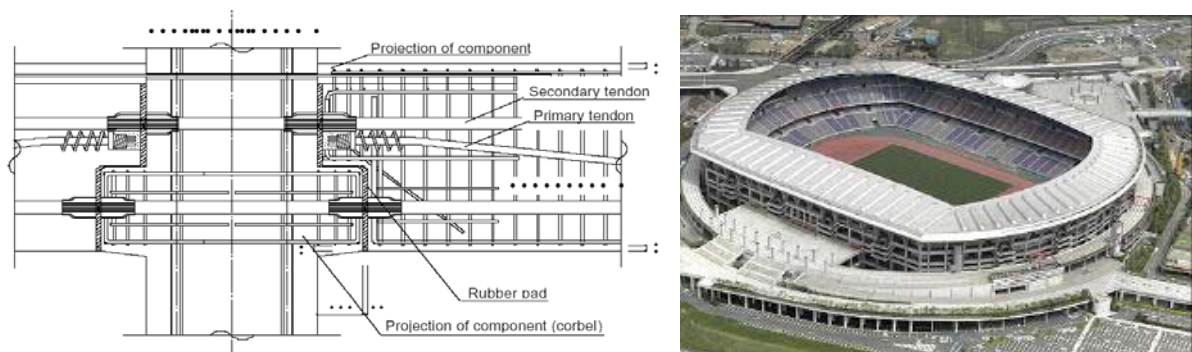


Figure 1.3 View of the International Stadium of Yokohama and a beam-column connection detail of the Mild-PRESS joint system [Nakano et al (2001)].

## 1.2 Manufacture and erection issues

One of the most important principles in the design of connections is to keep them simple. Maximum economy of precast concrete construction is achieved when connection details are kept as simple as possible, consistent with adequate performance and ease of erection. Furthermore, complex connections are more difficult to design, to produce and to control and will often result in poor fit in the field. This can contribute to slow erection and give less satisfactory performance.

In order to improve fabrication simplicity some of the precepts that should be considered during the design are listed here:

- Avoid congestion: It is very important to design the connections in such a way that sufficient room is left for concrete to be placed correctly between the different details.

- Allow alternatives: The producer should be allowed to use alternative methods or materials, provided the design requirements are met. Allowing alternative solutions will often result in the most economical and best performing connection.
- Avoid heavy connection items: Units requiring two persons for lifting may in some cases be acceptable, but the general rule is that one person should be able to handle it alone.



*Figure 1.4 Post-tensioning process after the beams are placed in a building project in Turkey with ductile connections of jointed systems.*

Hoisting precast pieces is usually the most expensive and time-consuming process of the erection. Connections should be designed so that the unit can be lifted, set, unhooked and tense in the shortest possible time, see Figure 1.4.

For fast erection it is necessary that the connections are adjustable to allow for dimensional deviations. Not only should the tolerances of the precast elements be considered, but also the possibility of incorrect placing of the elements. Connections should also be accessible during mounting.

On the other hand the erection of seismic resistant precast concrete construction differs from non-seismic precast by requiring tighter tolerances in limited number of key areas, such as:

- Seismic separations must not be reduced by accumulated tolerances.
- Rotation compatibility for pinned connections will require more careful attention to the location and thickness of bearing pads and clearances between beam-ends and supporting columns.

Seismic connections may also require access for specialised equipment (grouting, welding, or post-tensioning) and access for more than one worker.

### **1.3 Acceptance of Precast Concrete in Seismic Regions**

The use and development of precast concrete structures in seismic areas have been typically limited (with a few exceptions in Unites States, Japan and New Zealand), normally by the lack of confidence and knowledge about their performance in seismic regions as well as by the absence of sound seismic design provisions in major building codes. As a result of these doubts the accepted advantages of precast concrete over cast-in-place construction refers only to aspects of quality control and velocity of erection while its structural performance is disregarded.

This lack of confidence has been increased by incorrect design detailing rather than intrinsic limits of the structure when the performance of several prefabricated structures during earthquakes has been very poor.

In the special case of countries like Italy the only accepted philosophy of design of precast concrete structures among precasters is the emulation of cast-in-place concrete.

## **2 Project Description**

### **2.1 Purpose**

The purpose of this master's project was to acquire a better understanding of the behaviour and response of the precast prestressed beam-column concrete connections under seismic loading. This significant perception should lead to an increase in the development of the design and fabrication of precast prestressed structures in seismic regions.

### **2.2 Goal and objectives**

The main goal of this project was to select by means of conceptual analysis a precast beam-column concrete connection and to establish a two-dimensional FE-model of the selected precast prestressed beam-column concrete connection in the FE-program DIANA.

The results of this master's project were to be used as a part of a preliminary research in the experimental testing of a one-third scale sub-assembly specimen.

The project can be divided into 4 major parts:

1. Literature study and evaluation of the precast prestressed joint system and its features. Discussion of the different aspects and alternatives that need to be considered when designing the connection. Presentation of some possible solutions.
2. Preliminary global structural analysis of a frame and identification of important aspects for the detailed design.
3. Evaluation and application of appropriate and applicable constitutive models that reflect the expected behaviours of each material.
4. Applying the model in FE-analyses using the commercial FE-program, DIANA.
5. Verification of the FE-analyses results with analytical results.
6. Discussion and conclusions.

### **2.3 Scope and limitations**

This thesis work should concentrate on the analysis of precast prestressed concrete connections of ductile type for jointed systems in seismic design.

The analyses were to be carried out in the FE-program DIANA, with its implemented features, such as the material models for concrete and steel. Limitations in this

program could affect the relevance of the results of the analysis. The improvement of the material models is, however, outside the scope of this thesis.

The master's project was also limited to the analysis of connections with beams only coming from one direction. It was also assumed that this connection was part of a low-rise building (2 or 3 stories height).

## **2.4 Research approach and methodology**

An extensive research of literature to gather information concerning the subject of the thesis has been carried out mainly through internet. Scientific papers and reports have been provided by supervisors Davide Bolognini, Roberto Nascimbene and Björn Engström.

The main tool of this study has been the all-purpose finite element software DIANA. In addition the following programs were used: structural analysis software SAP, Microsoft Word, Microsoft Excel, Microsoft Equation, Microsoft Power Point, Matlab, Response-2000 and AutoCAD.

Since the researchers had no prior knowledge or experience of the finite element program DIANA, before this study began, it was necessary to become familiar with DIANA. Simple and complex examples concerning modelling of concrete structures were continually carried out during the first two weeks of the study period, whilst at the same time literature studies were made. DIANA's help manuals were constant partners during the learning process.

The next step, after achieving a basic understanding of DIANA, was to study the different types of precast prestressed beam-column concrete connections and to finally make a selection and design of the connection that was going to be analysed further, this was done by means of conceptual analysis and most of all with discussions between the author and the supervisors.

After the selection and design process was finished a study of the different types of elements and material models available in the program was done, subsequently the available models were narrowed to a few specific models that best suited this particular study. Again the DIANA manuals were of great help.

Following the finite element analysis conclusion and when results were in hand an analytical analysis was carried out mainly with the help of Excel sheets and the Matlab program.

## **2.5 Outline of the thesis**

This thesis is divided into 9 parts. The introductory part gives a background to the subjects treated in this thesis. In Chapter 3 the process of selecting the type of connection to be modelled is presented. Chapter 4 and 5 concern the global modelling of the structure and the selection and design of the studied connection.

A detailed description of the FE-analysis and constitutive models that were used is given in Chapter 6. In addition in Chapter 6 the FE-results are presented. Analytical results and comparisons with FE results can be found in Chapter 7.

Next possible improvements and recommendations for design are discussed in Chapter 8. At last in Appendix A the calculations from the analytical analysis are shown.

### 3 Conceptual analysis

In this chapter a list of possible solutions of ductile connections of jointed systems are presented and described. Finally an evaluation of alternatives is carried out in order to select the possible solutions that will be analysed further.

#### 3.1 Possible solutions of ductile connections

##### 3.1.1 Alternative 1

This alternative has been used in Japan and is documented in Nakano et al (2001). Structural members, beams and columns, are precast prestressed components. Structural frames are realized by connecting the beam and the column using prestressing tendons. The frame behaves as fully prestressed structures under design vertical load and under moderate earthquake load, and the connections between beams and columns behave as rigid joints and the joint interface remains in compressive state. Under higher levels of earthquake load the components rotate elastically to prevent damage to beams and columns. Seismic energy dissipation devices, such as damper and damping wall are installed when needed.

Two categories of prestressing tendons are provided, the first is prestressed up to 85% of the nominal yielding load and anchored at the end of the surface of each component. The other is placed trough adjacent components playing the role to connect the beams to the columns, with an effective prestressing force limited to 50% of the nominal yielding load. The shear force in the connection between beams and the columns is transmitted through corbels integrated into the columns. The beam section is rectangular. A detail of a beam-column connection of this type can be seen in Figure 3.1.

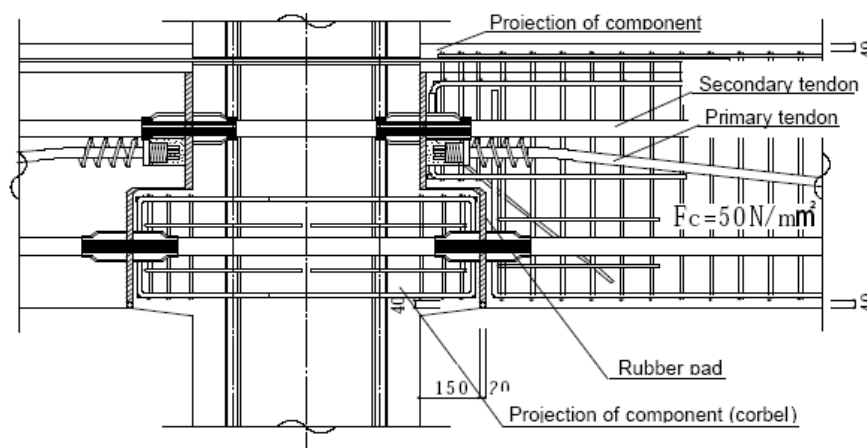


Figure 3.1 Detail of beam-column connection of alternative 1 [Nakano et al (2001)].

### 3.1.2 Alternative 2

This alternative was proposed in a research program in Turkey and is documented in Özdil et al (2002). The beam-column concrete connection has unbonded post-tension cables going through the components and located close to the beam mid-depth. Beams with I-sections are used, see Figure 3.2. This design uses short lengths of post-tensioning tendons.

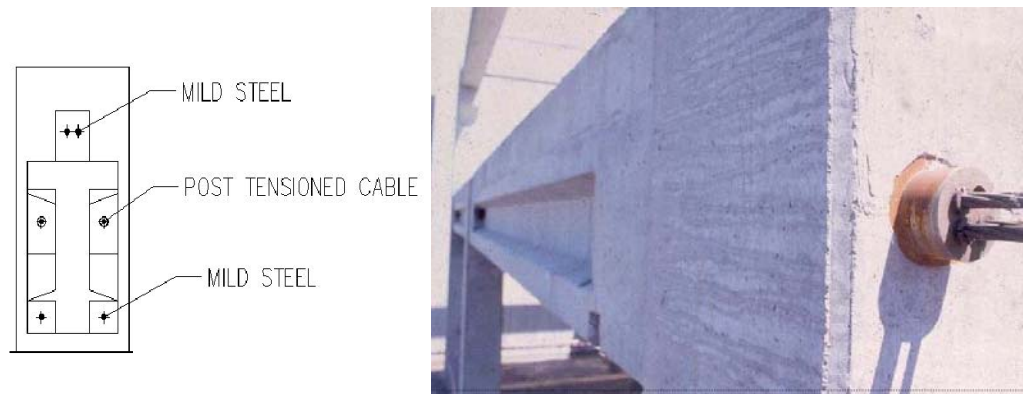


Figure 3.2 Section of beam-column connection of alternative 2 [Özdil et al (2002)].

### 3.1.3 Alternative 3

Alternative 3 is a variation of alternative 2. In this case corbels are added and instead of one layer of postensioning cables there are two. The cables are unbonded in similar lengths at each side of the beam-column interface. This design also uses short lengths of postensioning tendons.

Pretensioning steel could be placed in the beams to increase the flexural strength. Beam cables would be anchored at the end of each beam. A schematic sketch can be seen in Figure 3.3.

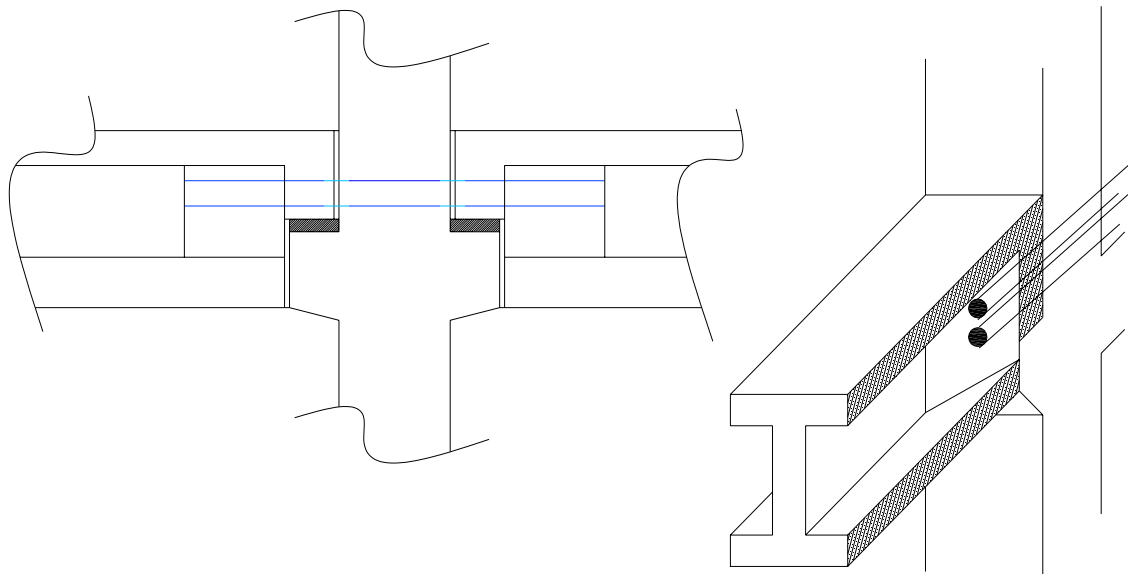


Figure 3.3 Schematic sketch of alternative 3.

### 3.1.4 Alternative 4

This alternative is classified as a hybrid connection. Rectangular beams and columns are connected by unbonded post-tension tendons. Additional flexural capacity and damping are provided with reinforcing bars slid through corrugated ducts in the beams and column, and grouted. There are short unbonded lengths in the beams. A 3D picture of alternative 4 can be seen in Figure 3.4.

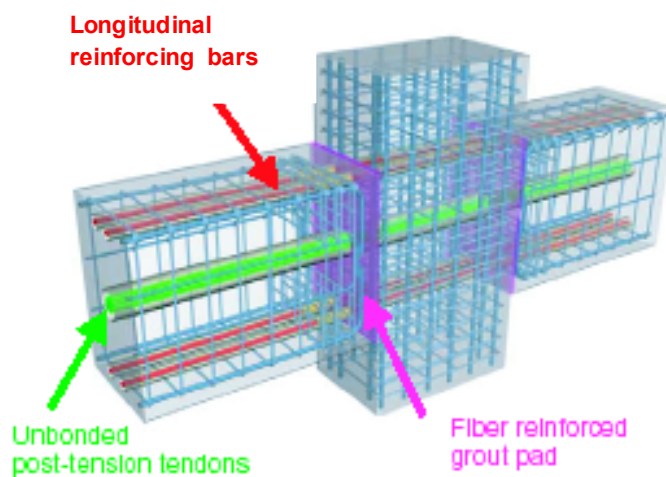


Figure 3.4 3D view of alternative 4, jointed hybrid connection [Pampanin (2003)].

### 3.1.5 Alternative 5

This next alternative consists of continuous rectangular beams with pretensioned strands bonded in external stub beams, but debonded over the interior beam length between the column faces. No additional reinforcing steel is provided across the beam-column interfaces. These full-length pretensioned beams are threaded over column reinforcing bars extending from the top of the columns, with reinforcing bar splices providing column continuity.

This type of connection was proposed in the PRESS program and is documented by Priestley et al (1999). A detail of the connection can be seen in Figure 3.5.

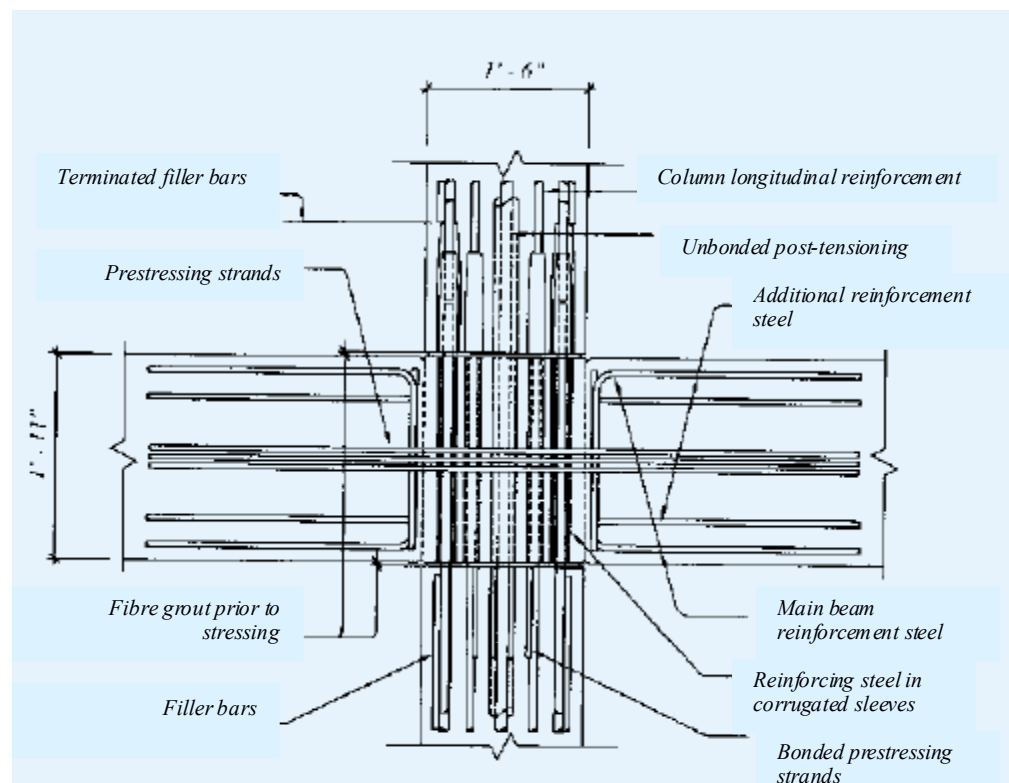


Figure 3.5 Alternative 5, pretensioned connection [modified from Priestley et al (1999)].

### 3.1.6 Alternative 6

This alternative is provided with a TCY-gap (TCY denotes tension/compression yielding), as illustrated in Figure 3.6. At the bottom of the connection, the beams are clamped to the column by unbonded post-tensioned threaded bars reacting through fibre grout pads over the bottom part of the connection only. Over the top two-thirds of the connection, a 25 mm gap is provided.

Reinforcement bars slides through corrugated ducts and is grouted in the beams and column. This type of connection was also proposed in the PRESS program and is documented in Priestley et al (1999).

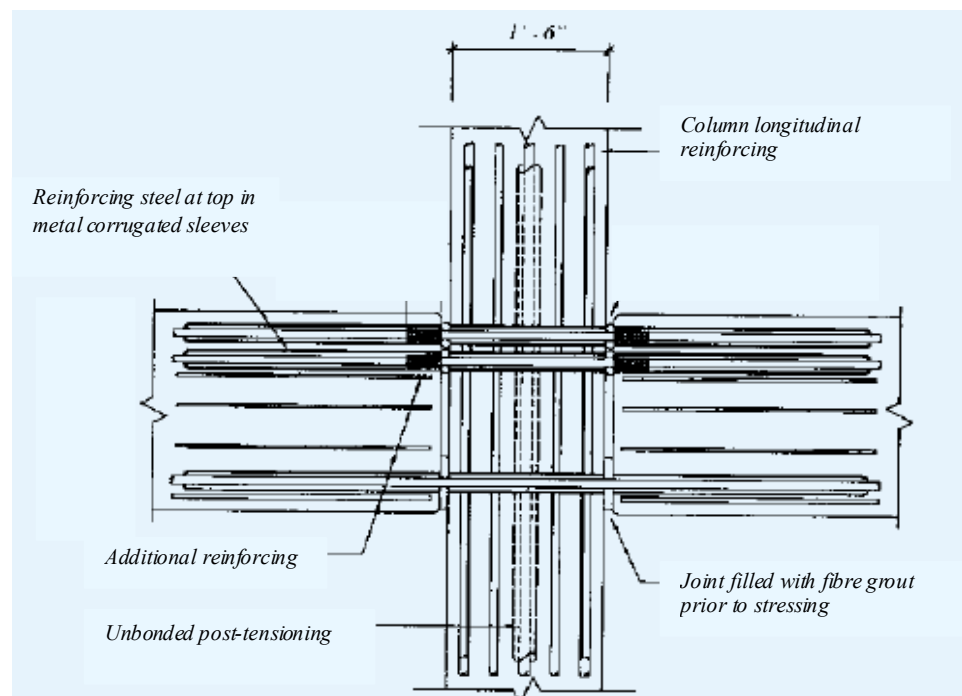


Figure 3.6 Alternative 6, TCY-gap connection [modified from Priestley et al (1999)].

### 3.1.7 Alternative 7

This type of connection was also incorporated in the 39-story Paramount building, see Figure 1.2. It uses a combination of the DYWIDAG Unbonded Multistrand Post-Tensioning System and grouted reinforcing steel to connect the precast beams and the column. Prestressing steel strands are inserted into ducts in the precast beam and anchorages are placed inside the precast columns. Stressing of the tendon is done at the column face.

This type of connection is documented in Englekirk (2002). A detail of the connection can be seen in Figure 3.7.

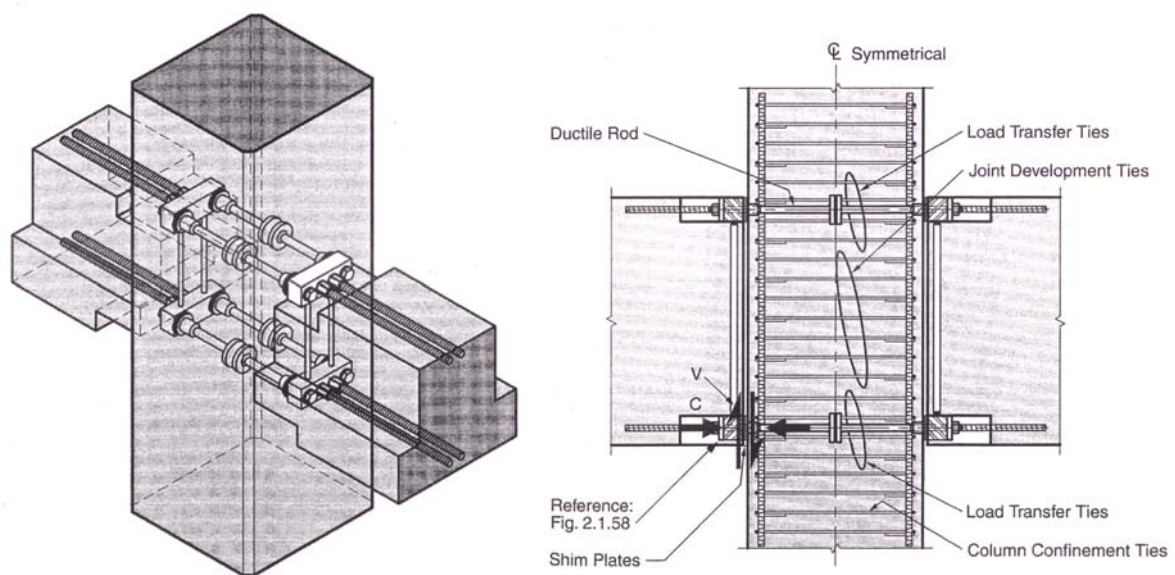


Figure 3.7 Isometric view of the Dywidag Ductile Connector system (DCC) and a view of the shear transfer mechanism.

### 3.1.8 Alternative 8

This alternative uses fully bonded reinforcing steel located in the top and bottom of the beam and fully bonded strands at mid depth of the beam. The reinforcing steel is placed at the outer edges of the beam. This design uses continuous post-tensioning strands that would run through the entire length of the structure.

More details on this connection can be seen in Stone et al (1995). A detail of the connection can be seen in Figure 3.8.

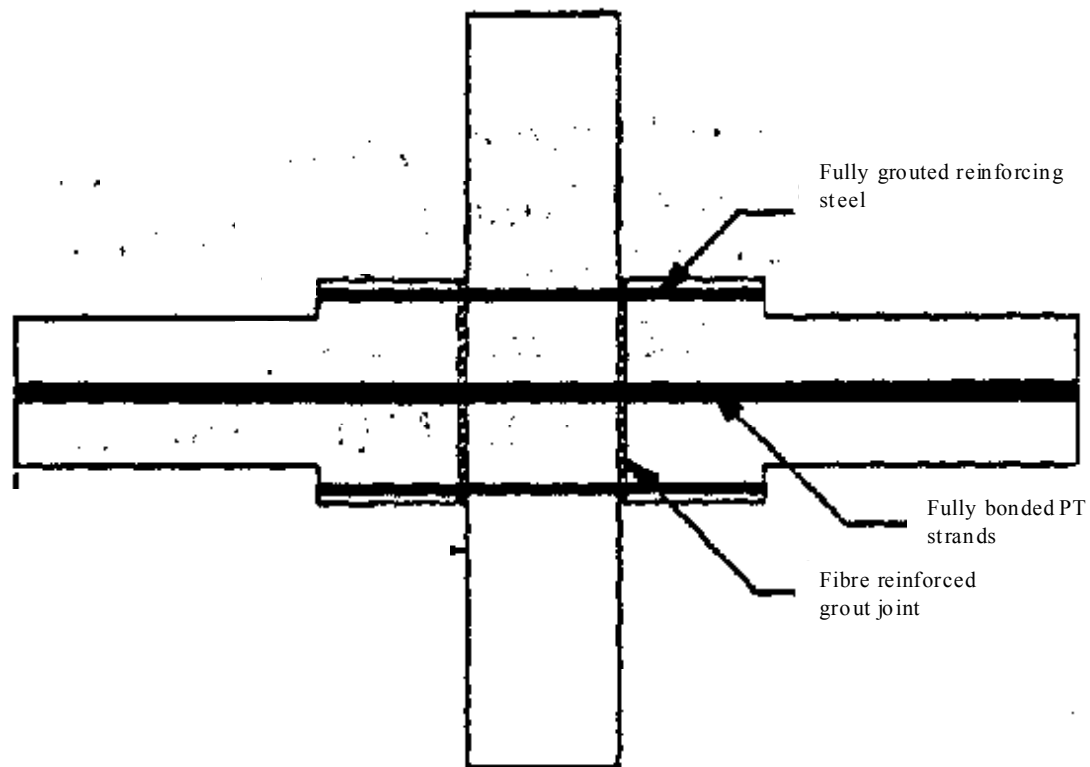


Figure 3.8 Details of alternative 8 connection [modified from Stone et al (1995)].

### 3.1.9 Alternative 9

This connection uses fully bonded reinforcing steel and unbonded post-tensioned steel, both located at the top and the bottom of the beam. This design uses short lengths of post-tensioning steel.

More details on this connection can be seen in Stone et al (1995). A detail of the connection can be seen in Figure 3.9.

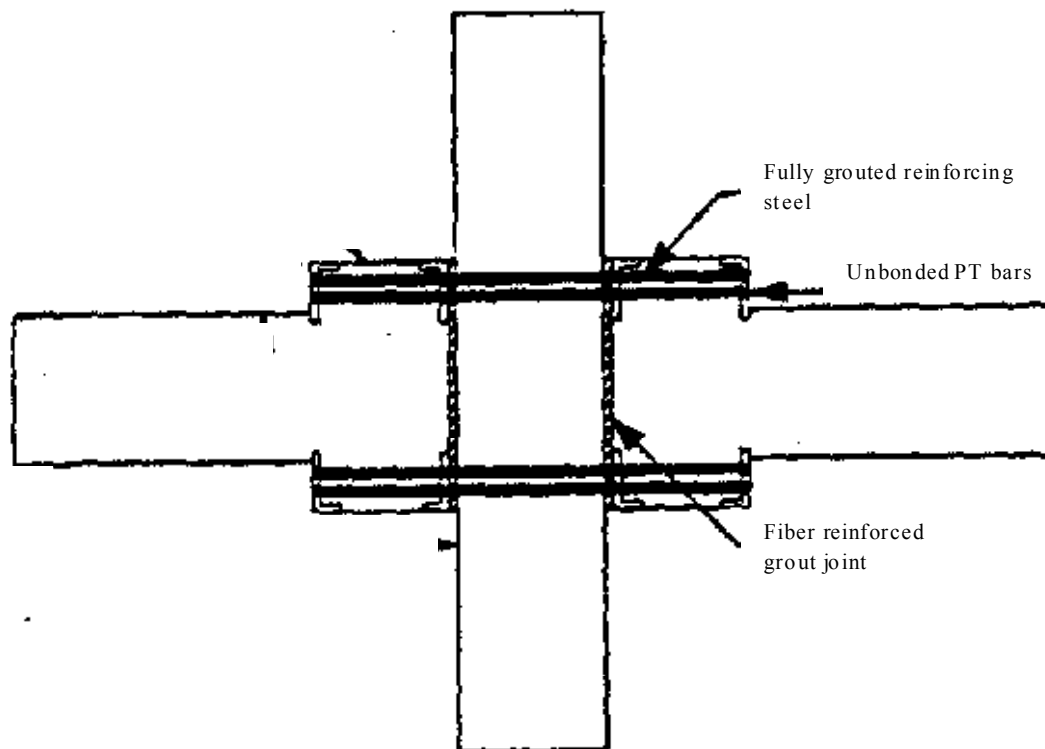


Figure 3.9 Details of alternative 9 connection [modified from Stone et al (1995)].

### 3.1.10 Alternative 10

This last alternative employs replaceable steel and this design also uses unbonded mild steel and post-tensioned steel located at the top and bottom of the beam. This design also uses short lengths of post-tensioning steel.

More details of this connection can be found in Stone et al (1995). A detail of the connection can be seen in Figure 3.10.

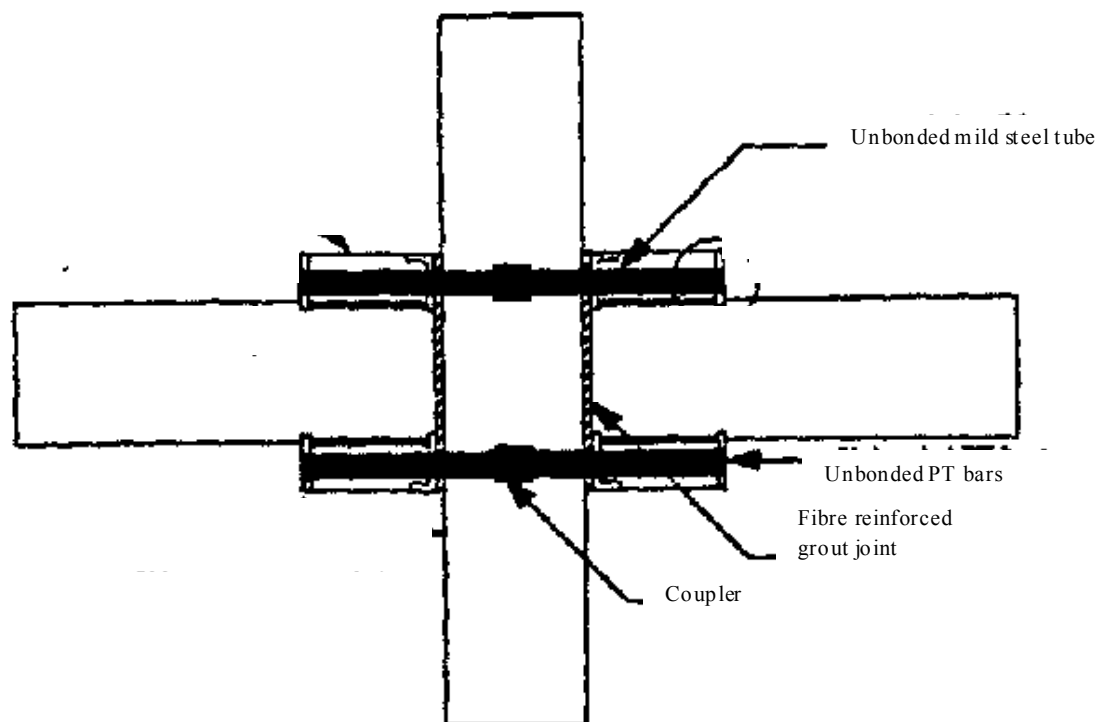


Figure 3.10 Details of alternative 10 connection [modified from Stone et al (1995)].

## 3.2 Evaluation of the connections

This section presents some decisive parameters regarding the design of connections and an evaluation of the connection alternatives presented in the previous section. This analysis results in a grading, from which the best alternative can be selected. Table 4.1 shows the grading system used. A compilation of the evaluation is found in Section 3.3, and conclusions from the analysis in Section 3.4.

*Table 3.1 Grading system used in the evaluation of alternative solutions.*

Grade	Meaning
0	Very Negative
1	Negative
2	Moderate
3	Positive
4	Very Positive

### 3.2.1 Decisive parameters

#### 3.2.1.1 Fabrication

One main advantage of precast structures is the industrialised process of manufacture, therefore the need for effective production methods may limit some of the alternative solutions.

Vertical tendons are much easier and faster to install than parabolic tendons. In addition irregular beam sections are more difficult to cast and to take out of the mould. Some of these alternatives require highly and technically skilful workers; this will represent a problem in some countries and also increased cost. Table 3.2 shows the grading of the alternatives with regard to fabrication.

*Table 3.2 Grading of alternatives regarding fabrication.*

Alternative	1	2	3	4	5	6	7	8	9	10
Grade	3	2	1	2	3	0	1	3	3	2

### 3.2.1.2 Erection

An additional main advantage of precast structures is the opportunity of fast erection. For beam-column connections corbels or direct support on the column element will improve efficiency of construction work and also assure job-site safety.

Connections that do not stipulate a corbel will need temporary supports during the erection. Table 3.3 shows the grading of the alternatives with regard to erection.

Table 3.3 Grading of alternatives regarding erection.

Alternative	1	2	3	4	5	6	7	8	9	10
Grade	4	1	4	0	2	0	0	1	0	1

### 3.2.1.3 Grouting and tensioning

Grouting and tensioning processes could be very difficult and delicate. If some parts of the ducts are not to be grouted, special items are needed, which could make the procedure more expensive and complicated.

The post-tensioning methods in some of these alternative solutions are very complicated. The construction of the Paramount building in San Francisco showed that the hybrid connection (alternative 4) required special techniques for post-tensioning, which will be less economical depending on the country. Table 3.4 shows the grading of the alternatives with regard to grouting and tensioning.

Table 3.4 Grading of alternatives regarding grouting and tensioning.

Alternative	1	2	3	4	5	6	7	8	9	10
Grade	2	4	4	0	4	1	1	1	2	1

### 3.2.1.4 Durability

Structural components that are fabricated in factory using high-grade concrete produced under rigorous quality control assure a higher grade of durability. Moreover components prestressed in factory will have less cracks in concrete. Under high seismic forces joints between components in the connection may open. These openings will try to close if the connections are provided with unbonded post-tensioned tendons. Table 4.5 shows the grading of the alternatives with regard to durability.

Table 3.5 Grading of alternatives regarding durability.

Alternative	1	2	3	4	5	6	7	8	9	10
Grade	4	2	4	3	3	3	4	2	3	3

### 3.2.1.5 Risk of damage and need for repair

It is of main concern for building owners if their buildings are usable or not after earthquakes. Information on possible cost and time for repair works should be a real concern for clients.

Some of the alternatives presented in Section 4.1 have design with this concern in mind. For example, for alternative 1 damage to the structure is restricted only to joint fill and energy dissipation devices. The expected damage could be easily predicted and this means that expense and time required for repair works could be estimated with high accuracy in the design phase. In alternative 7 a special ductile steel rod is placed inside the column that has the ability to react on the seismic load without damaging surrounding concrete. Table 3.6 shows the grading of the alternatives with regard to the risk of damage and need for repair.

Table 3.6 Grading of alternatives regarding risk of damage and need for repair.

Alternative	1	2	3	4	5	6	7	8	9	10
Grade	4	3	4	4	3	1	4	2	2	2

### 3.2.1.6 Tendon length and arrangement

The length of the tendons depends on the prestressing system and tendon arrangement. The tendons are placed in a parabolic shape or straight in these alternatives. Some of the alternatives presented are less economical with regard to the use of tendons and lengths. Alternatives 6 and 7 have no drawbacks in this respect. Table 3.7 shows the grading of the alternatives with regard to tendon length and arrangement.

Table 3.7 Grading of alternatives regarding tendon length and arrangement.

Alternative	1	2	3	4	5	6	7	8	9	10
Grade	1	4	4	2	2	4	4	2	3	4

### 3.2.1.7 Unbonding and self-centring capacities

The adoption of unbonded post-tensioned tendons gives to these connections high efficiency with a self-centring capability, which means that upon unloading from a large nonlinear rotation, the beam returns towards its original position with little permanent residual rotation. The self-centring capability means that the non-linear rotation occurs with little damage to the beam and that the prestressing force is sufficient to close the gaps upon unloading.

Unbonding of the post-tensioning steel also delays the non-linear straining (i.e. yielding) of the steel. The property that characterises alternative 5 is the self-centring ability. Table 3.8 shows the grading of the alternatives with regard to unbonding and self-centring capacities.

Table 3.8 Grading of alternatives regarding unbonding and self-centring capacities.

Alternative	1	2	3	4	5	6	7	8	9	10
Grade	4	3	3	4	4	1	3	1	3	2

### 3.2.1.8 Energy absorbing capacity

Seismic energy absorbing capacity of prestressed concrete structures is often considered to be less than that of reinforced concrete structures and steel structures. For the purpose to improve that situation, some of the alternatives are allowed to deform under severe earthquakes. The hybrid system (alternative 4) incorporates energy-absorbing capacity through the use of the ductile reinforcing steel. In alternative 1 energy dissipation devices are incorporated when needed.

For alternative 6 the TYC connection provides a high energy absorbing capacity. Table 3.9 shows the grading of the alternatives with regard to energy absorbing capacity.

Table 3.9 Grading of alternatives regarding energy absorbing capacities.

Alternative	1	2	3	4	5	6	7	8	9	10
Grade	3	2	2	3	1	4	3	2	2	2

### 3.3 Comparison

The results from the grading with regard to different decisive factors are compiled in Table 3.11. The comparison has been a way of gathering information about the different alternatives. The grading system also indicates the most promising alternatives to model and study further.

Table 3.11 Gathering of grades for the decisive factors.

<b>Alternative</b> <b>Factor</b>	<b>1</b>	<b>3</b>	<b>2</b>	<b>5</b>	<b>4</b>	<b>7</b>	<b>9</b>	<b>10</b>	<b>6</b>
<b>Fabrication</b>	3	1	2	3	2	1	3	2	0
<b>Erection</b>	4	4	1	2	1	0	0	1	0
<b>Grouting and tensioning</b>	2	4	4	3	1	1	2	1	1
<b>Durability</b>	4	3	2	3	3	4	3	3	3
<b>Risk of damage and need for repair</b>	4	3	3	3	4	4	2	2	1
<b>Tendon length and arrangement</b>	1	4	4	2	2	4	3	4	4
<b>Unbonding and self-centring capacities</b>	4	3	3	4	4	3	3	2	1
<b>Energy absorbing capacity</b>	3	2	2	1	3	3	2	2	4
<b>Total</b>	<b>25</b>	<b>24</b>	<b>21</b>	<b>21</b>	<b>20</b>	<b>20</b>	<b>18</b>	<b>17</b>	<b>14</b>

### 3.4 Conclusion

The different connection alternatives have been compared with regard to various different decisive parameters. The results from this comparison can be seen in Section 3.3.

In the bottom line of Table 3.11 the overall result can be observed, alternatives with best score are presented first. This result underlies the choice of the alternative that is investigated further, though it was not totally determining. Some of the properties weighted in this analysis are more valuable than others; this had some effect in the

final decision. For example, fabrication is an issue probably of higher importance than most of the other properties for this specific project.

The alternative 1 is the one with highest grade and it was selected for further analysis. This alternative has been used before in Japan and presents a promising design that could be tested and later implemented in Italy. The merits of this alternative are that it has a high grade of durability, uses common materials, enables rational construction methods to the industry and is easy to erect. Furthermore it has an acceptable energy absorbing capacity, negligibly small residual drift and the beam has a very high strength. Its primary weakness lies in a complicated detailed design of the beams end, but this could be modified in our own design.

Another promising alternative is alternative 3, but this alternative will probably require a three dimensional solid FEM model due to the complicated geometry in the beams end; for this it was discarded in this study. The hybrid connection, alternative 4, is also very attractive, but the fact that this type of connection requires advanced technical methods of construction made it less interesting for countries like Italy.

## 4 Preliminary Structural Analysis

In order to obtain information for a preliminary design of the selected type of the beam-column connection a global analysis of a monolithic frame was done with the software SAP2000 (see Figure 3.1). This chapter presents the structural model and the result of the global structural analysis.

The analysis was carried out twice (attempt 1 and attempt 2), and each attempt has two different load direction cases (direction used to carry the load in the slabs), see Figure 3.2 and 3.3.

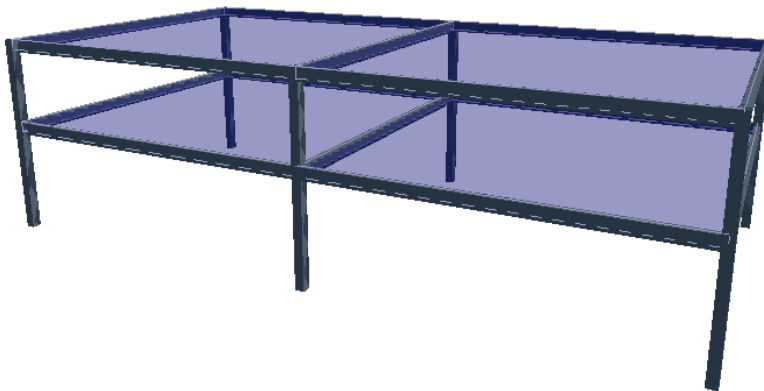


*Figure 3.1 3D view of the frame model used for the global structural analysis.*

### 4.1 Frame model

The characteristics of the frame were assumed according to the following:

- A 2 story 2 bay frame system.
- Each bay is 12,00 m long in both directions.
- Story height of the first floor is 4,00 m and for the second floor 3,00 m.
- The section of the columns is 320x320 mm, in a second analysis, if needed, the section would be increased to 450x450 mm.
- The section of the beams is 420 mm in height x 230 mm in width.
- In the first floor loads from infill panels are taken into account, see Table 3.2.

- In a first attempt the floor is assumed to be composed of hollow core elements of  $h = 0,36$  m and  $b = 1,20$  m. In the second attempt  $h = 0,30$  m was used. As mentioned previously two cases of load directions are studied. In case 1 the loads from the hollow core slabs are carried in the x-direction and in case 2 loads from the hollow core slab are carried in the y-direction, see Figure 3.2 and 3.3.

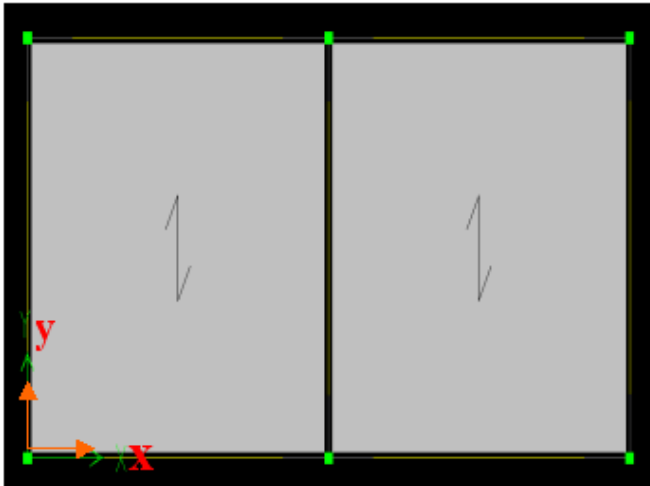


Figure 3.2 Case 1 regarding the bearing direction of hollow core elements.

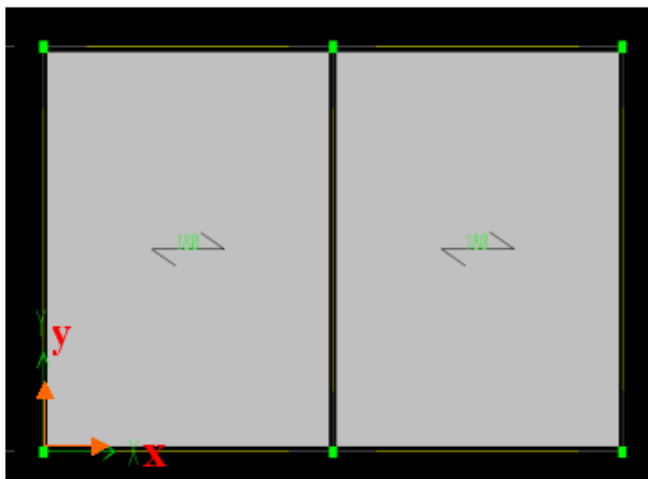


Figure 3.3 Case 2 regarding the bearing direction of hollow core elements.

- Since the objective of the investigation was to simulate the real structural behaviour, material parameters are represented by their mean values instead of the design values, see Table 3.1.
- Dead and snow loads are considered as well as live loads for small storage buildings according to the EC1, see Table 3.2. Wind loads are not considered.

Table 3.1 Assumed material properties for the reinforced concrete.

Unit	$f_{cm}$ [MPa]	$f_{ym}$ [MPa]	$E_c$ [GPa]	$\nu$	$\rho$ [kg/m <sup>3</sup> ]
Column	53,9	-	40,3	0,2	2 500
Beam	59,3	-	42,3	0,2	2 500
Reinf. steel	-	550	-	-	-

Table 3.2 Considered loads of the frame model used for the global structural analysis.

	Dead weight [kN/m <sup>2</sup> ]		Dead loads [kN/m <sup>2</sup> ]			Live loads [kN/m <sup>2</sup> ]		
	Attempt 1	Attempt 2		Attempt 1	Attempt 2		Attempt 1	Attempt 2
Infill panels	3,5	3,5	First floor	3	2,5	First floor	5	1,5
Hollow core elements	4,7	4,1	Roof	1	1	Roof (snow)	1,5	1,3

- Horizontal and vertical response spectra were assumed for the seismic loads according to EC8 as seen in Figure 3.4 and 3.5. A built in spectrum available in the program was also used for verification. Soil type C and a peak ground acceleration  $a_g = 0,35$  was selected. Behaviour factor for precast structures was also defined.

### Vertical Elastic Response Spectrum

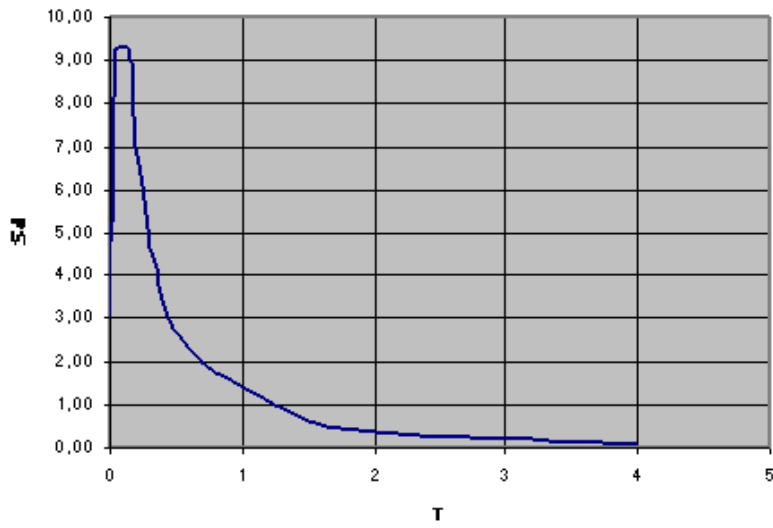


Figure 3.4 Vertical response spectra defined according to EC8.

### Horizontal Elastic Response Spectrum

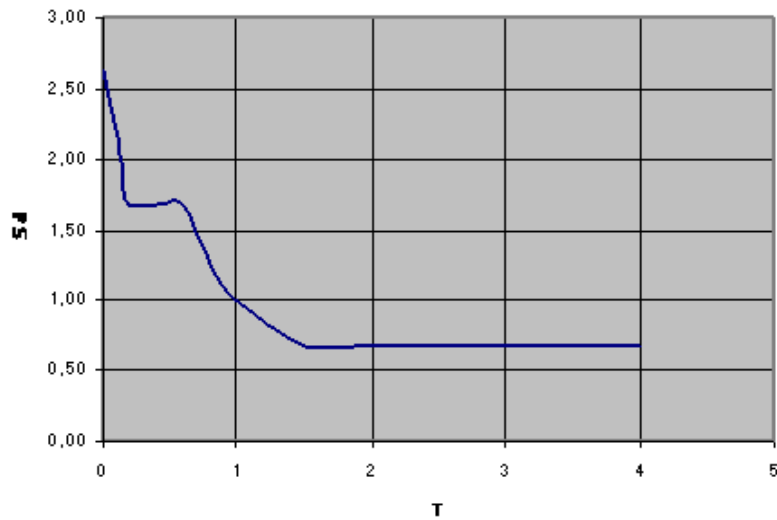


Figure 3.5 Horizontal response spectra defined according to EC8.

## 4.2 Results

In the first run the sectional forces turned out to be very high and the column not strong enough. In a second attempt the section of the column was increased, the thickness of the hollow core sections was diminished and the live and snow loads were also reduced, see Table 3.2.

Moment and shear force diagrams of an exterior frame that resulted from the second attempt are shown in Figure 3.4 for case 1 and Figure 3.5 for case 2. In Figure 3.5 the shady regions represent the superposition of maximum moment force diagrams for different load cases.

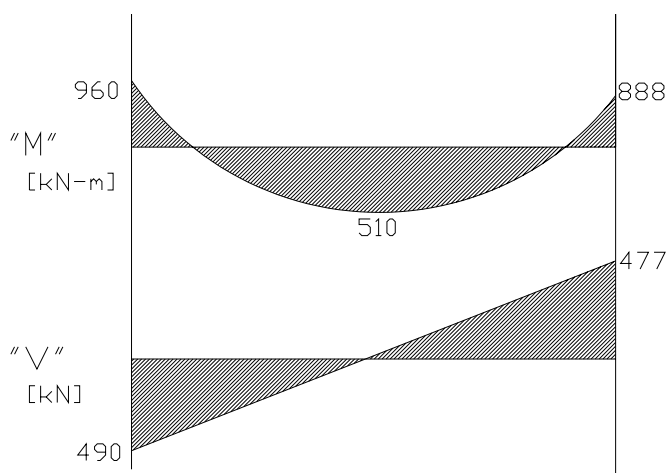


Figure 3.5 Moment and shear diagram for attempt 2, case 1.

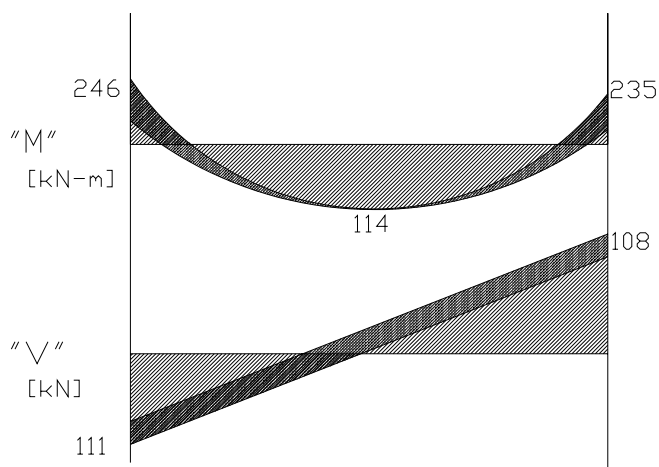


Figure 3.6 Moment and shear diagram for attempt 2, case 2.

The program also includes concrete frame design calculations according to EC2. This was used for the design and check of the column. The results for the reinforcement in the column were:

- Case 1:
  - Longitudinal reinforcement =  $4500 \text{ mm}^2$  (2,22%)
  - Shear reinforcement. =  $25 \text{ mm}^2$
- Case 2:
  - Longitudinal reinforcement =  $6400 \text{ mm}^2$  (3.16%)
  - Shear reinforcement =  $25 \text{ mm}^2$

## 5 Detailed Design and Final Geometry

The spans, storey height, beam and column sections and type of connection were already selected as presented in the previous chapters. This chapter concerns with the detailed design of the connection.

Currently there is no design procedure generally accepted for the design of this type of connections. In existing building codes seismic resistant reinforced concrete systems have, in general, been limited to cast-in-place walls and special moment resisting frames. While these two systems have shown to perform well during earthquakes, implementation of corresponding detailing rules into prefabricated structures is difficult. Therefore the guidelines used in this chapter, to develop the final detail and geometry of the connection, are taken from experimental reports and scientific papers.

### 5.1 Design concept

The specific design concept of the chosen structure can be summarized as follow:

- A ductile behaviour is realized by a weak ductile link at the beam-column interface. Yielding is localized to this interface with minimal damage to the precast beams.
- Prestressing tendons are classified into primary tendons and secondary tendons, the first are anchored at the end of the surface of each component and their role is to prevent cracking of the components, i.e. beams or/and columns. The secondary tendons are placed trough the connection and they play the role to connect beams and columns and provide self-centring capacity.
- The secondary tendons are post-tensioned and give reliable clamping force at the beam-column interface to resist vertical loads. At the required maximum drift, the secondary tendons remain elastic. Sufficient unbonded length of the secondary tendons should be provided.
- Vertical shear forces in the connection between the beams and the column are transmitted through corbels integrated into columns, friction created by the clamping force provided by the secondary tendons and friction created by the compressive resultant of the force couple induced by bending moment at the beam-column interface.
- Compression regions of the beam must be able to sustain large strains without degradation of its compressive resistance.
- The concrete in the end regions of the beam is confined so that it will not spall at the required maximum drift.

- The corbels also constitute a backup collapse prevention mechanism; in the unlikely event of secondary tendon failure or anchorage failure, the corbels will resist the vertical loads of the beams.

## **5.2 Sectional response**

In a prestressed member, prior to decompression, the section will behave in a manner comparable to an uncracked reinforced concrete section. The sectional properties for this state can be determined based on the gross concrete section. For the interval between decompression and yielding, the section properties are between that of an uncracked section and that of a cracked reinforced concrete section.

Under moderate earthquake load the beam-column connection behaves as a rigid unit and the interfaces between the structural members remain in the compressive state. Under strong earthquake load the beams rotate elastically to prevent damage to beams and columns.

## **5.3 Maximum prestress**

### **5.3.1 Steel stresses in secondary tendons**

The maximum stress in the tendons must be limited to ensure that no yielding of the tendons occurs at the maximum drift assumed in design. Yielding of the secondary tendons must prevent loss of the clamping force during load reversals. Limiting the initial prestress allows for greater strain capacity in the secondary tendons to accommodate the large story drift demands expected in a major earthquake.

The tendon's initial stress should not exceed 50% of the nominal yield strength, and the maximum stress should not exceed 80% of the nominal yield strength in order to avoid yielding under a severe earthquake.

### **5.3.2 Concrete stresses**

The maximum limit on the concrete compressive stress is determined by the concrete strength and by the provided confinement in the compression zones.

## **5.4 Energy dissipation**

Currently required in codes, the energy absorption capacity of new moment resisting systems should be equivalent to that of a corresponding conventional cast-in-place system. However, studies [Priestley (1993)] have shown that at high drift levels, the benefit of additional energy dissipation is unclear and that the system performance at high drift levels may be more dependent on the input ground motion than on the energy dissipation capacity. Therefore, while some energy dissipation is necessary for

displacement control, the drift capacity is considered to be a more appropriate performance requirement.

## **5.5 Detailing requirements**

### **5.5.1 Beam and column design**

The design shear capacity should be greater than the applied shear force. In addition the beam should be designed so that it can resist the design load acting as a simply supported beam.

### **5.5.2 Slab interaction**

It is important to prevent the slab from contributing to the connection strength and to prevent slab rotation to occur at the beam-ends. Measures may need to be taken to permit slab rotation adjacent to the beam-column joint and significant slab damage should be prevented during a maximum credible earthquake.

### **5.5.3 Protection of post-tensioned steel**

Measures should be taken to prevent corrosion of the post-tensioning steel. Over the ungrouted length, corrosion-inhibiting products are needed, while the bonded length can be protected by chloride free cementitious grout.

### **5.5.4 Concrete confinement**

The concentrated rotation, which occurs at the connection, induces large concrete strains in the extreme fibres of the beam. In order to retain the member integrity and minimize damage to unconfined concrete cover, the concrete must be confined. Steel angles could be used in the corners of the beam-ends at the beam-column interface, as well as close ties, which will increase the confinement of the concrete in a region that experiences large compressive strains.

### **5.5.5 Ties through weak planes**

Potential planes of shear cracking, usually where the cross section changes, should be identified. Shear reinforcement in the form of closed ties should be used across these crack planes.

### 5.5.6 Position of secondary tendons

The distance between the upper and lower tendons should be between  $0,35h$  and  $0,55h$  where  $h$  is the overall beam depth, in order to avoid yielding under a severe earthquake.

In addition the distance between the centroid of the beam section and the upper or lower tendon should be held within  $3/8$  of the overall beam depth.

## 5.6 Final geometry and design

The selected material properties for the design are the following (later on some of these values are used in the FE-analysis):

- Reinforcing steel:

Design values:  $f_{yd} = 374$  MPa,  $E_s = 200$  GPa (see Figure 5.2).

Mean values:  $f_{ym} = 550$  MPa,  $E_s = 200$  GPa (see Figure 5.3).

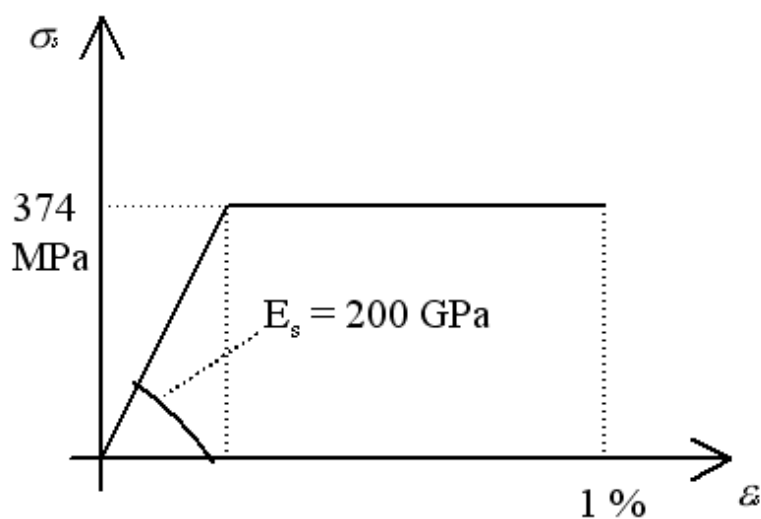


Figure 5.2 Design stress strain relation for reinforcing steel.

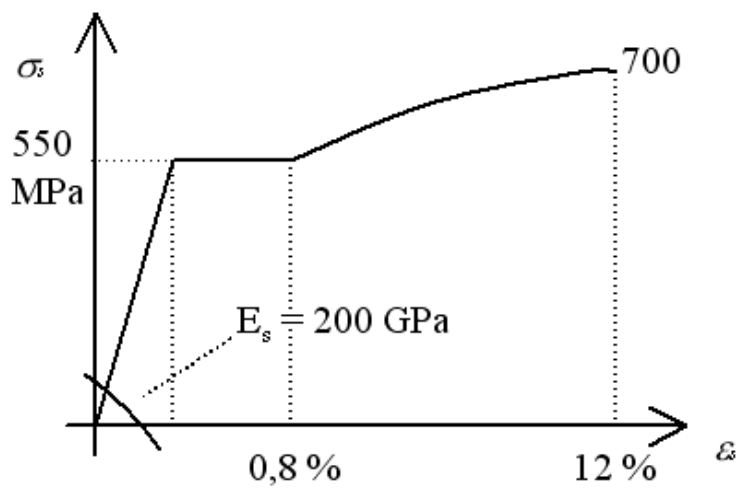


Figure 5.3 Mean stress strain relation for reinforcing steel.

- Prestressing steel:

Design values:  $f_{pd} = 1860$  MPa,  $E_p = 200$  GPa (see Figure 5.4).

Mean values:  $f_{pm} = 2000$  MPa,  $E_p = 200$  GPa (see Figure 5.4).

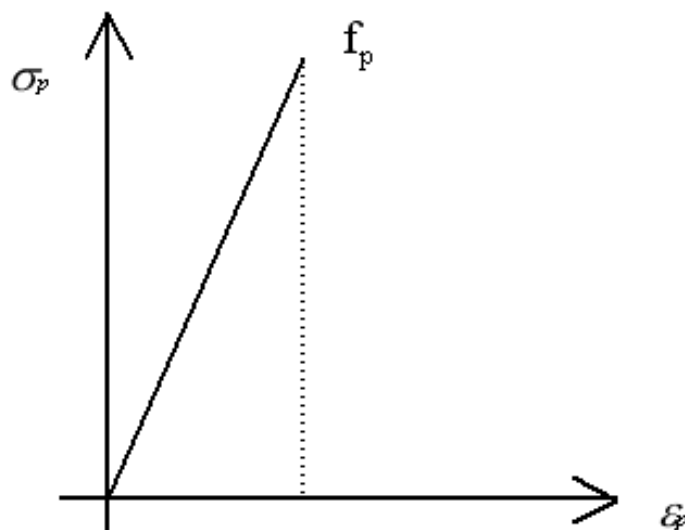


Figure 5.4 Assumed stress-strain diagram for prestressing steel.

- Concrete

Design values for columns:  $f_{cd} = 25,9$  MPa,  $E_{cm} = 40,3$  GPa (see Figure 5.5).

Mean values for columns:  $f_{cm} = 53,9$  MPa,  $E_{cm} = 40,3$  GPa (see Figure 5.5).

Design values for beams and mortar:  $f_{cd} = 28,5$  MPa,  $E_{cm} = 42,3$  GPa.

Mean values for beams and mortar:  $f_{cm} = 59,3$  MPa,  $E_{cm} = 42,3$  GPa.

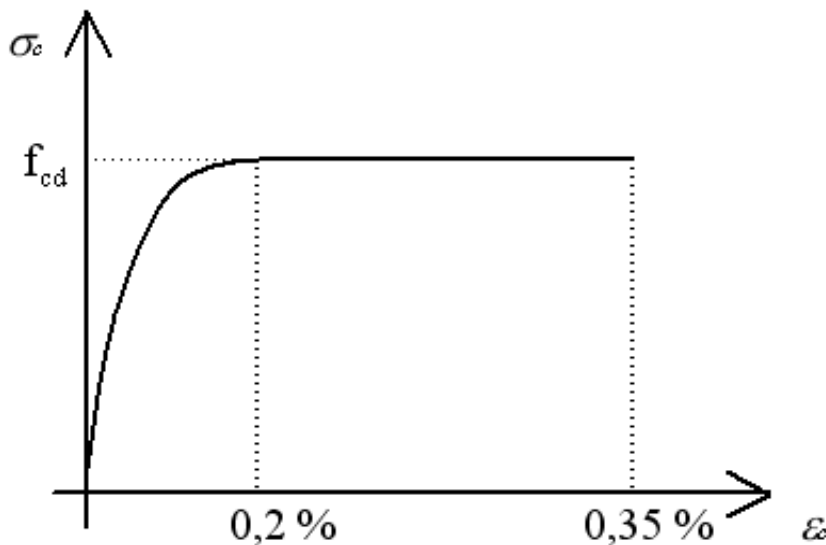


Figure 5.5 Stress-strain diagram for concrete in compression.

The final geometry of the connection can be seen in Figure 5.6. The beam-ends are supported by corbels and connected to the joint by secondary tendons. The beams have a length of 5775 mm from the face of the column to the mid section of the beam. The column has a height of 3500 mm. The beams and the column are reinforced with longitudinal and transverse reinforcement. The beams are also provided with primary tendons. The prestress in the primary tendons is limited to 75% of the nominal yield strength and for the secondary tendons the prestress is limited to 50% of the nominal yield strength. Mortar is placed in the vertical joints and a rubber pad is placed on the upper surface of the corbel. The secondary tendons are unbonded 50 mm before and after the interface with the column. The column section is 450 x 450 mm, the column reinforcement can be seen in Figure 5.6.

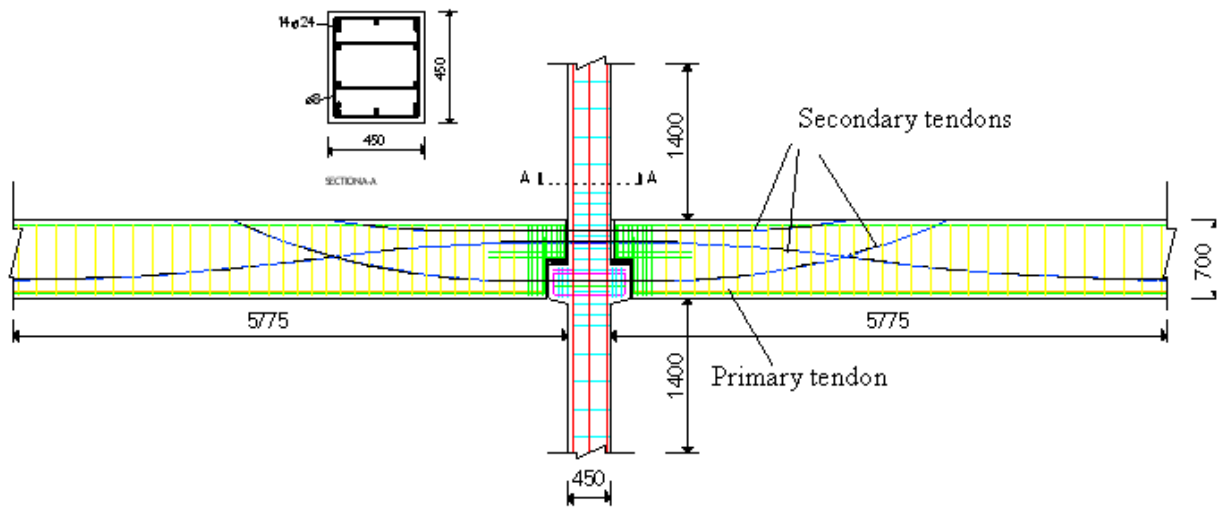


Figure 5.6 Design of the connection.

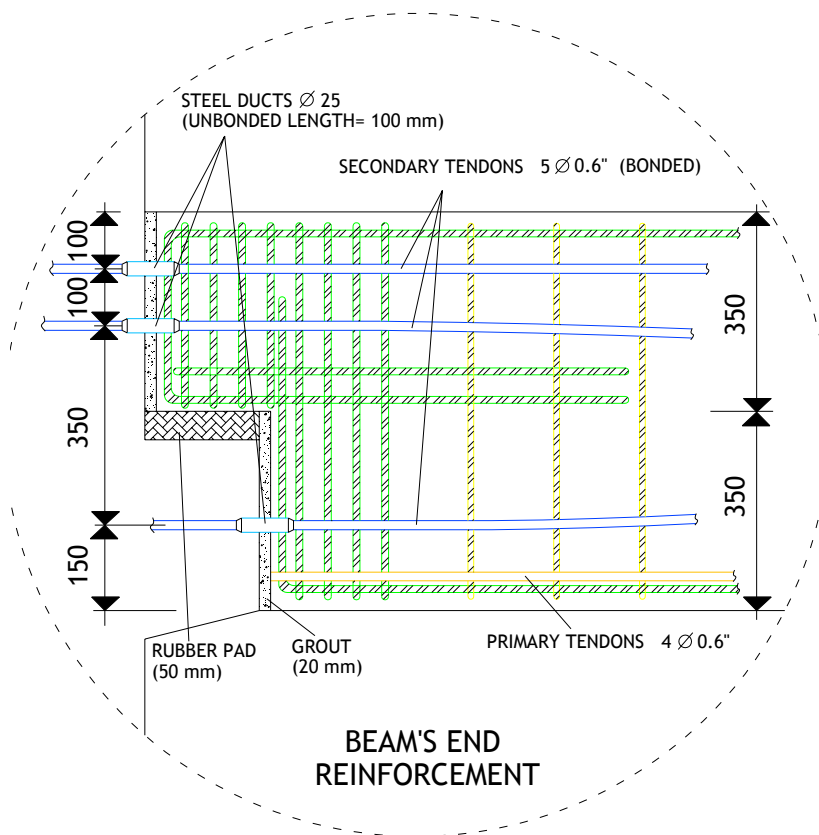


Figure 5.7 Description of the beam's end reinforcement.

The details of the beam's end reinforcement are shown in Figure 5.7. The beam section is 400 mm in width x 700 mm in depth. All the longitudinal reinforcing steel in the beams has 12 mm diameter. The vertical stirrups in the beam end have 12 mm diameter and a spacing of 50 mm. The stirrups away from the interface have 10 mm diameter and a spacing of 150 mm. The longitudinal reinforcing steel in the beam is looped with an angle in the beam end; this also helps to confine the concrete.

The corbel reinforcement is shown in Figure 5.8. The corbel section is 400 x 300 mm. This design should allow the beam to rotate without damage to highly strained regions.

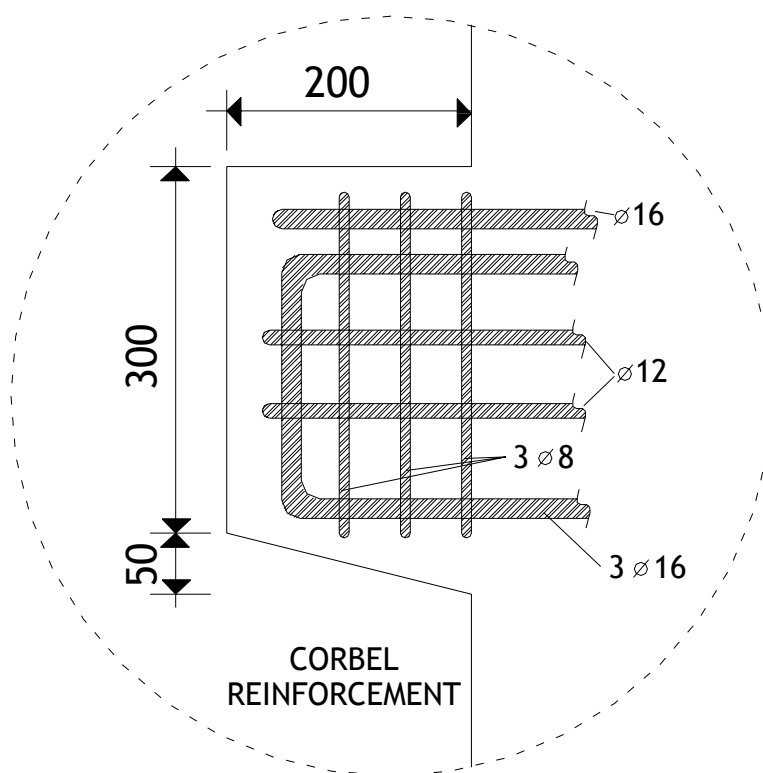


Figure 5.8 Detail of the corbel reinforcement.

## 6 Finite Element Analysis

In this study, the FEM analytical computer program DIANA V9 was used. DIANA is based on the displacement method and is aimed for modelling concrete structures due to the wide range of concrete material models and advanced numerical tools provided in the program. The non-linear mechanisms that were considered in the modelling are cracking and crushing of the concrete and yielding of the prestressing and the reinforcing steel. The finite element models were two-dimensional consisting of plane stress elements.

Since the objective of the investigation was to simulate structural behaviour in a realistic way, material parameters were taken by their mean values instead of the characteristic or design values.

This chapter describes the material models that were used in the analysis, the development of the finite element model, and finally the results.

The numerical models for the development of the finite element model are established in an iterative manner. Numerous parameters are thoroughly investigated until an estimate for the parameter can be identified. The confirmation of the parameters is an ongoing process, which begins at the individual material models and continues into the global analysis. Therefore several models with different parameters are analysed before the determination of the final one.

### 6.1 Material constitutive models

#### 6.1.1 Concrete

The behaviour of the concrete was modelled with the total strain based constitutive model. This constitutive model in DIANA is based along the lines of the modified compression field theory, which was developed by Vecchio and Collins (1986).

The original total strain model in DIANA relies on the approximation of the stress as a function of the strain, also for stress levels exceeding the elastic limit, that is, after the onset of cracking or crushing.

The principle is known as the coaxial stress-strain concept, which implies that crack-planes under non-proportional loading conditions will not remain in a fixed position. Therefore, the total strain model in DIANA is frequently also known as the rotating crack model.

The benefit of the coaxial stress-strain concept is that the constitutive modelling needs to be handled in the principal directions of the strain vector only. In an incremental/iterative FEM-procedure, this means that the strain tensor is always transformed to the principal directions before the material description is entered and the belonging principal stresses are determined.

Although the coaxial model operates in the principal stress-strain space, the mechanical behaviour in the principal directions is not independent. Hence, compressive strength is reduced by lateral cracking and increased by lateral confinement. The total strain model accounts for these effects, either according to design code regulations or by user specifications.

In cracked concrete the principal compressive stress is a function not only of the principal compressive strain,  $\varepsilon_2$ , but also of the coexisting principal tensile strain,  $\varepsilon_1$ . If the concrete is cracked in the lateral direction, the compressive stresses are reduced.

The reduction is introduced through reducing the peak stress value according to equation (6.1) [Vecchio and Collins (1993)]. It is assumed that the stress-strain curve is fully determined with its peak stress value and the corresponding strain value for a given base curve.

$$f_{2,\max} = f_c \cdot \frac{1}{(1 + K_c)} \geq f_c \quad (6.1)$$

and

$$K_c = 0.27 \cdot \frac{-\varepsilon_1}{(\varepsilon_{c0} - 0.37)} \quad (6.2)$$

$f_{2,\max}$  = Peak stress value in compression in cracked concrete,

$f_c$  = Uniaxial compressive strength,

$\varepsilon_{c0}$  = Compressive strain at maximum compressive stress (may be taken as -0.002).

As a base curve in compression, the parabolic curve shown in Figure 6.1 was chosen. The parabolic curve in DIANA is based on the fracture energy, according to Feenstra (1993). The compressive fracture energy in the present analysis is estimated from equation (6.3) [Lertsrisakulrat et al (1999)].

$$G_c = 3.0 \cdot f_c \quad (6.3)$$

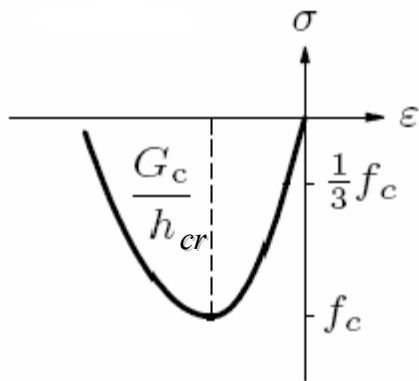


Figure 6.1 Parabolic stress-strain relation for concrete in compression.

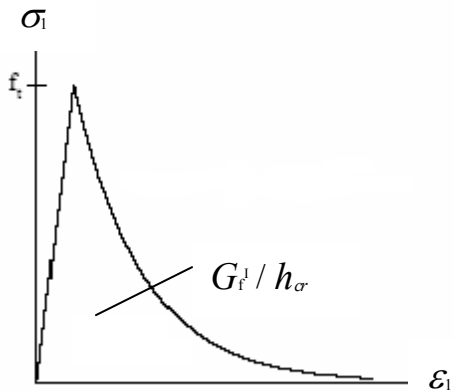


Figure 6.2 Exponential softening curve for concrete in tension.

The stress-strain diagram in tension was defined with a linear part until the tensile strength and an exponential softening branch, see Figure 6.2. The softening curve is determined from the tensile strength  $f_t$ , the mode-I fracture energy,  $G_f^I$  and the numerical crack bandwidth,  $h_{cr}$ . The numerical crack bandwidth is related to the dimensions of the finite element. For higher order two-dimensional elements, DIANA estimates its value as the square root of the element area, but in the case that embedded reinforcement is used the later is not valid and the crack bandwidth has to be calculated. The fracture energy in the present analysis was estimated from the CEB-FIP Model Code 1990 (CEB-FIP 1991) formula:

$$G_f^I = \alpha_F \cdot \left( \frac{f_{cm}}{10} \right)^{0.7} \quad (6.4)$$

where,

$\alpha_F$  = Coefficient, which depends on the maximum aggregate size,  $d_{\max}$

$f_{cm}$  = Mean cylinder strength in MPa.

### 6.1.2 Steel bars and tendons

A bilinear diagram defined the stress-strain relationship for the prestressing steel. A multilinear diagram that consisted of an elastic part, a yield part and a part with hardening defined the stress-strain relationship for the ordinary reinforcement.

For the reinforcement, an elastic-plastic model was used both in tension and compression, with Von Mises yield criterion.

Von Mises yield criterion states that yielding depends on the maximum and minimum principal stresses, plus the intermediate principal stress. Yielding occurs in Von Mises when a deviatoric part of the stress reaches a critical value in the principal stress space. The Von Mises yield criterion is commonly expressed as

$$\Phi = \frac{1}{2} \cdot [(\sigma_1 - \sigma_2)^2 + (\sigma_2 - \sigma_3)^2 + (\sigma_3 - \sigma_1)^2] - f_y^2 \quad (6.5)$$

where,

$\sigma_1$ ,  $\sigma_2$  and  $\sigma_3$  are the principal stresses

$f_y$  = yield strength.

Note that hardening is not included in this yield function. Since Von Mises yield criterion is independent of both the angle in the deviatoric plane and of the hydrostatic stress, the yield surface forms a circular cylindrical prism around the hydrostatic axis in the principal stress plane. Yielding of metals can normally be assumed to be independent of the hydrostatic stress and can thus be modelled with Von Mises.

### 6.1.3 Mortar and rubber pad

The rubber pad was modelled with a linear elastic stress-strain relation with a Poisson's ratio close to 0.5. For the mortar a total strain model was used, similar to the one for concrete.

## 6.2 Finite element model

In order to create an effective finite element model it is of great importance to take into account certain measures, such as minimising the number of elements and making appropriate simplifications. It is also essential to find a proper solution method by means of incrementation procedures, iteration methods and convergence criteria

When setting up the model, it is suitable and logical to build the model in a stepwise manner with the last steps being the non-linear parameters. The creation of the model should be an iterative procedure where important characteristics are gradually identified and obtained. An illustration of the steps involved in creating this finite element model is presented in Figure 6.3.

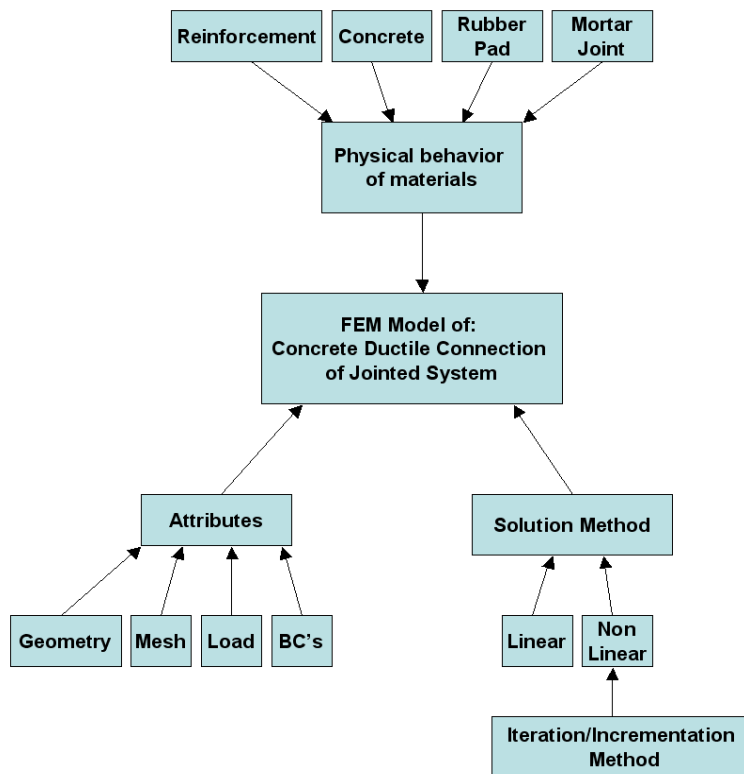


Figure 6.3 Flow chart illustrating the steps involved in creating a numerical model.

The present chapter will describe how the model was built. Properties of the model will also be presented.

## 6.2.1 Geometry

In order to better simulate the experimental specimen, a 1/3 scale was used for the entire model; additionally a 2D model was preferred. The creation of the geometry in DIANA is very simple; one way of doing it is by entering the coordinates to create points and later create lines to connect the points. Another way is creating the geometry in a CAD program and then import it into DIANA, but this could create problems later on when assigning properties to the geometry. A picture of the geometry layout in DIANA can be seen in Figure 6.4.

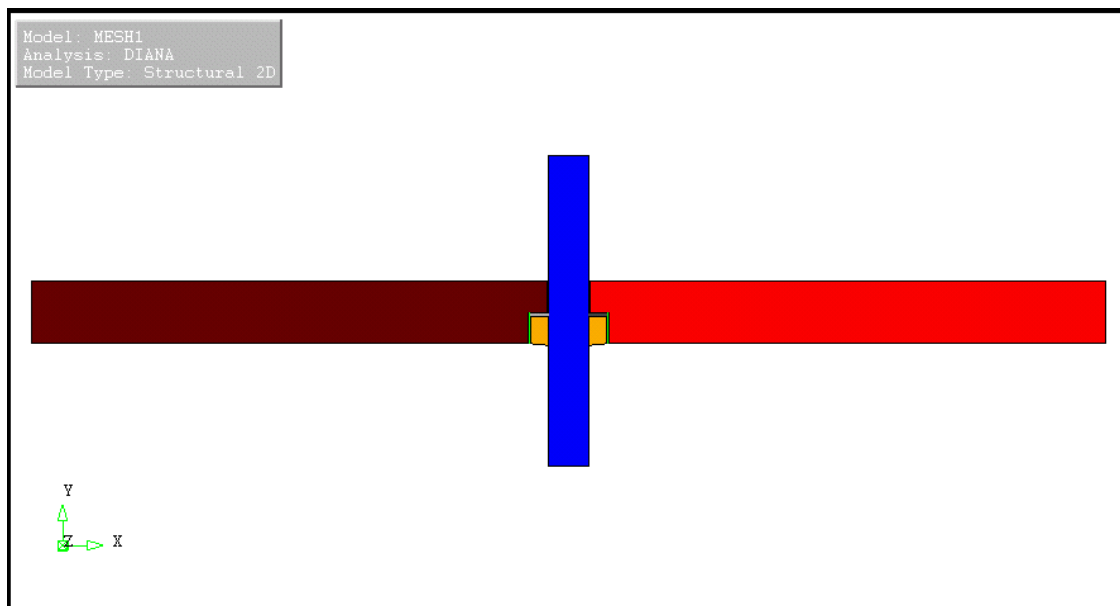


Figure 6.4 Geometry layout of the studied beam-column connection in DIANA.

Possible simplifications of the model, as symmetry, were discussed, see Figure 6.5, but due to the loading scheme this was not possible.

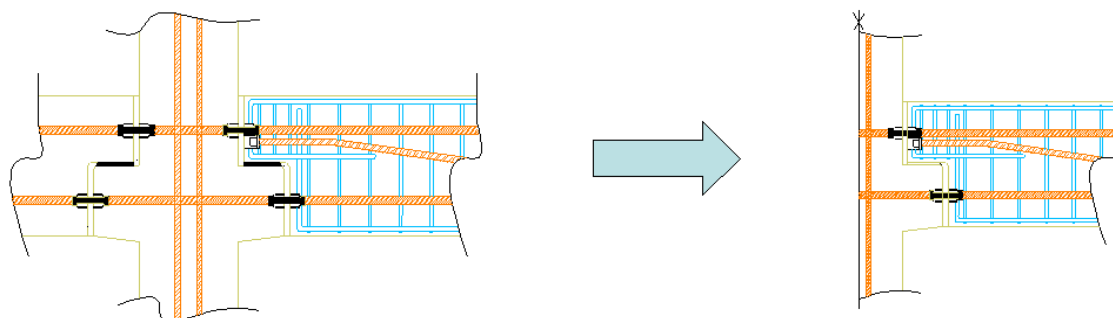


Figure 6.5 Symmetry simplification of the model that was discussed, but never used.

## 6.2.2 Mesh

Various possible meshes were discussed. The final decision was a dense mesh in the connection region and a coarse mesh elsewhere.

Several choices concerning elements and combination of different elements were considered but at the end concrete, mortar and rubber were modelled by eight-node quadrilateral isoparametric plane stress elements, and steel bars and tendons were modelled as embedded reinforcement.

In a first model during the linear analysis, instead of eight-node quadrilateral isoparametric plane stress elements, four-node quadrilateral isoparametric plane stress elements were used. However during the optimisation of the model it was decided to change to the eight-node quadrilateral isoparametric elements as they are more suitable for non-linear analysis of plane stress elements. This is also a recommendation given in DIANA's user manual. The mesh scheme and density is shown in Figure 6.6.

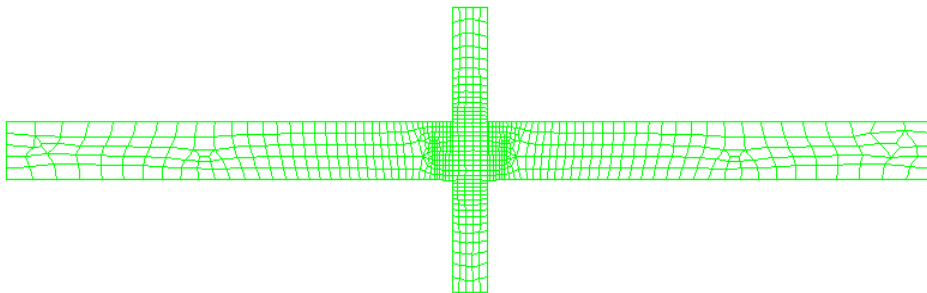


Figure 6.6 Mesh scheme.

The DIANA program provides a feature that evaluates the mesh quality. It is an option that identifies elements that fail quality tests, which includes angles, angle aspect ratios, positioning of the midsize node for higher order elements and the extent of warpage. After several tryouts the mesh passed all the quality tests, see Figure 6.7.

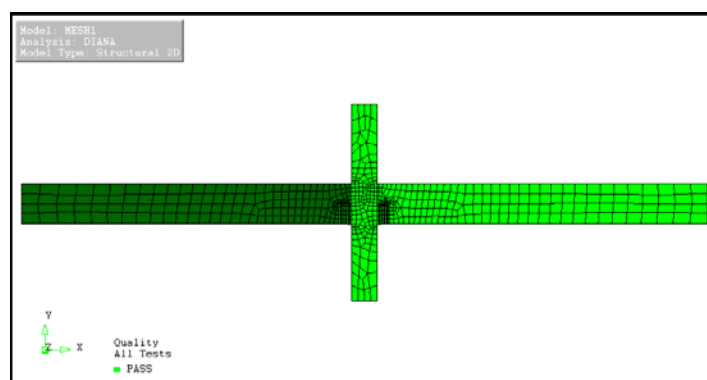


Figure 6.7 Mesh quality control in DIANA.

### 6.2.3 Boundary conditions

Several boundary choices were possible; some of the discussed ones are shown in Figure 6.8.

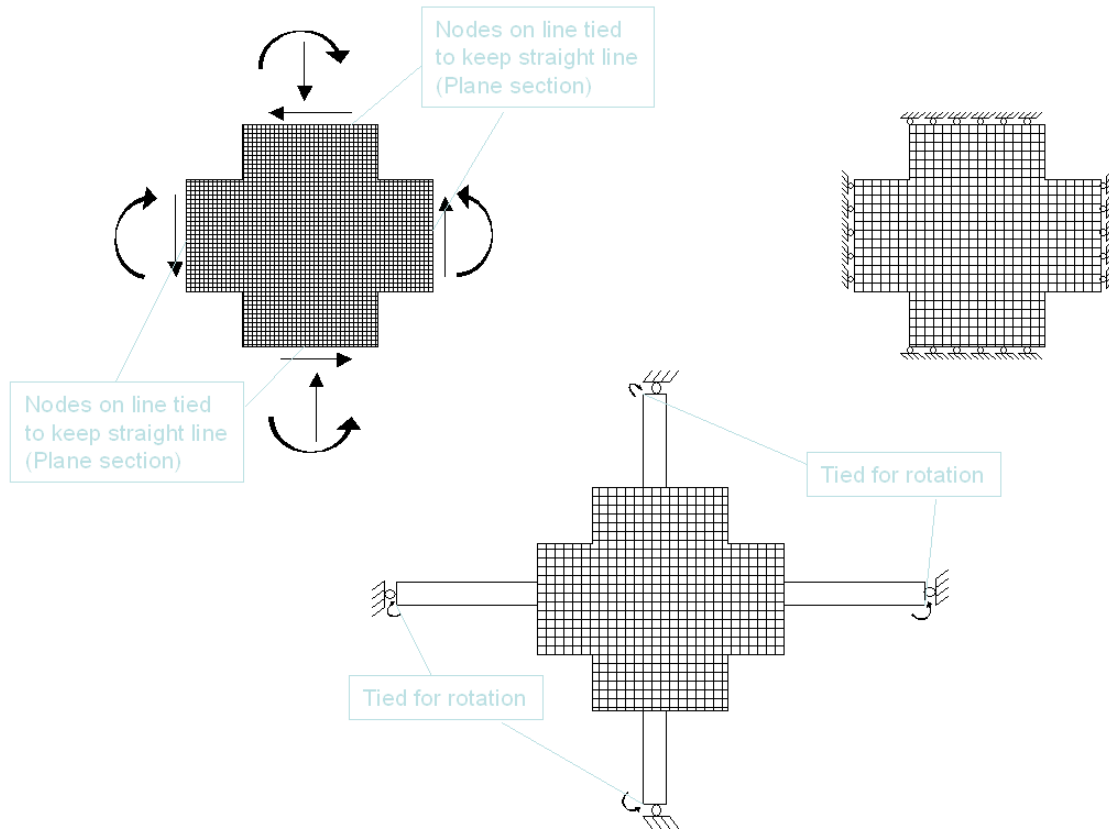


Figure 6.8 Different boundary conditions that were discussed.

The final decision was to try two approaches, one as shown in Figure 6.9, with the nodes at the end of the beam restricted in the x-direction and with the nodes at the column support restricted in the y-direction. The other approach was to restrict the nodes in the y-direction at the ends and with the nodes in the x- and y-direction restricted in the column support.

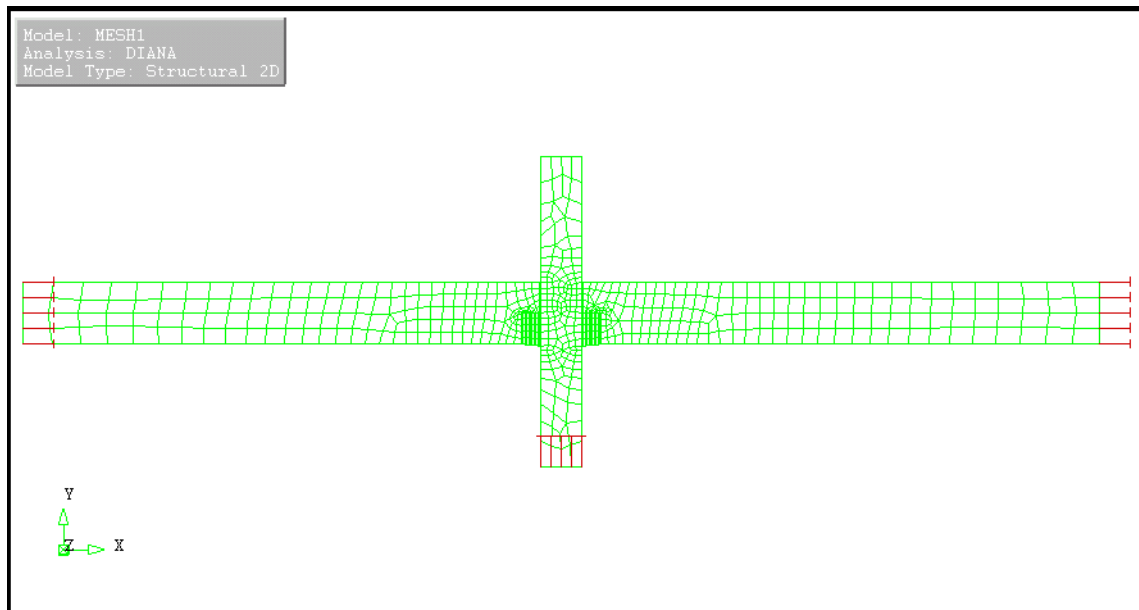


Figure 6.9 Boundary conditions, first alternative.

### 6.2.4 Loads and imposed displacement

The loading condition scheme is shown in Figure 6.10. An axial force of 594 kN was applied to the column, distributed loads of 60 kN/m, which represent the live load and dead load from slabs, were applied to the beams, and gravity loads from the dead weight of the structure was also applied.

In addition an imposed horizontal monotonic displacement up to a lateral drift of 5.0% was applied to the top of the column, see Figure 6.11.

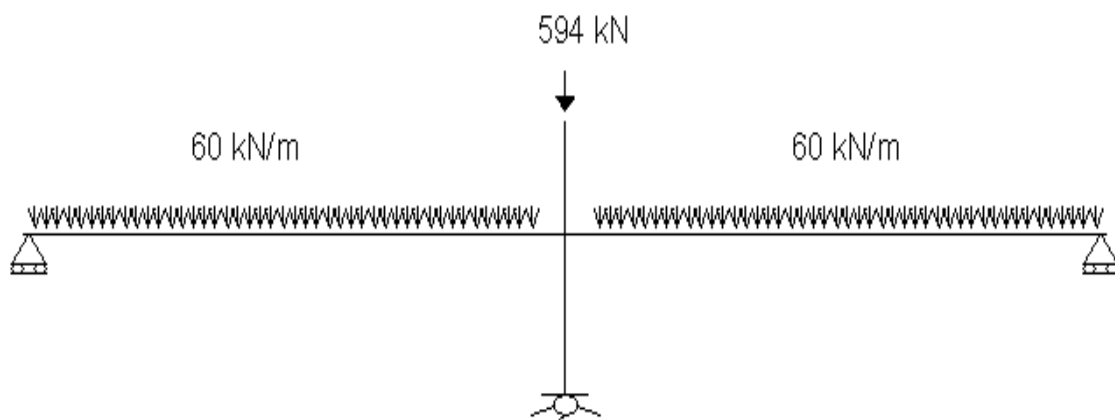


Figure 6.10 Loading conditions.

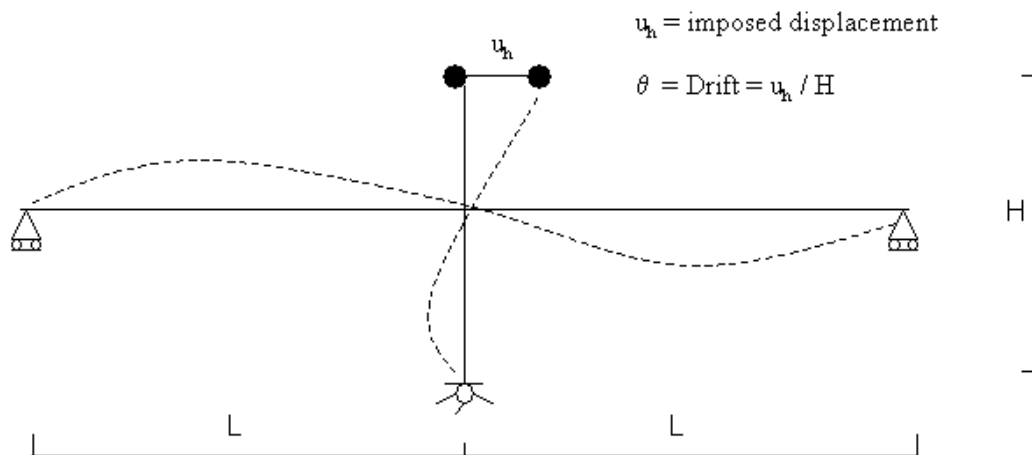


Figure 6.11 Imposed monotonic horizontal displacement applied at the top of the column.

Cyclic imposed displacement instead of monotonic imposed displacement would have been ideal but due to constraints from the material models of the DIANA program this was not possible.

The prestress applied to the primary tendons was of  $\sigma_{p0\infty} = 1050$  MPa after time dependent losses of prestress.

## 6.2.5 Post-tensioned tendons

For the post-tensioned tendons a special loading procedure was used, one that takes into account that the force in the tendon is influenced by various parameters. This is called *loss of prestress* and may be caused by subsequent prestressing of various tendons (elastoplastic shortening of steel and concrete), creep of the concrete (viscoelastic shortening), shrinkage of the concrete (shortening due to initial strain), and relaxation of the steel (viscoelastic extension). All these phenomena are incorporated in the DIANA numerical analysis.

It is also important to mention that other phenomena like the loss of prestress due to friction and penetration of the anchorage in the concrete was also taken into account in the model.

In the model two different approaches were used regarding the tensioning of the secondary tendons, one that they were tensioned at only one end and the other that they were tensioned at both ends.

For the tendons that were tensioned at both ends, DIANA calculates the distribution of tendon stress in a number of steps. The basic idea is that penetration leads to symmetric reduction of prestress in areas with initially reversed direction of friction,

and to additional uniform reduction if the required slip length is not available in those areas. Furthermore it is assumed that first tensioning takes place at both sides, followed by subsequent penetration at the first and the second anchorage. The procedure used by DIANA is illustrated in Figure 6.12. For more information on this reference is made to DIANA's user manual.

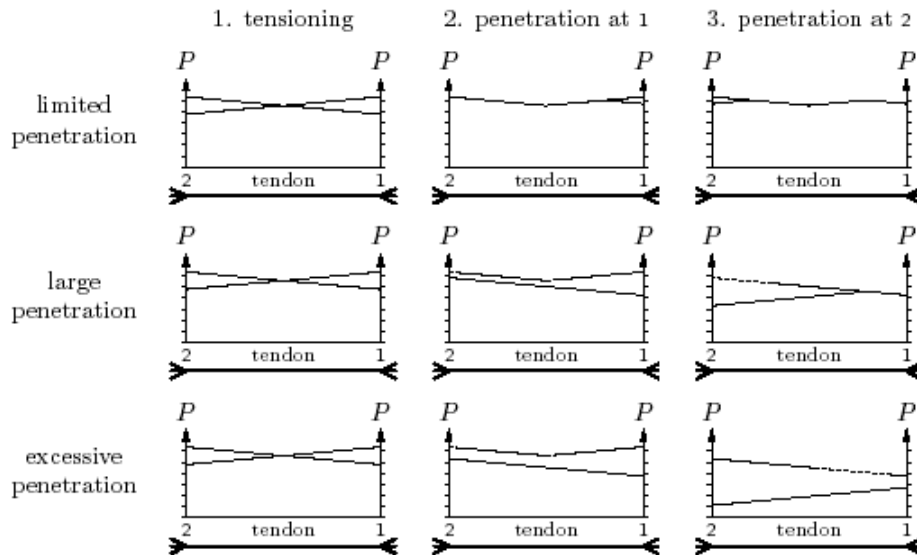


Figure 6.12 Tendon prestressed at both ends [De Witte et al (1999)].

## 6.2.6 Thickness and material properties

For plane stress elements the only physical property that is needed is the thickness, see Table 6.1 and Figure 6.13.

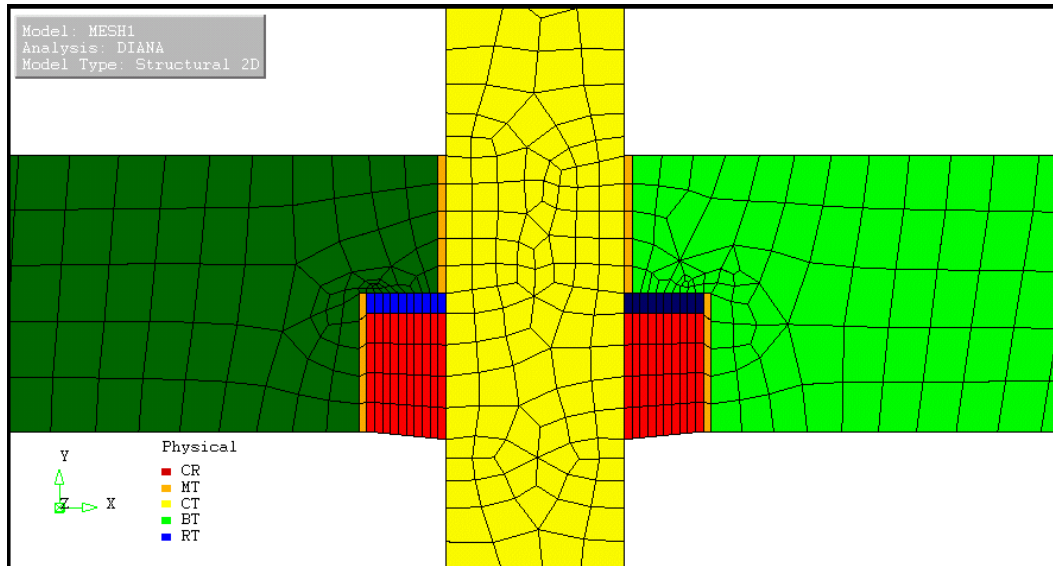


Figure 6.13 Physical properties in DIANA.

Table 6.1 Physical properties of the plane stress elements in DIANA.

No	Notation in Diana	Descp.	t [mm]	t scaled [mm]
1	CT	Column	450	150,00
2	CR	Corbel	400	133,33
3	BT	Beam	400	133,33
4	MT	Mortar	400	133,33
5	RT	Rubber	400	133,33

For the tendons and the reinforcing steel the physical input is the cross-sectional area. In Figure 6.14 a layout is shown of how the tendons and reinforcing steel are presented in DIANA.

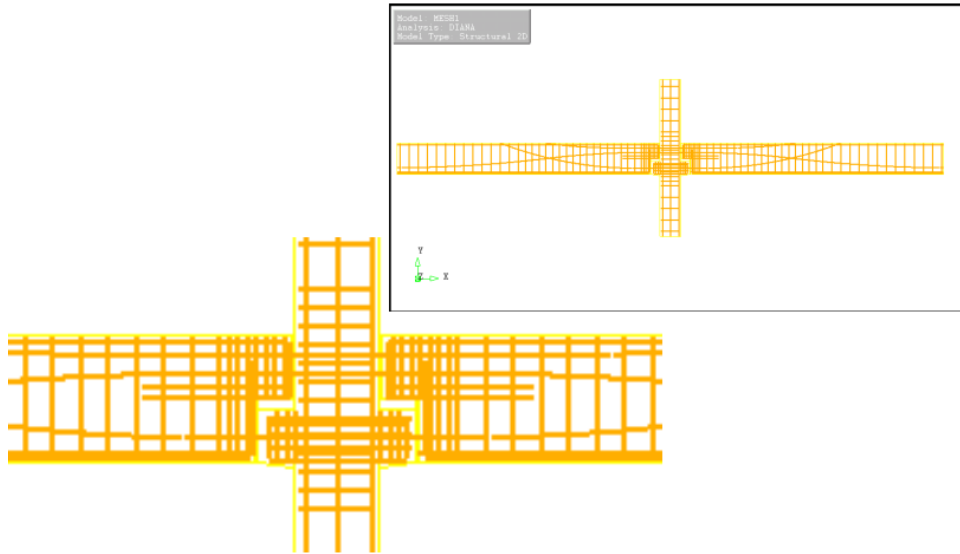


Figure 6.14 View of the reinforcement in DIANA.

For the concrete, mortar and rubber the material parameters for linear and non-linear analysis are listed in Table 6.2. The material parameters were applied to different parts of the model; see Figure 6.15 for a view of the parts. For the tendons and the reinforcing steel the elastic and plastic input is listed in Table 6.3.

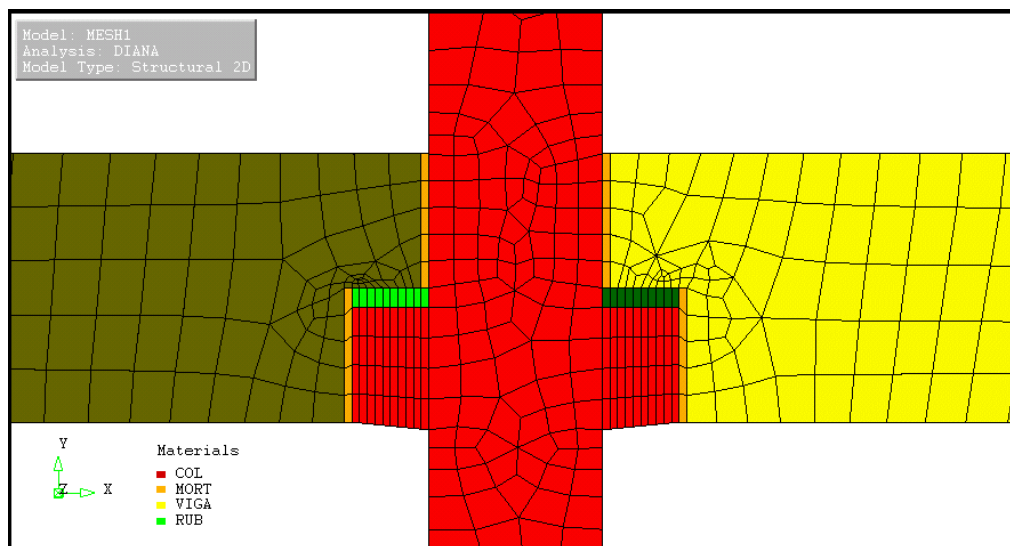


Figure 6.15 Material properties in DIANA.

Table 6.2 Material properties for the plane stress elements in DIANA.

No	Notation in Diana	Descp.	Elastic Input			Plastic Input				
			E [GPa]	$\nu$	$\rho$ [kg/m <sup>3</sup> ]	f <sub>cm</sub> [MPa]	f <sub>t</sub> [MPa]	Tensile F.E.	Compressive F.E.	Beta
1	COL	Column	40,3	0,2	2500	53,9	3,5	0,1	161	0,01
2	VIGA	Beam	42,3	0,2	2500	59,3	3,8	0,1	177,9	0,01
3	MOR	Mortar	42,3	0,2	2000	59,3	3,8	0,1	177,9	0,01
4	RUB	Rubber	0,05	0,5	1522	-	-	-	-	-

Table 6.3 Material properties for the prestressing and reinforcement steel in DIANA.

No	Notation in Diana	Descp.	Elastic Input			Plastic Input	
			E [GPa]	$\nu$	$\rho$ [kg/m <sup>3</sup> ]	f <sub>ym</sub> / f <sub>pm</sub> (MPa)	Hard. curve
5	PCB	Tendon (Bond)	200	-	-	2000	Hard. Curve 2
6	PCNB	Tendon (No Bond)	200	-	-	2000	Hard. Curve 2
7	RCB	Mild steel (Bond)	200	-	-	550	Hard. Curve 3

### 6.3 Preliminary linear analysis

First a linear analysis was performed in order to check the model and to estimate the size of the first load steps of the nonlinear analysis.

After the analysis is done DIANA checks whether any badly shaped elements exist. There were no such warning messages in the analysis-progress window or in the standard output file, so its possible to inspect and accept the analysis results.

Another inspection is to check if the support forces under gravity loads in the column agree with hand calculations. The result from a hand calculation was 3,572 kN, which agrees well with the results from the analysis, see Figure 6.16.

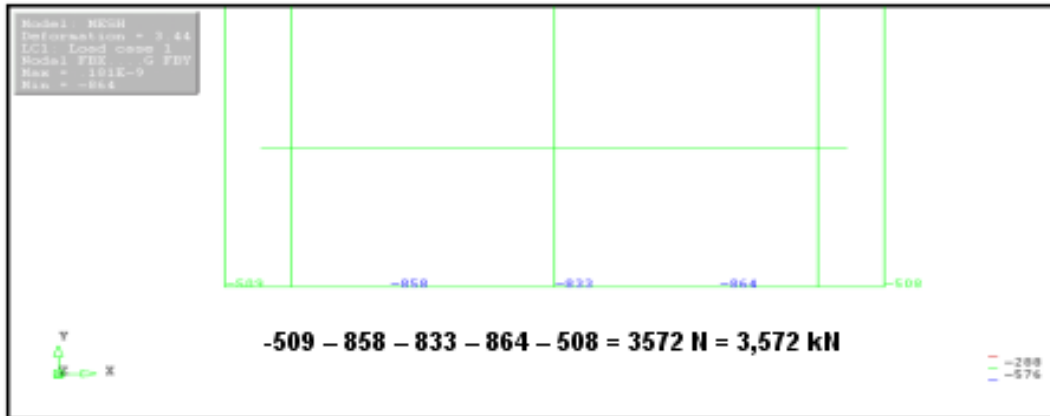


Figure 6.16 Verification of the forces in the column support under gravity loads.

A plot of the deformed mesh (in red) after post-tensioned of the secondary tendons is shown in Figure 6.17 and a plot of the deformed mesh for all loads (vertical loads, prestressing loads and imposed horizontal displacement) is presented in Figure 6.18. Both figures have been amplified with different amplification factors in order to exaggerate the deformations. Therefore the two displays may not be compared as such. Note that in Figure 6.17 the deformation is not totally symmetrical; this is because in this particular model there was only one active anchor at the secondary tendons.

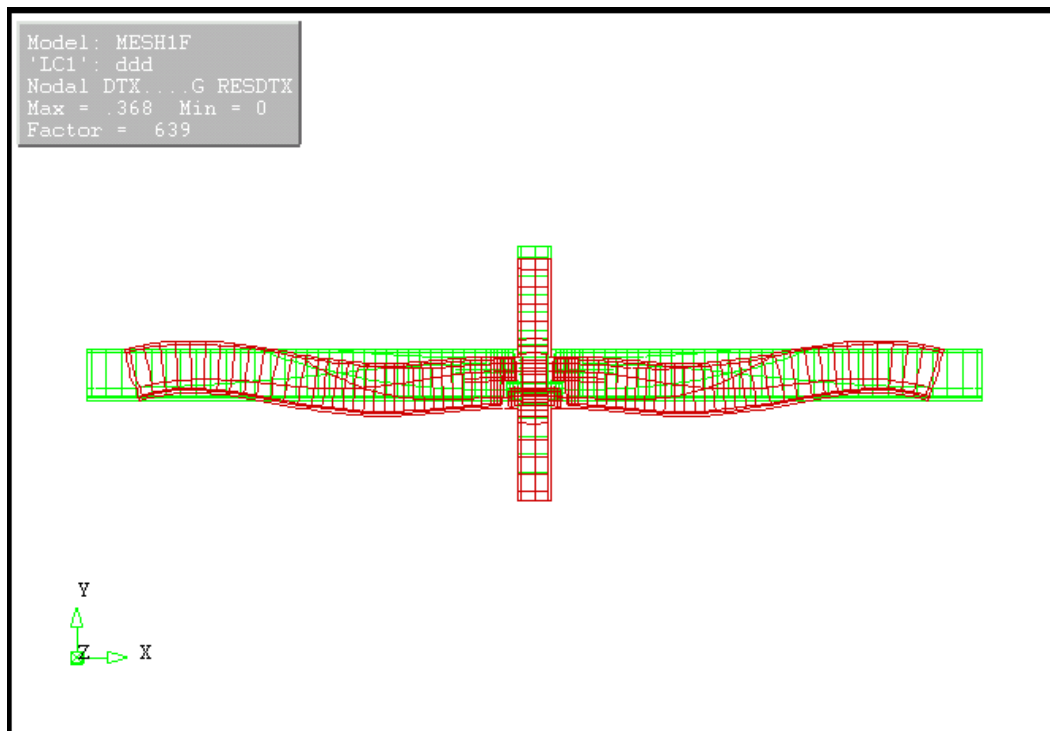


Figure 6.17 Deformed mesh (639x) relative to undeformed mesh for vertical loads after post-tensioning of the secondary tendons.

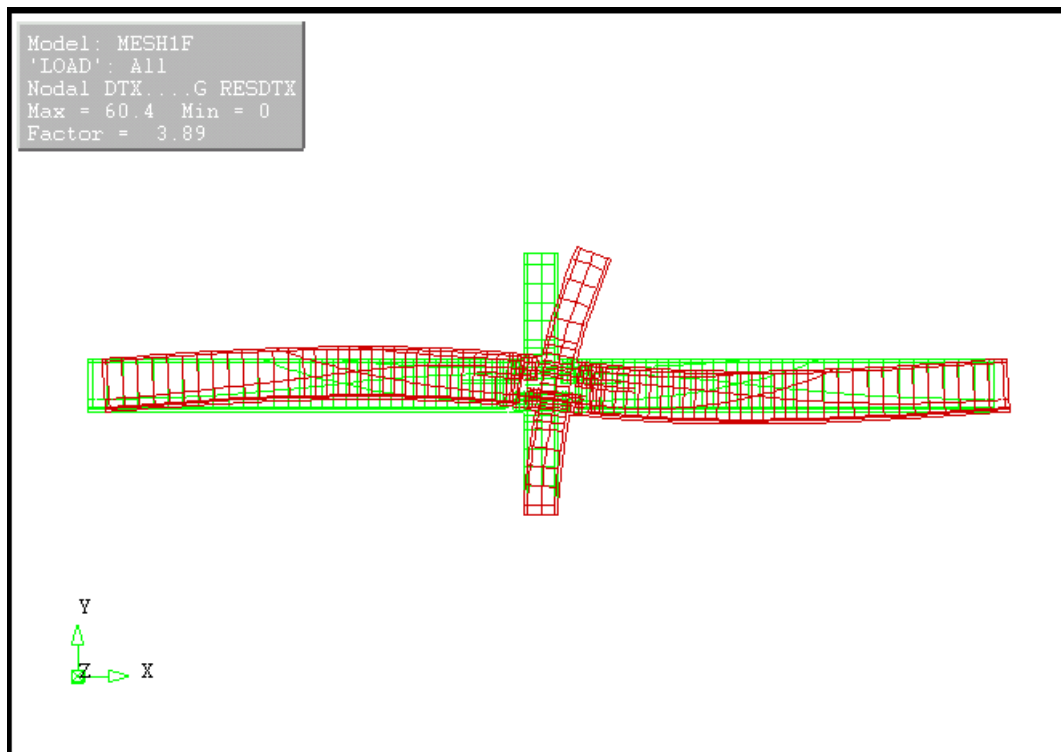


Figure 6.18 Deformed mesh (3,89x) relative to undeformed mesh for all loads (vertical loads, prestressing loads and imposed horizontal displacement).

To check the behaviour of the model the stresses from the linear elastic analysis are displayed. A stress contour plot of the stresses in the x-direction before the application of the imposed horizontal displacement is shown in Figure 6.19.

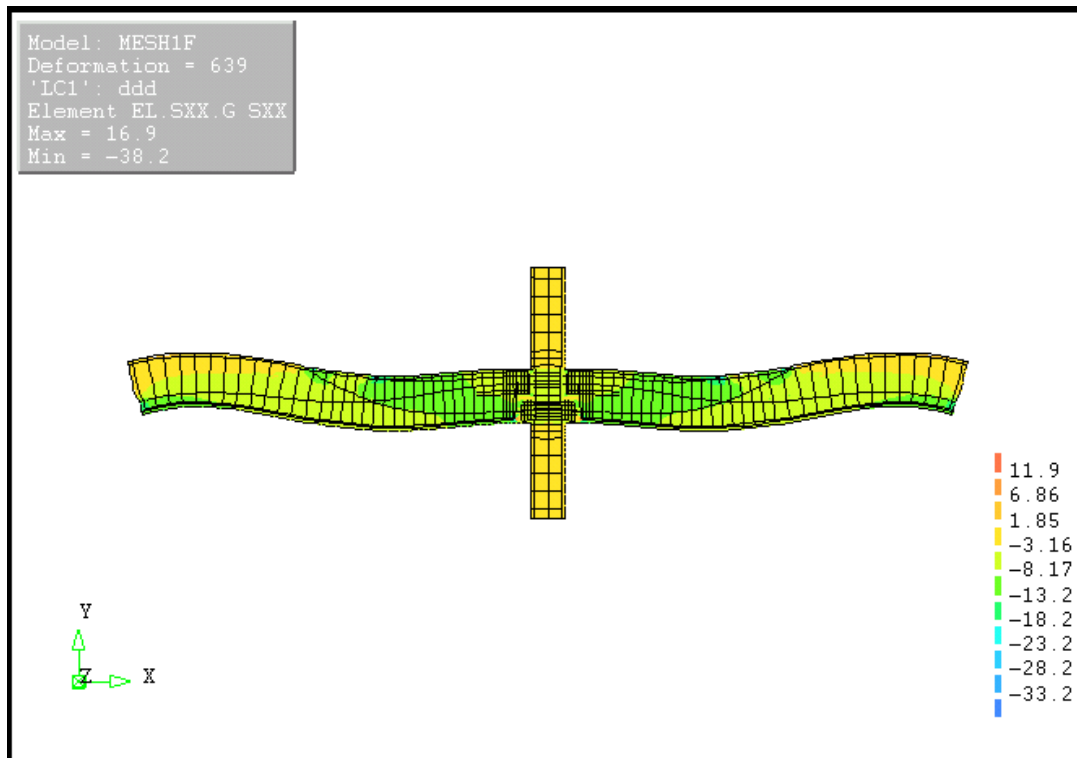


Figure 6.19 Plot of element stresses in the x-direction under the deformed mesh before the application of the imposed horizontal displacement.

The results indicate that the maximum tensile stress is 16,9 MPa, which is far beyond the tensile strength of the concrete and could imply that a non-linear analysis is already needed. However this region with high tensile stress is very small and located in the mortar-beam interface next to the primary tendon anchor (see Figure 6.20). This phenomenon can be explained. The program does not take into account that in real life the pretensioning process of the primary tendons is done before the assemblage of the connection. Therefore when the program applies the pretensioning on the primary tendons, the regions close to the anchor sustain large deformations.

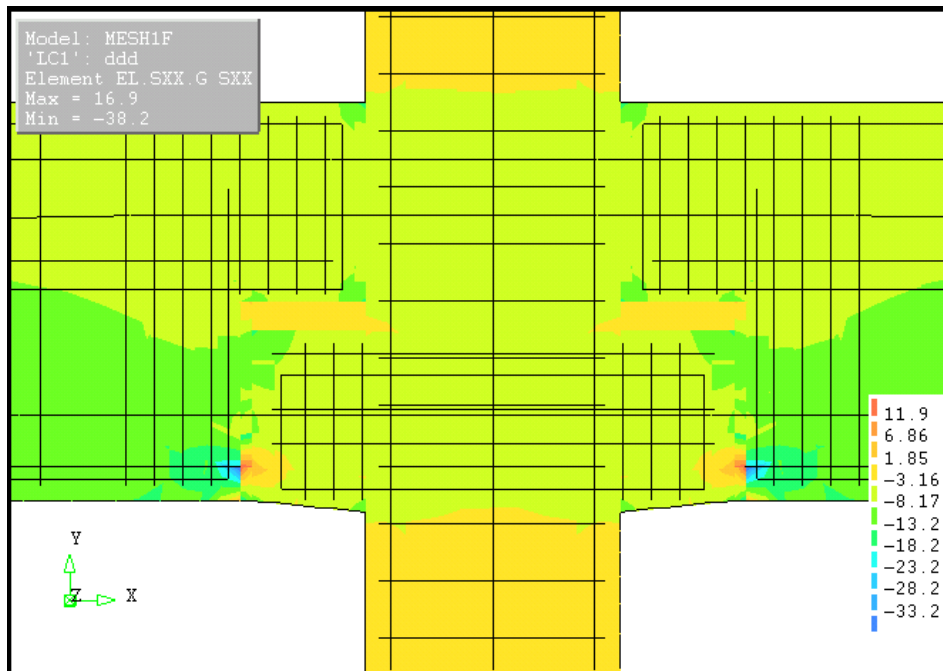


Figure 6.20 Zoomed view of the stresses in the x-direction before the application of the lateral loads.

On the other hand the results from the analysis including the imposed horizontal displacement indicate the need of a non-linear analysis. Stresses in the x- and y-direction show that elements close to the upper column-beam interface have surpassed all limits, see Figures 6.21, 6.22, 6.23 and 6.24.

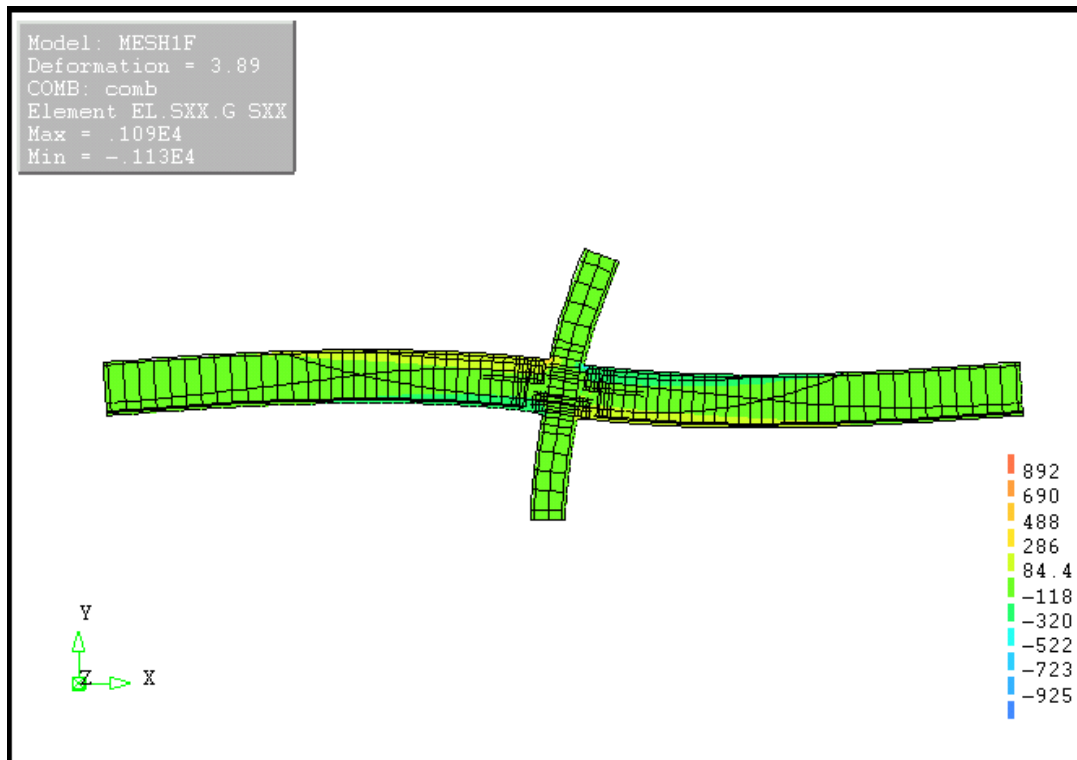


Figure 6.21 View of the stresses in the x-direction for all loads (vertical loads, prestressing loads and imposed horizontal displacement).

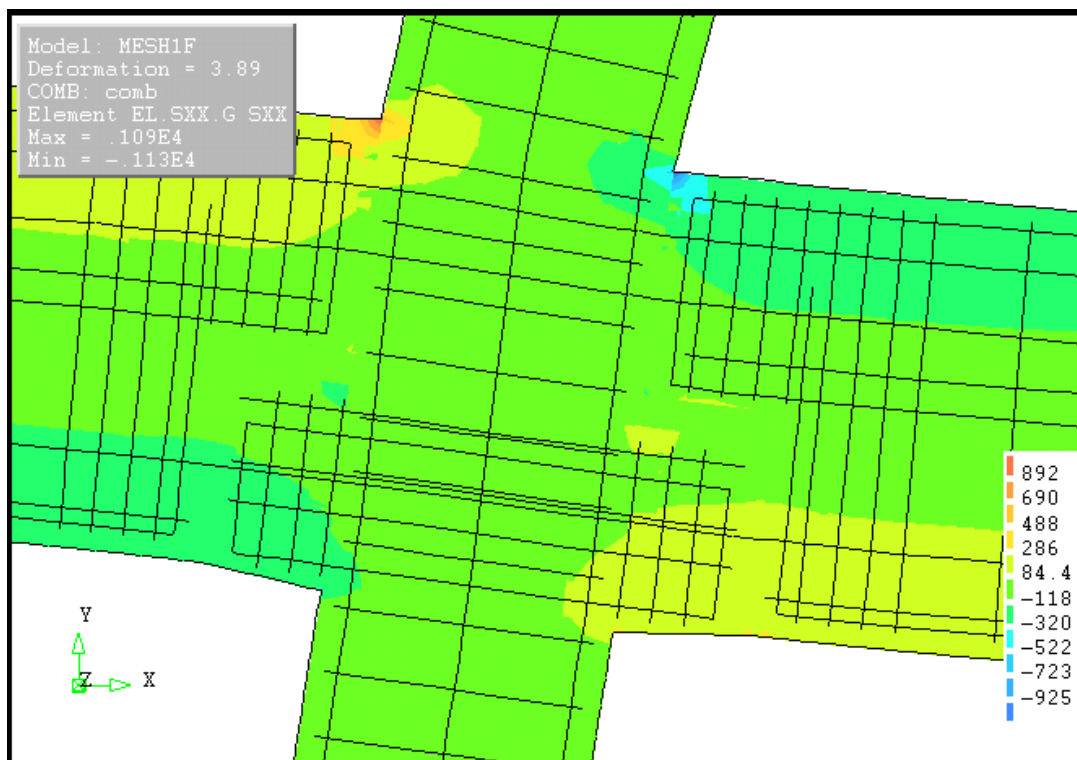


Figure 6.22 Zoomed view of the stresses in the x-direction for all loads (vertical loads, prestressing loads and imposed horizontal displacement).

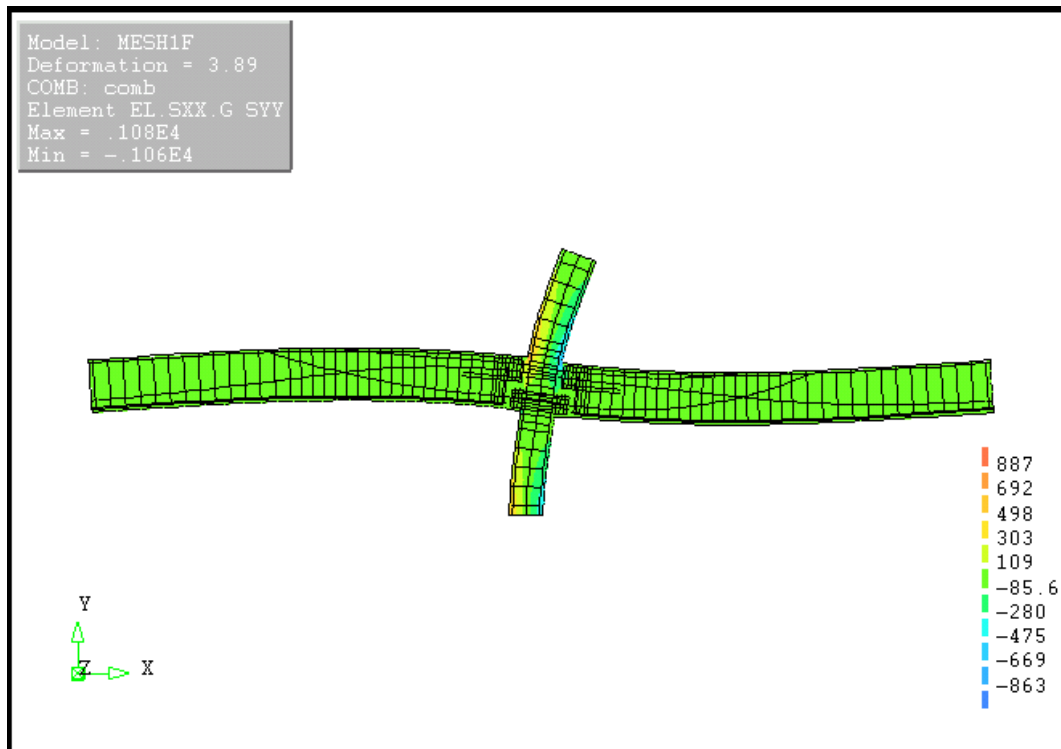


Figure 6.23 View of the stresses in the y-direction for all loads (vertical loads, prestressing loads and imposed horizontal displacement).

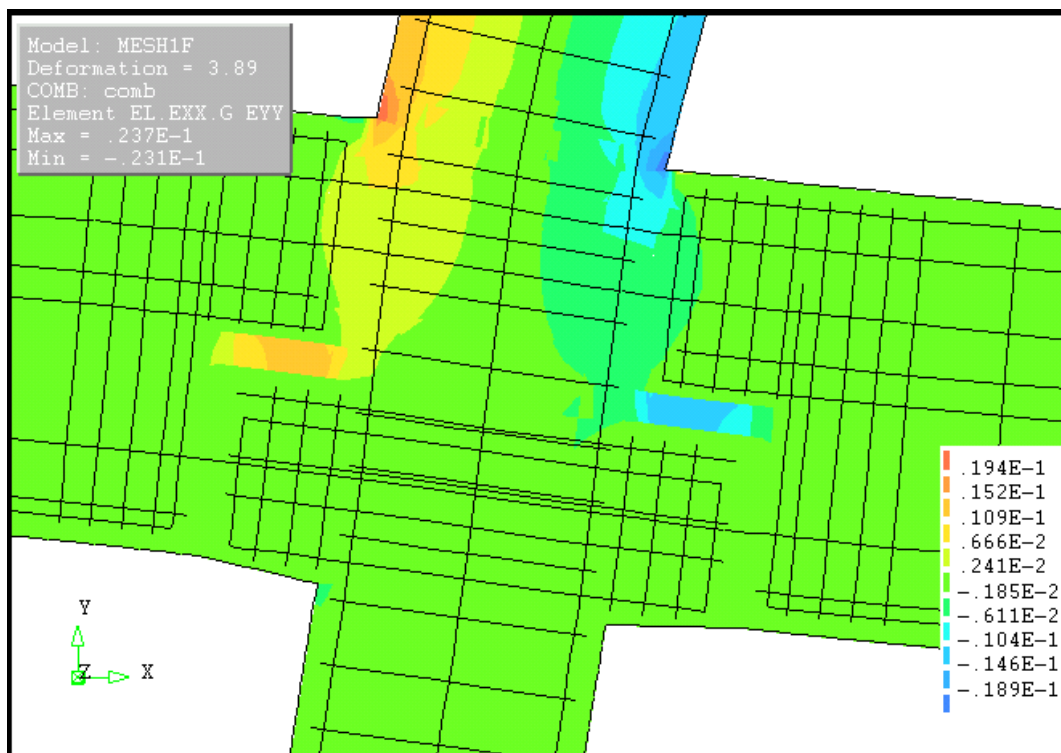


Figure 6.24 Zoomed view of the stresses in the y-direction for all loads (vertical loads, prestressing loads and imposed horizontal displacement).

The deformations and the stress plots seem reasonable for every load stage analysed but the results demonstrate that a non-linear analysis is needed in order to assess a more realistic behaviour of the connection.

## 6.4 Non-linear analysis

In the non-linear analysis the lateral drift, i.e., the horizontal imposed displacement at the top of the column was applied as depicted in Tables 6.4, 6.5 and 6.6. In order to have better results several analysis with different loading steps were used, the first with large early steps (which should be completely linear) and two other with smaller steps.

During the application of the load horizontal imposed displacement steps presented in Tables 6.4, 6.5 and 6.6 all the other loads had to be already present. Hence the prestressing was applied in a start step and then all the gravity loads were applied in 3 equal load steps.

The finally selected loading procedures were chosen by trial and error to achieve convergence within a reasonable number of iterations. For convergence criteria the program DIANA offers 3 types of norms: displacement, force and energy norms. In these analysis the displacement norm was used.

The iteration scheme applied for the non-linear analysis was the Broyden–Fletcher–Goldfarb–Shanno (BFGS), a Quasi-Newton method (also called “Secant method”). In addition the line search algorithm was used.

Table 6.4 Loading procedure 1.

Steps	# of steps x increment	Total increment	Total disp. [mm]	Drift (%)
5 to 11	6 x 0,1	0,6	36	3,09
12 to 36	25 x 0,01	0,85	51	4,37
37 to 136	100 x 0,005	1,35	81	6,94

Table 6.5 Loading procedure 2.

Steps	# of steps x increment	Total increment	Total disp. [mm]	Drift (%)
5 to 15	11 x 0,02	0,22	13,2	1,13
16 to 47	32 x 0,01	0,54	32,4	2,78
48 to 61	12 x 0,008	0,636	38,16	3,27
62 to 81	20 x 0,001	0,656	39,36	3,37
82 to 92	11 x 0,008	0,744	44,64	3,83
93 to 112	20 x 0,01	0,944	56,64	4,85

Table 6.6 Loading procedure 3.

Steps	# of steps x increment	Total increment	Total disp. [mm]	Drift (%)
5 to 15	11 x 0,02	0,22	13,2	1,13
16 to 47	32 x 0,01	0,54	32,4	2,78
48 to 61	12 x 0,007	0,624	37,44	3,21
62 to 81	20 x 0,004	0,704	42,24	3,62
82 to 95	13 x 0,002	0,73	45,5	3,90

### 6.4.1 Displacements

In Figure 6.24 the deformed mesh for some selected steps from loading procedure 3 are shown in the same scale. As seen the displacement before the application of the horizontal imposed displacement is practically imperceptible. Later on with the application of load steps in the horizontal imposed displacement the structure deforms. The column tends to deform much more compared with other elements and probably in step 95 the steel bars in the column have failed.

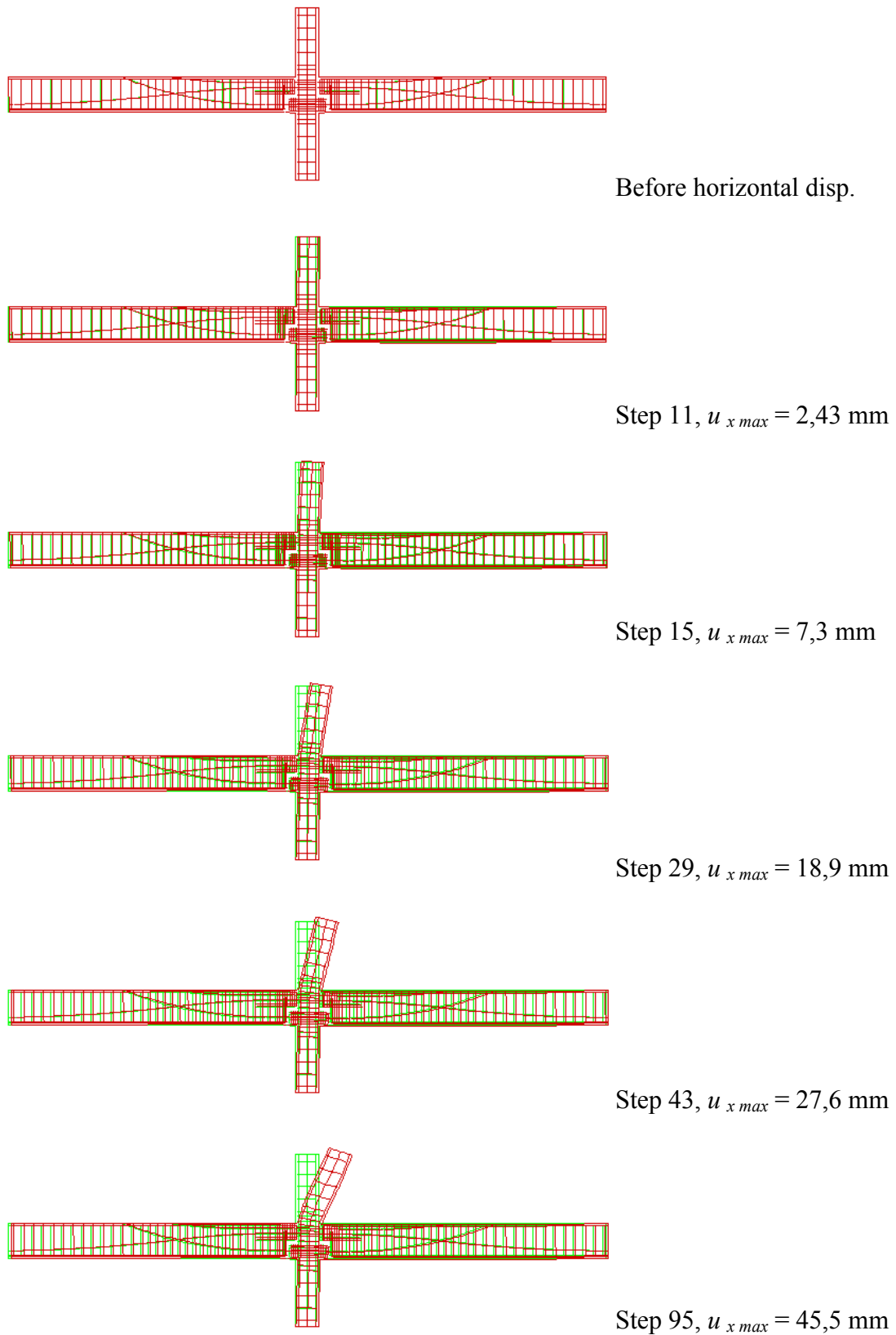


Figure 6.25 Displacement sequence for different load steps for load procedure 3.

## 6.4.2 Cracking and stresses

The crack-strain results or EKNN (name in DIANA) at the integration points (first crack at integration point) are presented at different load steps in order to show the cracking sequence. These crack-strains represent how much the cracks are opened. These displays have the same orientation as the cracks and their colour indicates the width of the crack.

Furthermore, the result S1 (name in DIANA) at the integration points is shown, which is the first principal stress  $\sigma_1$ , i.e., the most positive (tensile) principal stress. These results are visualized as vectors, oriented in the direction of the principal stress and with size and colour modulated according to the magnitude of the stress.

The third result that is shown is EP3 (name in DIANA), which represents the third principal plastic strain  $\varepsilon_{p3}$ , i.e., the most negative (compressive) plastic strain. These results are displayed as contour plots, scaled by the plastic strain at the last step.

Steps from loading procedure 3 are presented here are step 9 (before the application of the lateral drift), step 11 (start of the application of the lateral drift), step 15 (after first yielding of the longitudinal steel in the column), step 29, step 43 and step 95 (last converged step).

- Results for load step 9: The connection is subjected only to vertical and prestressing loads. A symmetric crack distribution in the bottom surface of the corbels can be identified, see Figure 6.26 top left and bottom left. These cracks are believed to occur due to the application of prestress in the primary tendons, which in real life will not occur as the tensioning of primary tendons is finished before the assemblage.

The principal stresses are all less than, or equal to 3,5 or 3,8 MPa, which are the values specified for the tensile strength  $f_t$  of the column and beam concrete respectively, except for the bottom surface of the corbels. In the regions close to the active anchors of each primary tendon, significant tensile stresses can be noticed, see Figure 6.26 right centre and bottom right.

The plastic strain is very small in all elements (Figure 6.27).

- Results for load step 11: At this load step a new crack pattern is found. The largest crack occurs in the top region of the left beam-column interface. Now the maximum stresses have a new direction. And still the plastic deformations are very small, see Figures 6.28 and 6.29.

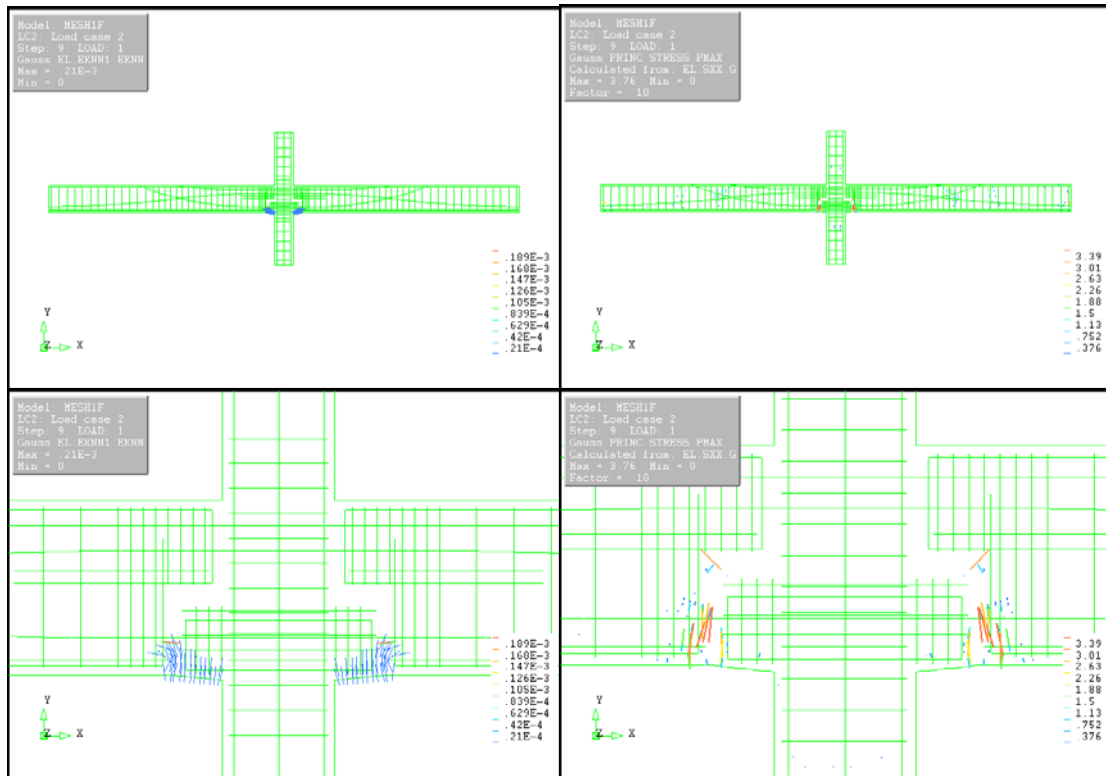


Figure 6.26 Results of crack-strain and 1<sup>st</sup> principal stress for load step 9.

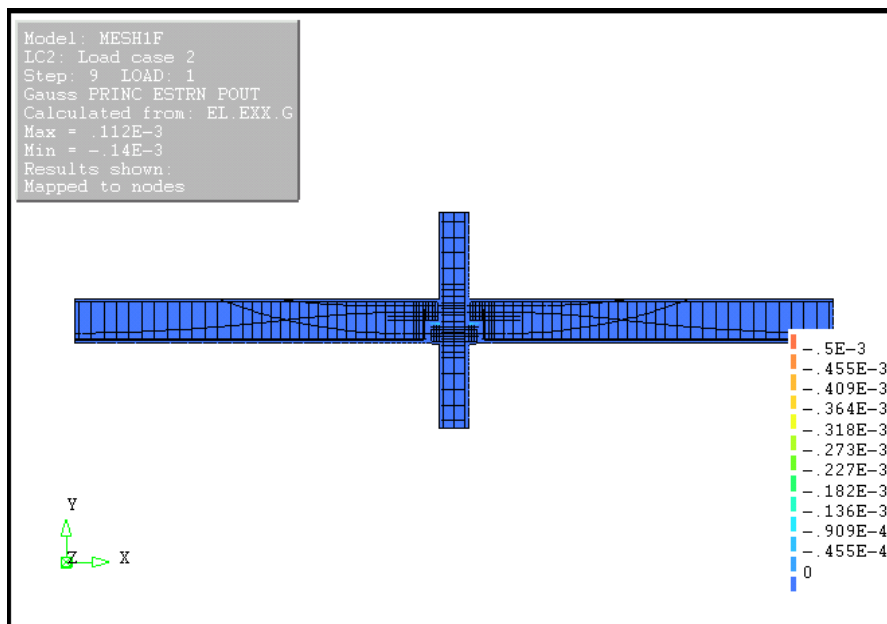


Figure 6.27 3<sup>rd</sup> principal plastic strain for load step 9.

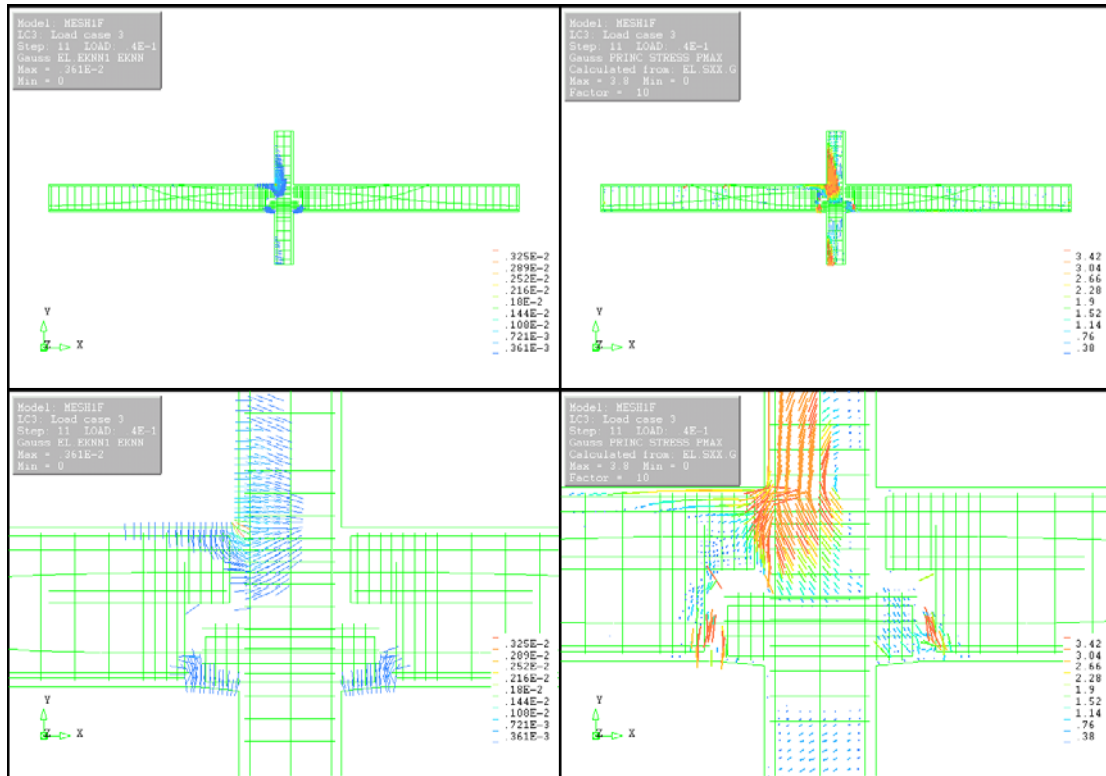


Figure 6.28 Results of crack-strain and  $1^{st}$  principal stress for load step 11.

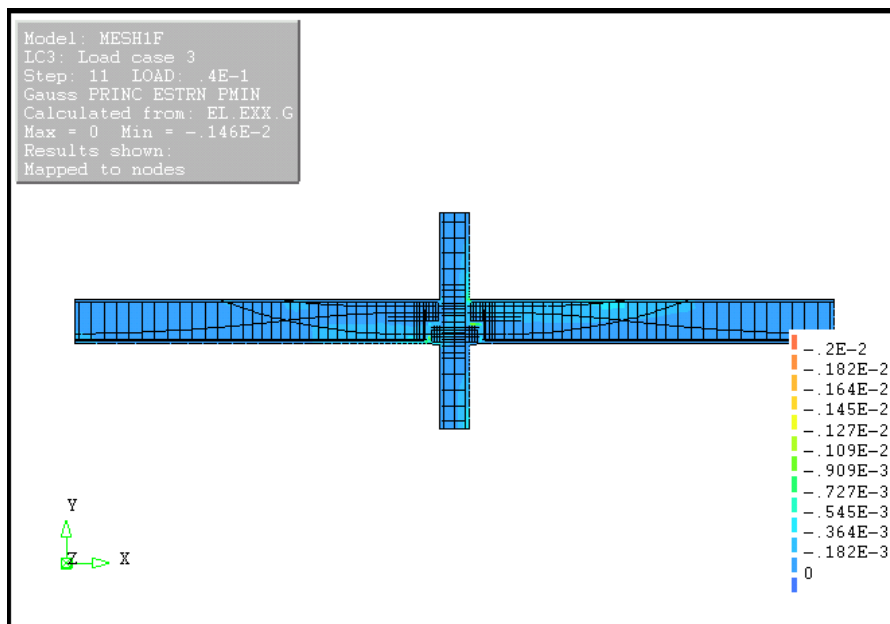


Figure 6.29  $3^{rd}$  principal plastic strain for load step 11.

- Results for load step 15: At step 15 the crack pattern found in step 11 has extended into the connection zones. Cracks appear almost all over the left side of the column; also some small cracks appear in the top region of the beams. The directions of the tensile stresses tend to rotate. Moreover, significant plastic deformation can be observed at opposite corners of the beam-column interfaces, see Figures 6.30 and 6.31.
- Results for load step 29: At step 29 the horizontal imposed displacement has been more than doubled. The crack pattern is still extending; the maximum crack strain is much bigger than in the last step, and red values appear in the same location. The direction of the tensile stress keeps rotating; the pattern is very similar, but many more locations in the connection are in red, especially around the corbels. Considerable high tensile stresses appear in some locations in the beams. As the loading has increased, the plastic deformations have also increased, specifically in the interior of the upper part of the column next to the joint interface. Inside the connection a diagonal pattern of high compression strains is found, which could be expected, see Figures 6.32 and 33.

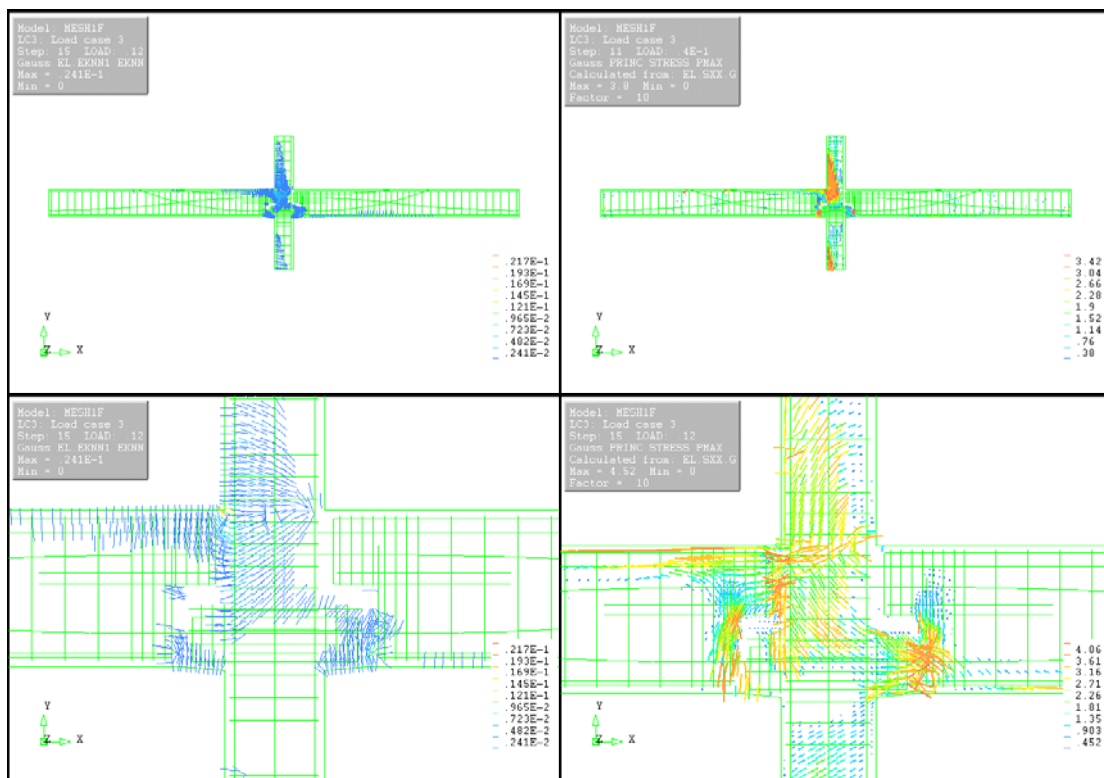


Figure 6.30 Results of crack-strain and 1<sup>st</sup> principal stress for load step 15.

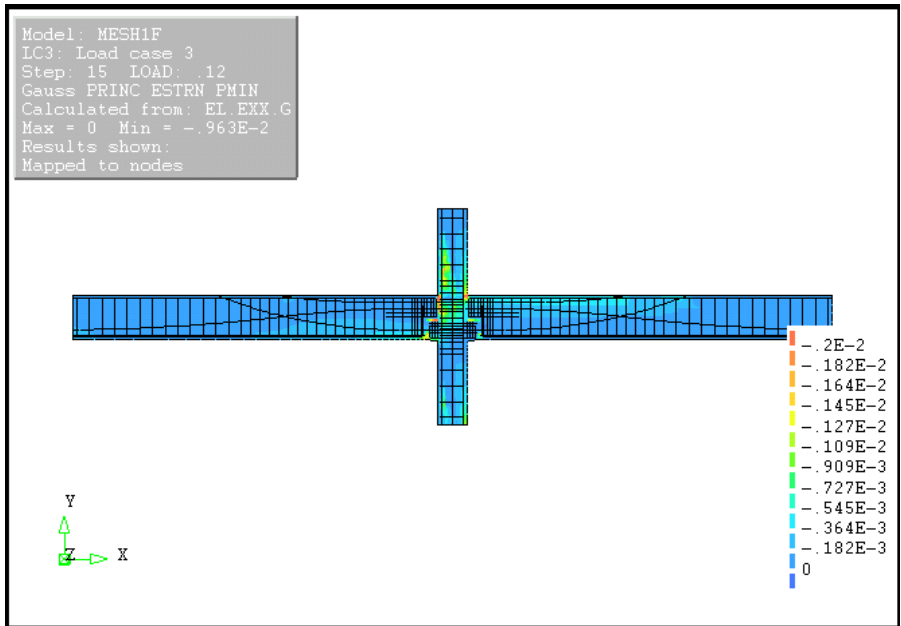


Figure 6.31 3<sup>rd</sup> principal plastic strain for load step 15.

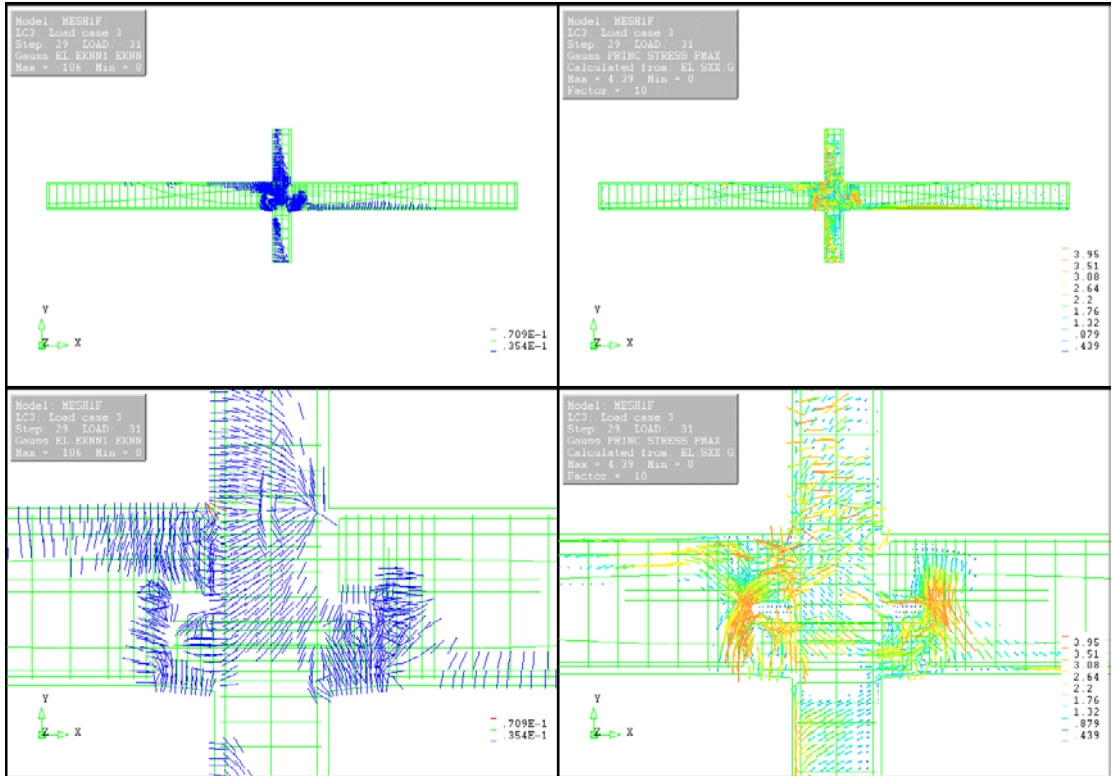


Figure 6.32 Results of crack-strain and 1<sup>st</sup> principal stress for load step 29.

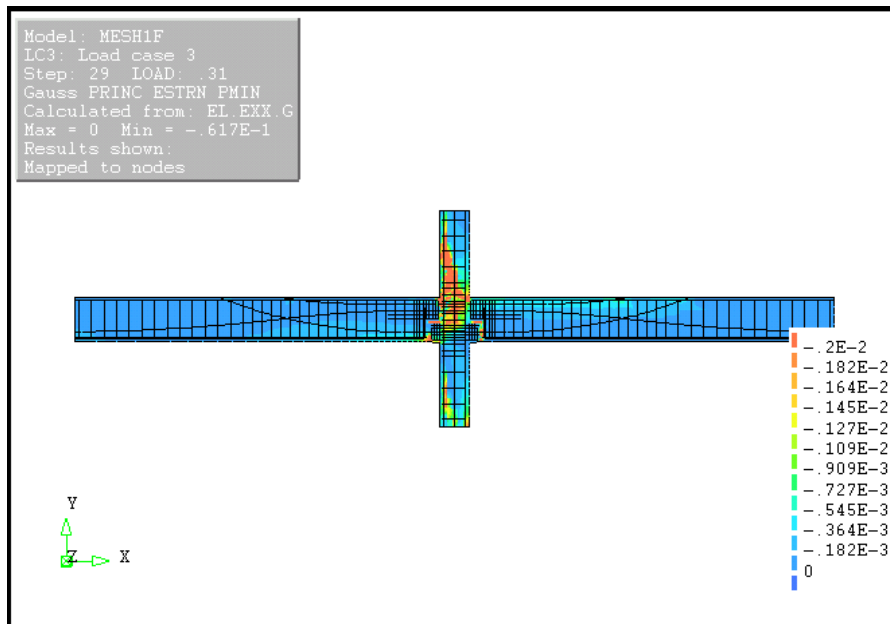


Figure 6.33 3<sup>rd</sup> principal plastic strain for load step 29.

- Results from load step 43: The results in step 43 show patterns similar to those in load step 29 but more pronounced. The cracks in the beams are mostly limited to the concrete cover, except for the regions close to the joint interface, see Figures 6.34 and 6.35.
- Results for load step 95: In this final step the top part of the column is practically fully cracked as well as the left column-beam interface. The cracks in the regions of the beams away from the joint interface are still very much limited to the concrete cover, see Figures 6.36 and 6.37.

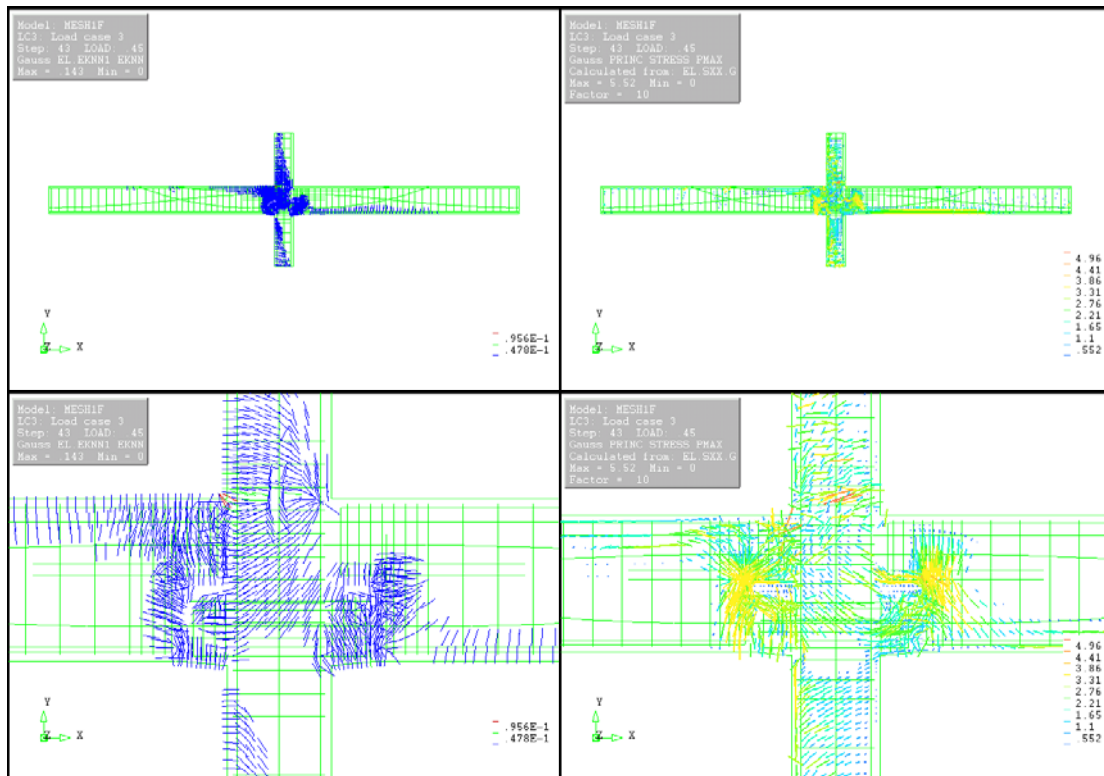


Figure 6.34 Results of crack-strain and 1<sup>st</sup> principal stress for load step 43.

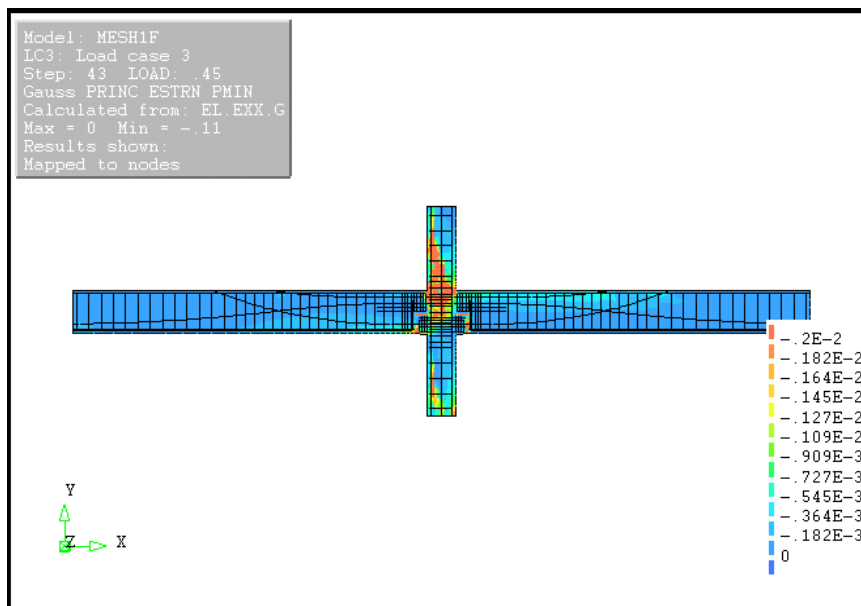


Figure 6.35 3<sup>rd</sup> principal plastic strain for load step 43.

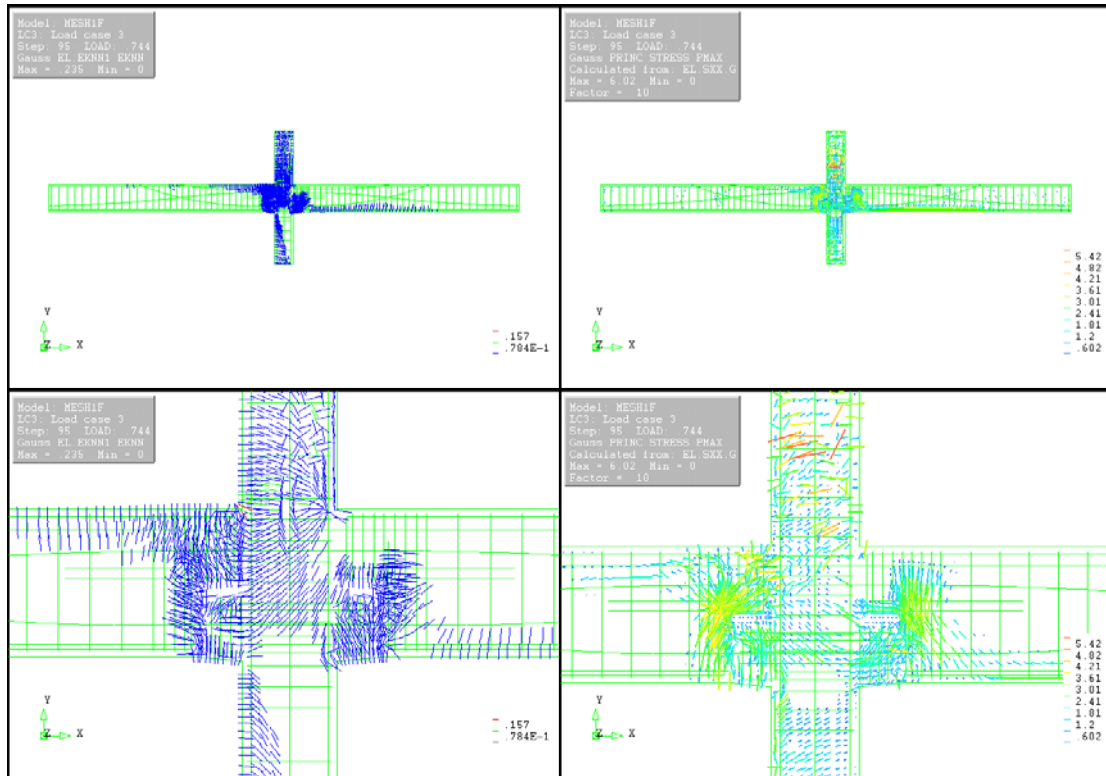


Figure 6.36 Results of crack-strain and 1<sup>st</sup> principal stress for load step 95.

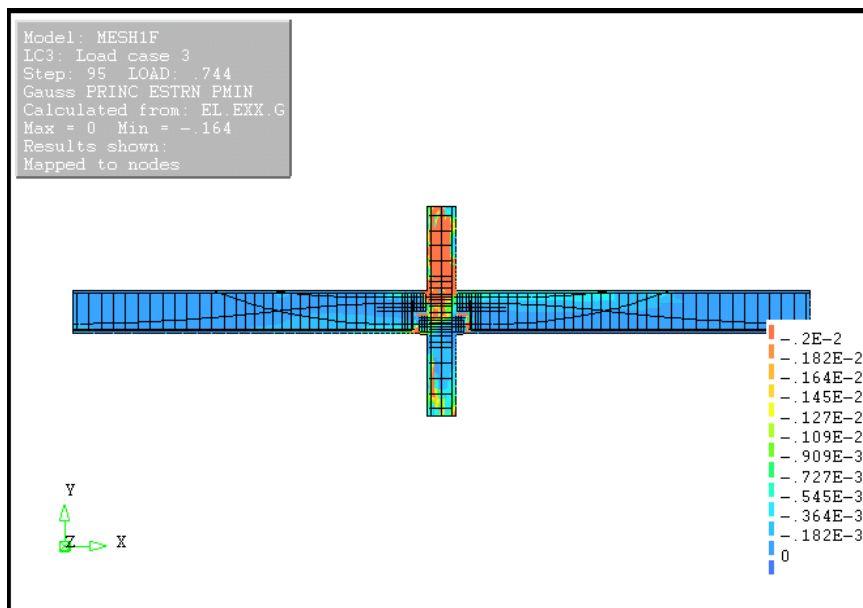


Figure 6.37 3<sup>rd</sup> principal plastic strain for load step 95.

### 6.4.3 Loss of prestress in the tendons and yielding of reinforcing steel

The tendons should be in the linear elastic field. If the tendons reach the limit of proportionality, the prestressing effect is lost.

The pre-tensioned tendons (primary tendons) had some loss of prestress, around 15%, must probably due to the change of moment sign when the vertical loads were applied. On the other hand none of the post-tensioned cables (secondary tendons) had any loss of prestress, see Figures 6.38 and 6.39.

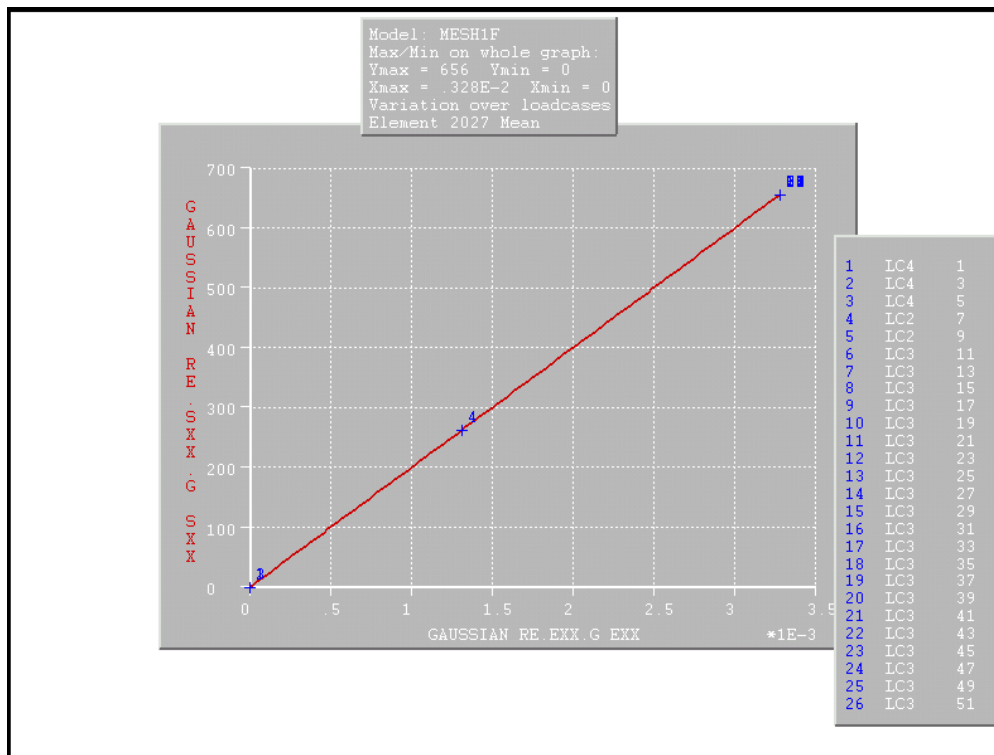


Figure 6.38 Stress-strain diagram for post-tensioned tendons (secondary tendons), section A-A next to the joint, see Figure 7.4.

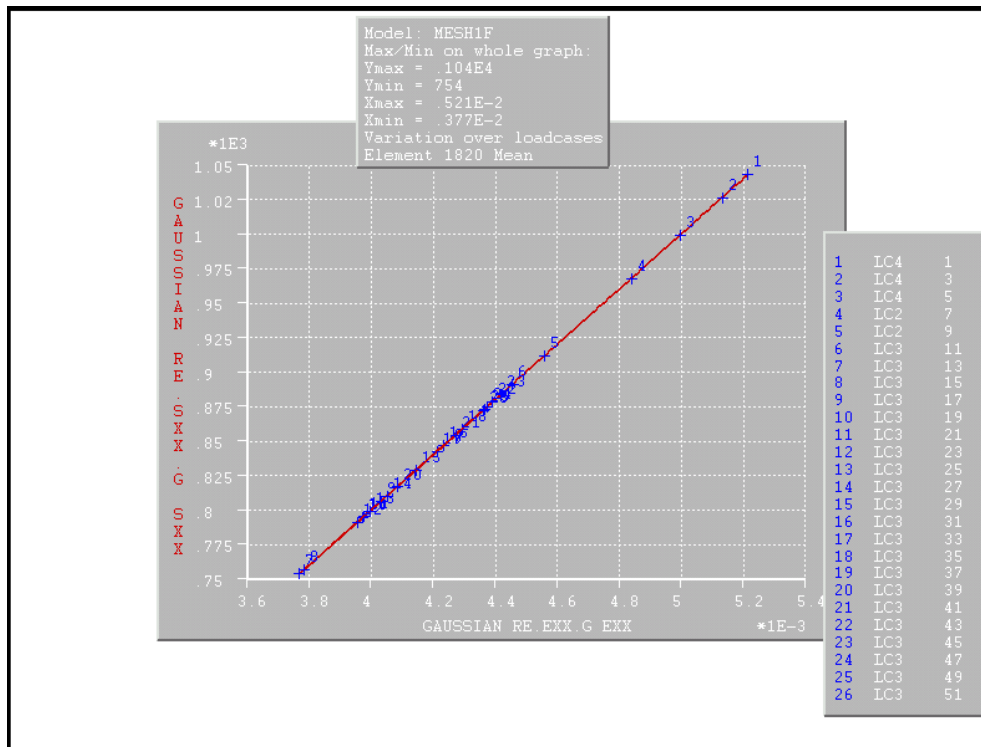


Figure 6.39 Stress-strain diagram for pre-tensioned tendons (primary tendons), section A-A next to the joint, see Figure 7.4.

The reinforcing steel and tendons in the beams never reached yielding, see Figure 6.40. Yielding was reached in the column longitudinal steel, close and inside the joint at a drift of 2,06%, see Figure 6.41. These yielding values were almost the same in all 3 loading procedures.

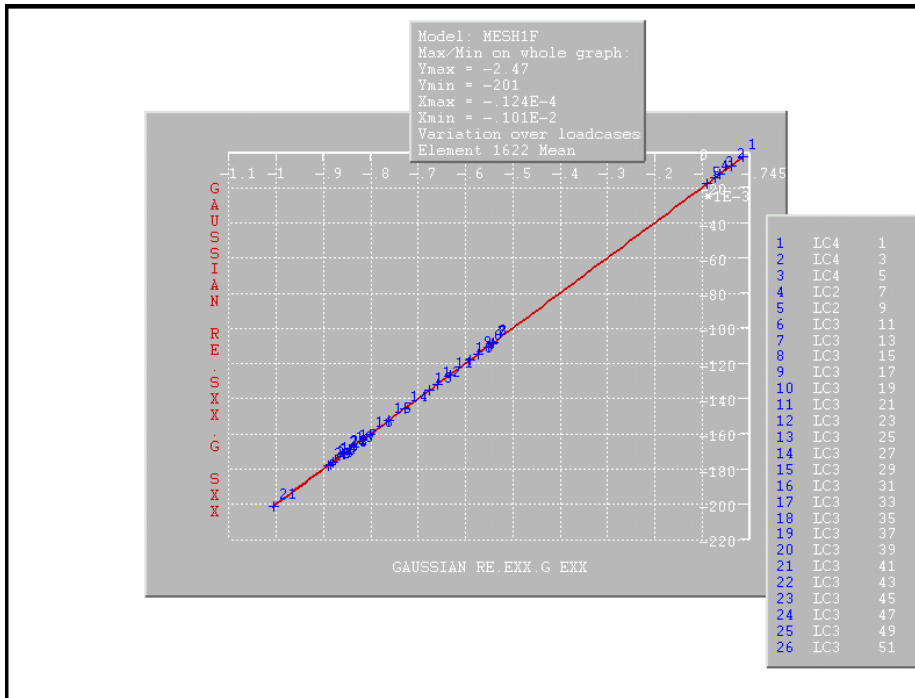


Figure 6.40 Stress-strain diagram for longitudinal beam steel, section A-A next to the joint, see Figure 7.4.

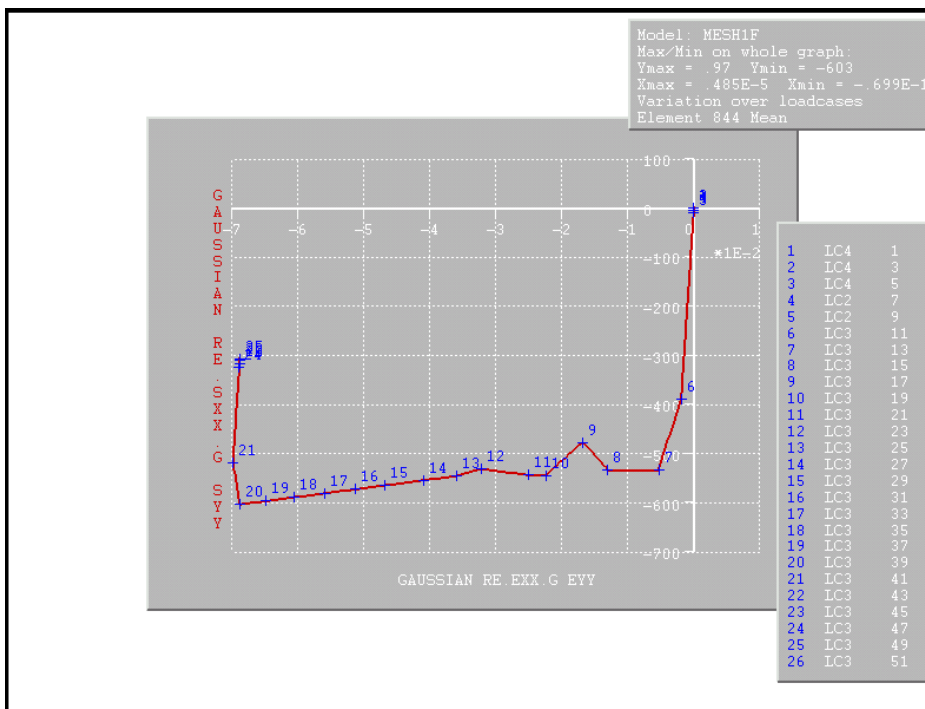


Figure 6.41 Stress-strain diagram for longitudinal column steel, section next to the joint.

### 6.4.4 Force-drift curve

Probably this is the most important result from this non-linear analysis. From the results the drift was calculated simply as horizontal displacement/height ratio, see Figure 6.11. Then, for a certain drift, the force is read as the sum of the support reactions in the horizontal direction at the base, joint A, see Figure 6.42.

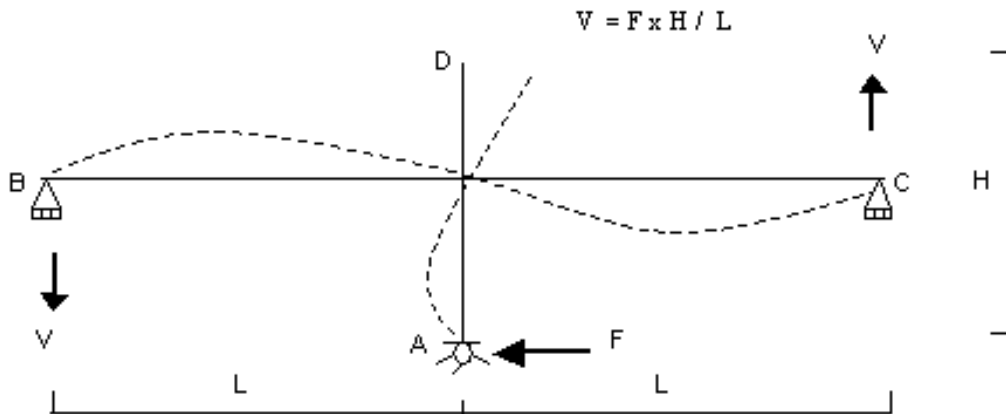


Figure 6.42 Support reactions.

Different loading step procedures were used as explained in the beginning of this section. As a result 3 different force-drift curves are plotted, see Figure 6.43.

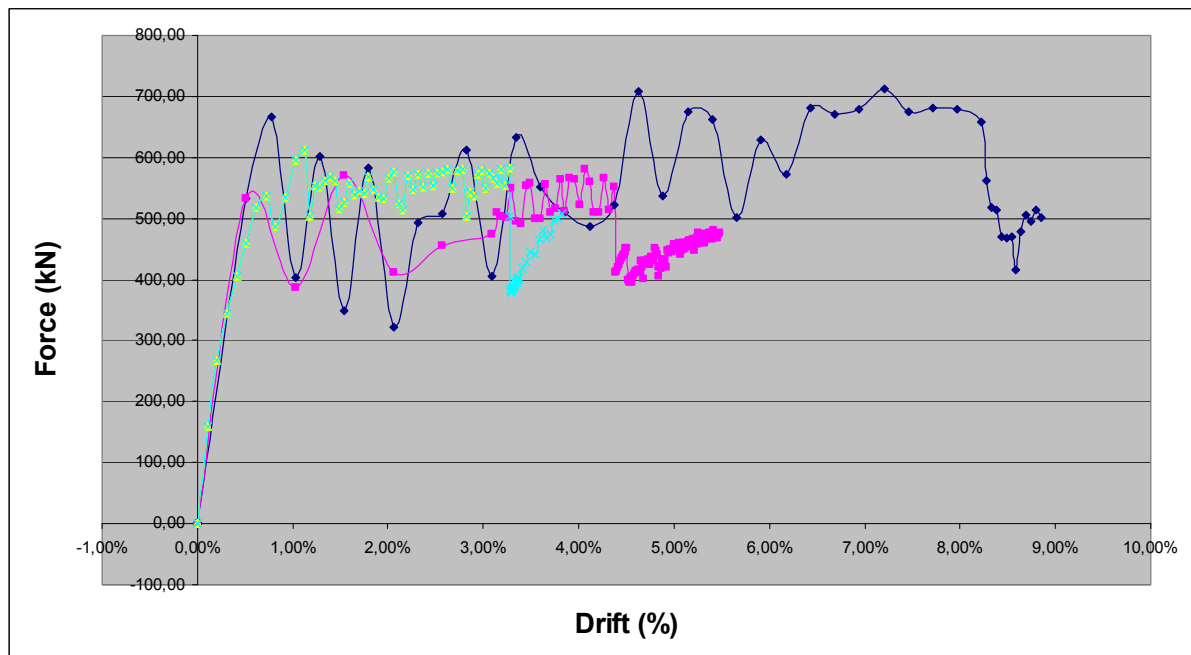


Figure 6.43 Force-drift diagram for different load-step procedures.

The results look satisfactory and seem to comply with a simplified tri-linear idealization, Figure 6.44, of the force-deflection curve behaviour for a typical debonded precast prestressed concrete beam-column joint that is proposed by Priestley (1993).

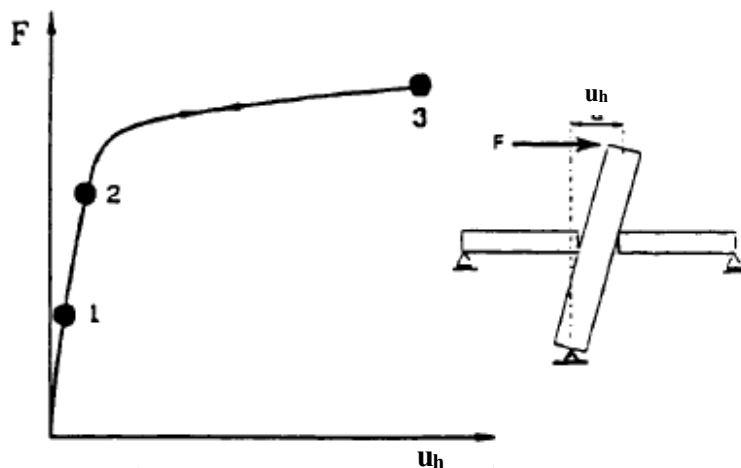


Figure 6.44 Trilinear idealisation of force-drift relation [modified from Priestley (1993)].

Therefore the presentation of the outcomes could be explained with a sequence of events in the specimen:

1. Decompression point: Defines the beginning of the crack formation, when the concrete at the extreme fibre of the beam-column connection reaches zero stress, after the initial pre-compression imposed by the post-tensioned tendons.
2. Linear limit point: Defines the end of the elastic range, which does not correspond to a clear stress-strain state in the section, as typical in a reinforced concrete section after the yielding of the steel. The crack is assumed to have propagated to the centroidal axis.
3. Failure of the steel: A third last point of the curve can be defined at the point of failure at the steel stress-strain curve.

Now the 3 events are identified in Figure 6.45. At a drift of 4,32% the longitudinal steel in the column failed, this determines point 3 from the trilinear idealization. Point 2 is determined from the first yielding in the steel and point one when the first cracks appeared.

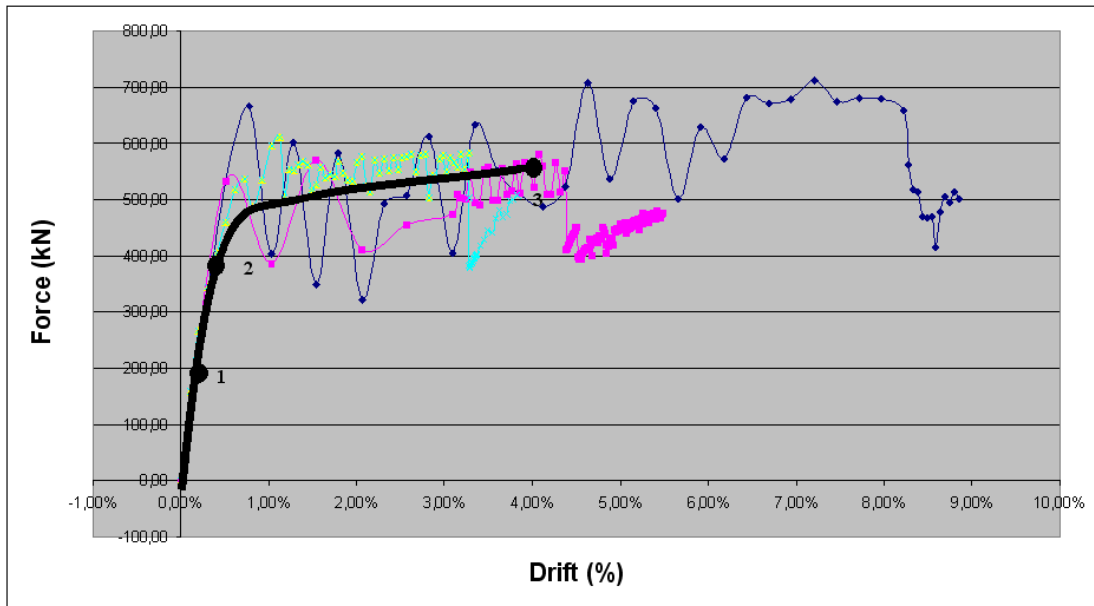


Figure 6.45 Force-drift diagram for different load-step runs with identification of 3 critical events.

## 7 Results Validation with Analytical Modelling

Ductile beam-column connections of jointed systems that incorporate unbonded prestressing steel at the critical sections, causing strain incompatibility between steel and concrete, cannot be analysed by classical section analysis methods.

Different alternative approaches have been proposed in literature to analytically investigate the behaviour of such particular types of connections. The one used in this chapter is proposed by Pampanin et al (2001). Some modifications were adopted for this particular case.

### 7.1 Moment rotation analysis procedure

The section analysis approach proposed by Pampanin et al (2001) provides a simple procedure to calculate a moment-rotation relation based on a typical section analysis, which can account for member compatibility.

In order to satisfy both equilibrium and member compatibility a trial and error process is utilized. While the equilibrium equation can still be formulated at the critical section, the deformation compatibility relationship must consider the global behaviour of the connection, including beam and column elements as well as the connection zone.

The analysis was made with the help of Microsoft Excel sheets and Matlab. The procedure is explained in the following steps:

- **Calculate the rotation:** The horizontal displacement  $u_h$  in the top of the column from one of the drift results in DIANA is used to calculate the column rotation  $\theta$ , according to Eq. (7.1) and Figure 7.1.

$$\theta = \arctan \frac{u_h}{H} \quad (7.1)$$

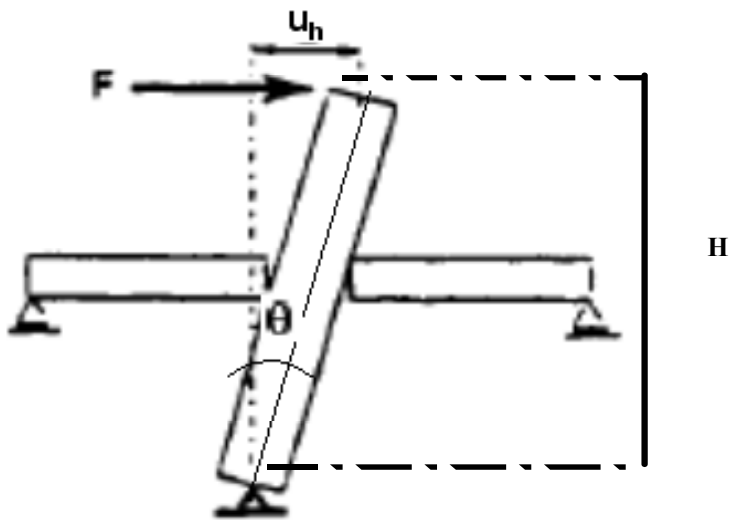


Figure 7.1 Column rotation and displacements.

The effective rotation  $\theta_b$  of the beam developed at the beam-column interface due to the opening of the crack is then related to the rotation of the column: according to Eq. (7.2) and Figure 7.2.

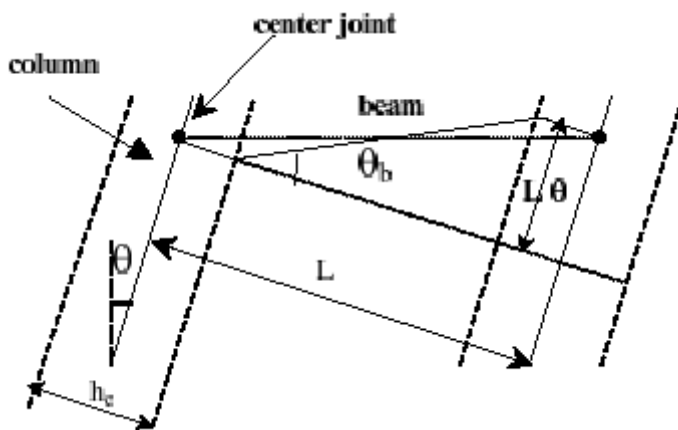


Figure 7.2 Interstorey drift and beam rotation [Pampanin et al (2001)].

$$\theta_b = \frac{\theta}{\left(1 - \frac{h_c}{L}\right)} \quad (7.2)$$

where:

$h_c$  = Column depth.

$\theta$  = Column rotation.

$L$  = Idealised length of beam (from centre to centre of the joints).

- **Guess the initial neutral axis  $x$  of the beam:** Start with a value of  $\frac{1}{4}$  of the depth of the beam and later, if needed, update the value.

- **Evaluation of the strains in unbonded post-tensioned tendons:** The increase of the strains in the post-tensioned tendons due to the beam deformation is taken into account as

$$\varepsilon_{pt} = \frac{n \cdot \Delta L_{pt}}{l_{ub}} \quad (7.3)$$

where:

$n$  = Number of total openings along the beam at beam-column interfaces.

$l_{ub}$  = Unbonded length of the tendons.

$\Delta L_{pt}$  = Elongation (elastic + plastic) at the level of the tendons.

$$\Delta L_{pt} = \theta_b \cdot (d_i - x) \quad (7.4)$$

where:

$d_i$  = Effective depth of the tendons in the beam section.

- **Member compatibility condition or monolithic beam analogy:** For the calculation of the concrete strain we assume conventionally that the point of contraflexure occurring in the beam due to the lateral loads is at mid span. The end displacement of two different cantilever schemes is compared in Figure 7.3. In the precast case, the opening of a gap at the beam-column interface results in an imposed rigid rotation.

The displacement contribution from the imposed rigid rotation, summed with the elastic deformations, gives the total displacement for the precast cantilever. Meanwhile in the monolithic cantilever the total displacement would be given by the sum of an elastic and a plastic contribution, where the later is approximated by rigid rotation about the beam end.

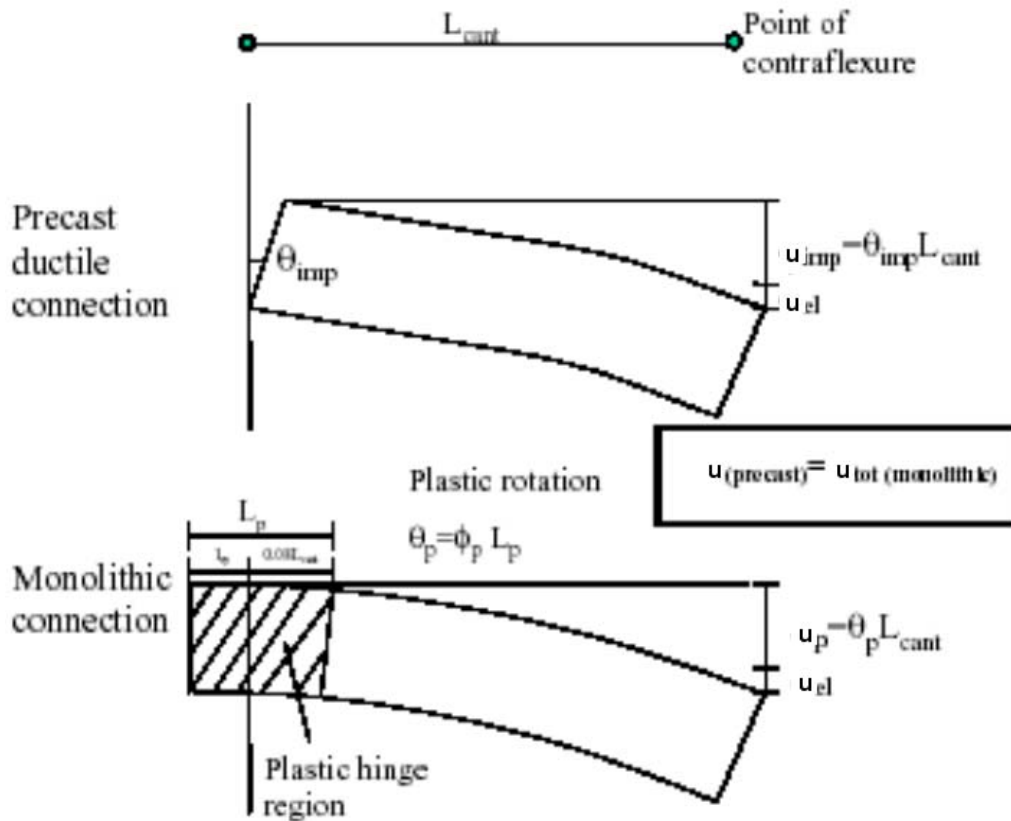


Figure 7.3 Monolithic beam analogy [modified from Pampanin et al (2001)].

When imposing the same total displacement and assuming that the two beams are identical in terms of geometry and reinforcement, the elastic deformations would be the same and the plastic contributions can be equated. In the precast case the inelastic deformation is localised at the interface, and in the monolithic one it is distributed along a plastic hinge.

Using, in the monolithic case, the ultimate curvature  $\phi_u$  and yielding curvature  $\phi_y$  concepts [Paulay and Priestly (1992)] and combining the equations presented in Figure 7.3 the concrete strain results in Eq. (7.10). For more information on this matter reference is made to Pamapanin et al (2001).

$$u_{tot\_(\text{precast})} = u_{tot\_(\text{monolithic})} \quad (7.4)$$

$$u_{imp} + u_{el} = u_p + u_{el} \quad (7.5)$$

$$u_{imp} = u_p \quad (7.6)$$

$$\theta_{imp} \cdot L_{cant} = u_p \quad (7.7)$$

$$u_p = \theta_p \cdot \left( L_{cant} - \frac{L_p}{2} \right) = (\phi_u - \phi_y) \cdot \left( L_{cant} - \frac{L_p}{2} \right) \quad (7.8)$$

$$\phi_u = \frac{\varepsilon_{cc}}{x} \quad (7.9)$$

where

$\varepsilon_{cc}$  = Compressive concrete strain at extreme fibre

Combining equations (7.7), (7.8) and (7.9) yields:

$$\varepsilon_{cc} = \left[ \frac{\theta_{imp} \cdot L_{cant}}{\left( L_{cant} - \frac{L_p}{2} \right) L_p} + \phi_y \right] \cdot x \quad (7.10)$$

where:

$L_{cant}$  = Length of the corresponding cantilever.

$L_p$  = Plastic hinge length.

$\theta_{imp}$  = Imposed rigid rotation.

Finally the concrete stress distribution in the compressive zone is determined from the assumed value of the extreme concrete strain  $\varepsilon_{cc}$ . The introduced additional condition

on the global member displacement satisfies the member compatibility and results in a simple relationship between concrete strain and neutral axis position. For each guessed value of the neutral axis position, the member compatibility relationship provides a unique value of concrete strain, which should satisfy the section equilibrium conditions.

- **Section equilibrium:** The concrete resultant is calculated from the previous concrete strain and compared with:

$$\sum P = P_{pt1} + P_{pt2} + P_{pt3} \quad (7.11)$$

with:

$$P_{pti} = P_i + \Delta\sigma_p \cdot A_{pt} \quad (7.12)$$

where:

$\Delta\varepsilon_{pti}$  = Additional strain of the post-tensioned tendons due to frame displacement.

$\Delta\sigma_p$  = Additional stress in the tendons due to their additional elongation.

$P_i$  = Initial tensile force in post-tensioned tendon, before frame displacement.

Then section equilibrium is checked and if it is violated, a new value of the neutral axis depth should be guessed, resulting in a trial and error procedure to find the final value.

- **Moment capacity:** At last the moment resistance of the section is calculated by taking the moment around the concrete resultant.

$$M_R = \sum P_i \cdot z_i \quad (7.13)$$

where

$$z_i = d_i - \frac{x}{2} \quad (7.14)$$

## 7.2 Comparison of moment-drift curve

The analytical results and the finite element results from DIANA were compared with a moment-drift curve instead of the force-drift curve, as that is how the analytical procedure states it. To calculate the moment in the beam from the finite element analysis results, simple equilibrium considerations (using the force that is read as the sum of the support reactions in the horizontal direction at the base values, see Figure 6.42) permit to achieve the value of the moment at a desired section, see Figures 7.4 and 7.5.

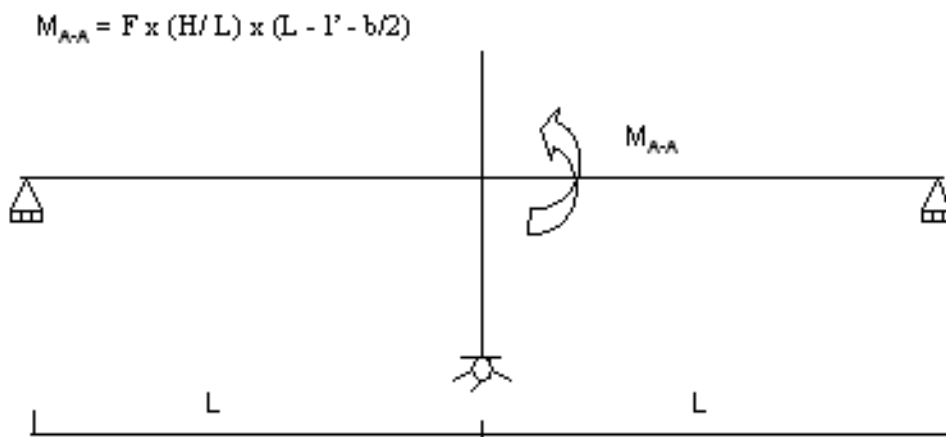


Figure 7.4 Moment at the section A-A.

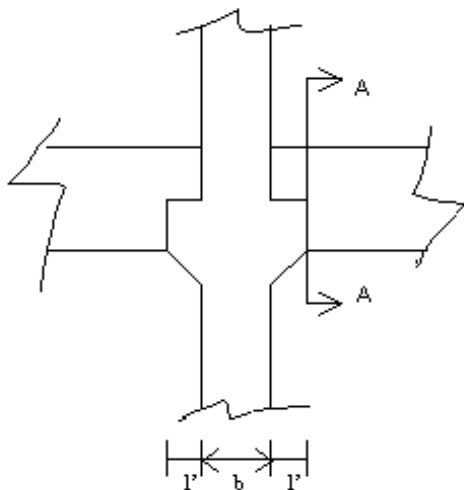


Figure 7.5 Joint details.

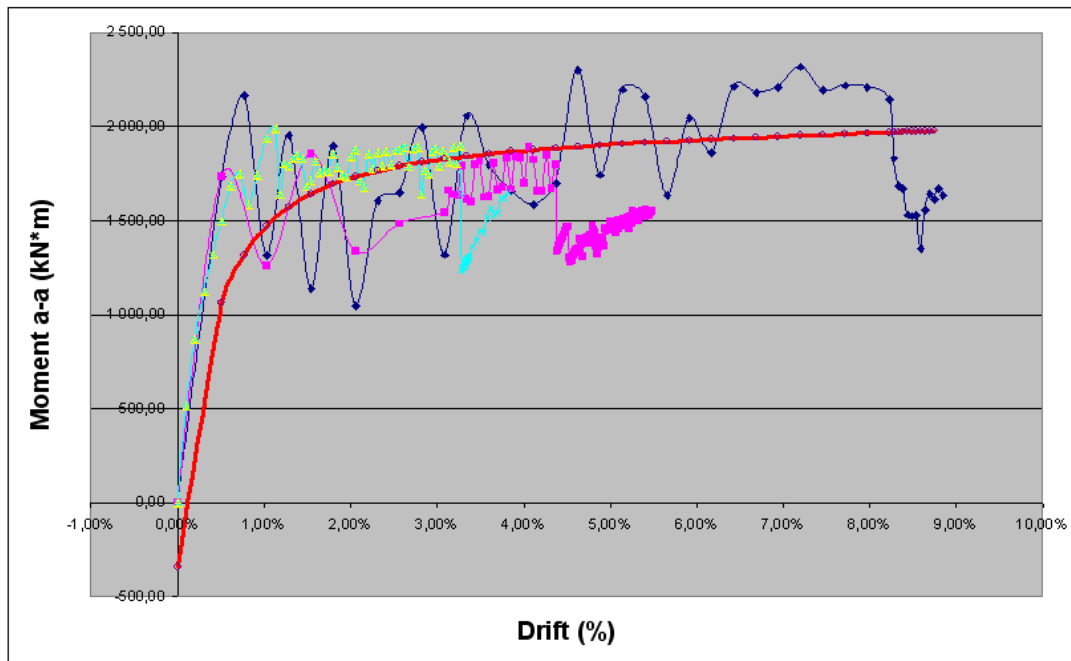


Figure 7.6 Moment-drift comparison of FEM results with analytical results.

The comparison of the results is shown in Figure 7.6; the red line represents the analytical results and the other lines the results from DIANA assuming different loading procedures. As previously mentioned the calculations were made in Excel and checked with Matlab, see Appendix A.

The results from the analytical calculations proposed by Pamapanin et al (2001) turned out to be quite satisfactory especially in the non-linear part of the curve. In the elastic part there seems to be a shift that could be due to several factors. One possible factor is that in the analytical calculations the hypothesis that the columns rotates rigidly is not totally true in the FE analysis.

## 8 Recommendations and Conclusions

The results from the FEM analysis and the comparison with the analytical calculations showed to be satisfactory. In any case the design of the connection can be further improved for future research.

### 8.1 Column capacity

The results showed that the capacity of the column was small compared to the capacity of the beams, since the steel in the column failed before any yielding appeared in the beams. This issue reminds of the “weak-column strong-beam” problem. This also means that if the design of the column is upgraded, the response of the connection will also be improved.

Several measures could be taken to upgrade the column, for example:

- Increase the lever-arm of the sectional force resultants by increasing the sectional height of the column. Increase the amount of reinforcing steel.
- Prestress the column by pretensioning.
- Prestress the connection by vertical post-tensioned tendons.

### 8.2 Recommendations for further research

Some further research could be carried out before a connection design is selected for experimental studies:

- Self-centring capabilities and limited residual drift are some of the notable features that should be checked; therefore it would be interesting to study the cyclic behaviour of the connection.
- Analysing the same connection in a 3 dimensional model and comparing the results with those from this investigation would be valuable.
- Modelling and designing another promising solution of a ductile connection and comparing it with the results of this investigation would also be appealing.

### **8.3 Final conclusions**

The structural response of the selected and designed ductile beam-column connection of jointed systems under imposed monolithic lateral loads was satisfactory. The following summarizes the conclusions:

- Damage to the beams was minimal; most of the cracks in the beams were limited to the regions close to the interface and to the concrete cover.
- As expected there was no loss of prestress in the secondary tendons, i.e. they remained in the elastic range.
- The structure achieves drift of 4%, which is higher than the drift of 2 to 3% that is normally assumed in design of structures.
- The analytical calculations provided an excellent confirmation of the FEM results.

## 9 References

- CEB-FIB (2003) State-of-art report: *Seismic Design of Precast Concrete Building Structures*, International Federation for Structural Concrete (fib), bulletin 27, Lausanne, Switzerland, 2003, 254 pp.
- CEB-FIP (1991): CEB-FIP Model Code 1990. Comité Euro-International du Béton.
- De Witte F. C., Kikstra W. P. (1999): *DIANA R9 User's Manual, Nonlinear Analysis*, TNO Building and Construction Research, Delft, The Netherlands.
- Englekirk R. (2002): Design-Construction of The Paramount – A 39-Story Precast Prestressed Concrete Apartment Building. *Precast/Prestressed Concrete Institute, PCI Journal*, Vol. 47, No. 4, July-August 2002, pp. 56-71.
- Feenstra, P. H. (1993): *Computational Aspects of Biaxial Stress in Plain and Reinforced Concrete*, PhD thesis, Delft University of Technology, Holland.
- FIB (1994): *Planning and Design Handbook on Precast Building Structures*, SETO Ltd, London, England, 1994, 138 pp.
- Lertsrisakulrat, T., Watanabe, K., Matsuo, M., Niwa, J. (1999): *Localized Fracture Length and Fracture Energy of Concrete in Compression*, Japan, September 1999, 6 pp.
- Nakano K., Tanabe K., Machida S., Wada A. (2001): *Damage Controlled Seismic Design by Precast Prestressed Concrete Structure with MILD-PRESS-JOINT, Part 1. Basic concept of design*. Summaries of technical papers of annual meeting, Architectural Institute of Japan, Japan, September 2001, pp. 119-1244.
- Pampanin S. (2003): Alternative Design Philosophies and Seismic Response of Precast Concrete Buildings, *International Federation for Structural Concrete (fib), FIB Journal Structural Concrete*, Vol. 4, No. 4, December 2003, pp. 203-211.
- Pampanin S., Priestley M.J.N., Sritharan S. (2001): Analytical Modelling of the Seismic Behaviour of Precast Concrete Frames Designed with Ductile Connections. *Journal of Earthquake Engineering, Imperial College Press*, Vol. 5, No. 3, 2001, pp. 329-367.
- Priestley M.J.N., Sritharan S, Conley J.R., Pampanin S. (1999): Preliminary Results and Conclusions from the PRESS Five-Story Precast Concrete Test Building, *Precast/Prestressed Concrete Institute, PCI Journal*, Special Report, November-December 1999, pp. 42-67.
- Priestley M.J.N. (1996): The PRESS Program – Current Status and Proposal Plans for Phase III, *Precast/Prestressed Concrete Institute, PCI Journal*, Vol. 41, No. 2, March-April 1996, pp. 22-40.
- Priestley, M.J.N. (1993): Myths and Fallacies in Earthquake Engineering – Conflicts between Design and Reality, *Bulletin of the New Zealand National Society for Earthquake Engineering*, Vol. 26, No. 3, pp. 329-341.

- Stone W., Cheok G., Stanton J.F. (1995): Performance of Hybrid Moment-Resisting Precast Beam-Column Concrete Connections Subjected to Cyclic Loading, *ACI Structural Journal*, No. 92-S22, March-April 1995, pp. 229-249.
- Tanabe K., Matuzaki Y., Yamada M. (2001): *Damage Controlled Seismic Design by Precast Prestressed Concrete Structure with MILD-PRESS-JOINT, Part 2. Kernel of Structural Design and Examples*, Summaries of technical papers of annual meeting, Architectural Institute of Japan, Japan, September 2001, pp. 125-131.
- Vecchio F. J., Collins M. P. (1993): Compression Response of Cracked Reinforced Concrete, *Journal of Structural Engineering*, ASCE, 119.
- Vecchio F. J., Collins M. P. (1986): The Modified Compression-Field Theory for Reinforced Concrete Elements Subjected to Shear, *ACI Journal*, Proceedings V. 83, No. 2, Mar.-Apr. 1986, USA, pp. 219-231.
- Özdil E., Arioglu E., Yorulmaz M., Manzak O., Alper T. (2002): *Full Scale Testing of Post Tensioned Moment Resisting Connections of a Precast Concrete Structure*, Yapi Merkezi Prefabrication Incorporated, Istanbul, Turkey, 2002, 10 pp.

# APPENDIX A      ANALYTICAL ANALYSIS CALCULATIONS IN MATLAB

```
% --- Analytical Calculations using Pampanin et al (2001) model ---  
  
% --- Clear Everything ---  
  
clear  
  
close all  
  
clc  
  
% --- Model parameters ---  
  
h=3500;                    %Height of column  
hc=450;                    %Depth of column  
lb=6000;                   %Length of beam  
hb=750;                    %Depth of beam  
d1=100;                    %Position of tendon 1  
d2=500;                    %Position of tendon 2  
d3=550;                    %Position of tendon 3  
lub=100;                   %Unbonded length of the tendons  
n=1;                        %Number of total openings along the beam  
lsp=50;                    %Spandrel length  
ey=0.00275;                %Yielding strain of mild steel  
lcant=lb/2-hc/2;            %Distance form the interface and the point of contraflexure  
phiy=0.5*ey*(lb/hb);        %Yielding curvature for reinforced frames  
lp=lsp+(0.08*lcant);        %Plastic hinge length  
  
beta=0.8;  
  
fm=50405;  
  
b=400;  
  
Ept=200000;                %Young modulus for steel  
Tin=700;                    %Initial tendon force
```

```

Apt=465;                                %Area of the tendons

% --- Fix the rotation ---

delta=0;

teta=atan(delta/h);

tetab=teta/(1-(hc/lb));

% --- Guess of the initial neutral axis ---

ci=0.13;

% --- Equilibrium ---

tol=0.1;

R=0;

T=0;

C=0;

while (R>tol)

    % --- Evaluation of the strain in unbonded post-tensioned tendons ---

    dpt1=tetab*(d1-ci);

    dpt2=tetab*(d2-ci);

    dpt3=tetab*(d3-ci);

    ept1=(n*dpt1)/lub;

    ept2=(n*dpt2)/lub;

    ept3=(n*dpt3)/lub;

    % --- Calculation of the strain in the concrete ---

    ec=(((teta*lcant)/((lcant-(lp/2))*lp))+phiy)*ci;

    % --- Concrete compressive force ---

    C=ci*beta*b*fm;

    % --- Tendon forces ---

    f1=ept1*Ept;

    f2=ept2*Ept;

    f3=ept3*Ept;

```

```
Tpt1=(f1*Apt)+Tin;  
Tpt2=(f2*Apt)+Tin;  
Tpt3=(f3*Apt)+Tin;  
if Tpt1 < 0  
    T=Tpt2+Tpt3;  
else  
    T=Tpt1+Tpt2+Tpt3;  
end  
R=(T-C);  
end  
c=C/(beta*b*fm);  
ci=c;
```